Fluidized granular matter : sedimentation and dense flows

Laciel Alonso Llanes

UNIVERSITÉ DE STRASBOURG

En cotutelle avec l'Université de La Havane

(Cuba)

ÉCOLE DOCTORALE ED413

Sciences de la Terre et de l'Environnement

UMR 7063

THÈSE présentée par :

Laciel ALONSO-LLANES

soutenue le : **23 septembre 2022**

pour obtenir le grade de : **Docteur de l'université de Strasbourg**

Discipline/ Spécialité : Geophysique / Physique de la Matière Granulaire

Matière granulaire fluidisée :
sédimentation et écoulements denses

THÈSE dirigée par :

Mr. TOUSSAINT Renaud	Directeur de recherche CNRS, université de Strasbourg
Mr. ALTSHULER Ernesto	Professeur, université de La Havane

RAPPORTEURS :

Mr. SANTUCCI Stéphane	Chargé de recherche, ENS Lyon
Mr. RAMOS Osvanny	Maître de conférences HDR, ILM Lyon

AUTRES MEMBRES DU JURY :

Mme. LINDNER Anke	Professeure, université de Paris
Mr. MEGHRAOUI Mustapha	Professeur, université de Strasbourg
Mr. BATISTA-LEYVA Alfo J.	Professeur, université de La Havane
Mr. SÁNCHEZ-COLINA Gustavo	Maître de conférences, université de La Havane

UNIVERSITE DE STRASBOURG

RESUME DE LA THESE DE DOCTORAT

Discipline :	Geophysique
Spécialité (facultative) :	Matière Granulaire
Presente par:	**ALONSO – LLANES Laciel**
Titre :	Matière granulaire fluidisée : sédimentation et écoulements denses
Unité de Recherche :	Institut Terre et Environnement de Strasbourg (ITES) – UMR 7063
Cotutelle :	Faculté de Physique, Université de La Havane
Ecole Doctoral :	Sciences de la Terre et de l´environnement – ED 413
Location :	ITES, Universite de Strasbourg, Strasbourg
Directeur de Thèse :	**TOUSSAINT Renaud** (DR CNRS, Université de Strasbourg)
Co-Directeur de Thèse :	**ALTSHULER Ernesto** (PR, Université de La Havane)

Université de Strasbourg

VNIVERSIDAD DE LA HABANA

Université de Strasbourg
Université de La Havane

Doctoral School **Sciences de la Terre et de l'Environnement**

University Department **Institut Terre et Environnement**

Thesis defended by **Laciel Alonso Llanes**

Defended on **September 23, 2022**

In order to become Doctor from Université de Strasbourg and from Université de La Havane

Academic Field **Geophysics**

Speciality **Physics of granular matter**

Fluidized granular matter: sedimentation and dense flows

Thesis supervised by Renaud Toussaint
Ernesto Altshuler

Committee members

Referees	Stéphane Santucci	Researcher at ENS Lyon
	Osvanny Ramos	HDR Associate Professor at ILM
Examiners	Anke Lindner	Professor at Université de Paris
	Mustapha Meghraoui	Professor at UNISTRA
	Alfo J. Batista-Leyva	Professor at UH
	Gustavo Sánchez-Colina	Associate Professor at UH
Supervisors	Renaud Toussaint	Senior Researcher at UNISTRA
	Ernesto Altshuler	Professor at UH

Université de Strasbourg

VNIVERSIDAD DE LA HABANA

Université de Strasbourg
Université de La Havane

École doctorale **Sciences de la Terre et de l'Environnement**

Unité de recherche **Institut Terre et Environnement**

Thèse présentée par **Laciel Alonso Llanes**

Soutenue le **23 septembre 2022**

En vue de l'obtention du grade de docteur de l'Université de Strasbourg et de l'Université de La Havane

Discipline **Geophysique**

Spécialité **Physique de la Matiere Granulaire**

Matière granulaire fluidisée : sédimentation et écoulements denses

Thèse dirigée par Renaud Toussaint
Ernesto Altshuler

Composition du jury

Rapporteurs	Stéphane Santucci	chargé de recherche à l'ENS Lyon
	Osvanny Ramos	MCF HDR à l'ILM
Examinateurs	Anke Lindner	professeure à l'Université de Paris
	Mustapha Meghraoui	professeur à l'UNISTRA
	Alfo J. Batista-Leyva	professeur à l'UH
	Gustavo Sánchez-Colina	MCF à l'UH
Directeurs de thèse	Renaud Toussaint	directeur de recherche à l'UNISTRA
	Ernesto Altshuler	professeur à l'UH

This thesis has been prepared at the following research units.

Institut Terre et Environnement
Batiment Descartes
5, rue René Descartes
67084 Strasbourg cedex
France

☎ (33)(0)3 68 85 03 37
✉ secretariat@ites.unistra.fr
Web Site https://ites.unitra.fr/

Facultad de Física
San Lázaro y L
14000 La Habana
Cuba

☎ (53)(7)878 50 05
✉ secretaria@fisica.uh.cu
Web Site https://fisica.uh.cu/

Fluidized granular matter: sedimentation and dense flows

Abstract

Granular media are ubiquitous in nature and of utmost importance for Earth sciences. A distinguishing feature of these is that although their constituent particles are solid, as a whole they may behave as solids, liquids or gases. During the penetration of an intruder into a granular bed, solid and fluidlike behaviors coexist and, under certain conditions, this penetration may involve rotation of the object. However, despite significant research efforts devoted to understanding of the penetration, rotation has been a topic rarely documented in the literature. Another scenario involving solid and fluidlike behaviors is that of granular heap. Many complex phenomena have been found in the dense flows established on its surface, such as the transition between continuous and intermittent flows (CIT). In spite of the many advances in the physics of granular flows, the study of these during the continuous regime in situations of greater practical utility such as growing heaps is not common. This thesis studies the sedimentation of solid intruders in granular cells under different conditions: close to a vertical wall, in a horizontally agitated cell or with different initial orientations, with particular emphasis on the rotation described by them. On the other hand, the CIT in a growing granular heap is also studied.

Keywords: granular media, sedimentation, settling, penetration, tilting, dense flows, flow transition

Matière granulaire fluidisée : sédimentation et écoulements denses

Résumé

Les milieux granulaires sont omniprésents dans la nature et revêtent une importance capitale pour les sciences de la Terre. Ils se distinguent par le fait que, bien que leurs particules constitutives soient solides, dans leur ensemble, ils peuvent se comporter comme des solides, des liquides ou des gaz. Lors de la pénétration d'un intrus dans un lit granulaire, les comportements solide et fluide coexistent et, dans certaines conditions, cette pénétration peut impliquer une rotation de l'objet. Cependant, malgré d'importants efforts de recherche consacrés à la compréhension de la pénétration, la rotation a été un sujet rarement documenté dans la littérature. Un autre scénario impliquant des comportements de type solide et fluide est celui du tas granulaire. De nombreux phénomènes complexes ont été découverts dans les flux denses établis à sa surface, tels que la transition entre les flux continus et intermittents (CIT). Malgré les nombreuses avancées dans la physique des écoulements granulaires, l'étude de ceux-ci en régime continu dans des situations de plus grande utilité pratique comme les tas en croissance n'est pas courante. Cette thèse étudie la sédimentation d'intrus solides dans des cellules granulaires dans différentes conditions : près d'une paroi verticale, dans une cellule agitée horizontalement ou avec différentes orientations initiales, avec un accent particulier sur la rotation décrite par celles-ci. D'autre part, le CIT dans un amas granulaire en croissance est également étudié.

Mots clés : milieux granulaires, sédimentation, décantation, pénétration, basculement, écoulements denses, transition d'écoulement

Abstract

Granular media are ubiquitous in both industrial processes and in nature, and since most soils are granular, they are of utmost importance to Earth sciences. Granular matter is composed of conglomerates of rigid macroscopic particles of many different materials, sizes and shapes, which interact with each other predominantly by contact and friction. Although the particles that compose them are solid, as a whole, and depending on the manner in which they are handled, they may behave as solids, liquids or gases. In some cases it's even possible to describe them with the laws governing these states of matter, however, their behavior is often very different from a conventional solid, liquid or gas.

In the granular state of matter, solid or fluid like behaviors usually coexist. Such is the case for the penetration of a solid intruder in a granular bed: during the first moments the sinking is usually smooth, there, the intruder transfers its momentum fluidizing the particles of the medium; then, when it has lost enough speed, the jamming begins due to the friction between grains and the networks of contacts that transmit the forces until the intruder comes to a complete detention at a certain depth. The first part of the process may resemble the sinking of an object in a conventional fluid, however, the second part distinguishes it from any behavior expected in any liquid. Many real world scenarios can benefit from understanding how objects sink in granular matter, particularly if confinement effects are taken into account. However, in spite of the substantial research efforts devoted to understand the impact and penetration of low-velocity projectiles into granular beds, intruder-wall interactions have rarely been documented in the literature. In the first chapter of the thesis, the penetration dynamics of a cylindrical object close to a vertical wall into a quasi-2D granular medium it is described in detail. By following the path of the cylinder as it penetrates the granular bed, we describe two different types of motion: its center of mass moving horizontally away from the sidewall while it rotates about its axis of symmetry. While repulsion is associated with the loading of force chains between the intruder and the wall, rotation may

be associated with frictional forces between the grains and the intruder. Finally, we show the analogies between the settling of twin intruders released far from any boundary and that of an intruder released near a vertical wall.

The rotation of intruders into a granular medium has been another topic rarely documented in the literature, its reason may be associated with the interest of first establishing bridges between the development of knowledge of static granular matter and its dynamic flow. This has led studies to concentrate on quasi-static penetration situations where, due to experimental limitations, intruders are not allowed to rotate. On the other hand, shaken granular beds have received a certain degree of attention, due to the growing interest for engineers and geoscientists to understand how man-made structures such as buildings, and massive rocks laying on granular soils respond to fluidization associated to seismic waves. However, the performance of objects initially laying on the surface of a granular bed submitted to lateral shaking has been rarely studied. In that sense, we study the behavior of cylindrical objects when they sink (with the axis parallel to the force of gravity) in a dry granular fluidized bed due to lateral oscillations. We find that while sinking, cylinders with foundations attached to their bottom base (consisting of a thin ring) tend to tilt while those with flat bases remain practically vertical. We also find that the tilt scenario tends to predominate regardless of the base of the intruders when sufficiently strong horizontal vibrations are used. Through DEM simulations we were able to reproduce this behavior and find a possible cause, in addition to analyzing the influence of the change in the aspect ratio of the intruder when incorporating different rings. Our findings may shed light on the behavior of buildings and other man-made constructions during earthquakes.

In order to advance our understanding of the rotation exhibited by flat-bottom intruders, we study a situation that, while still not quasi-static, is simpler than penetration into the agitated granular medium. We then analized the penetration of a cuboid intruder released at different angles of attack inside a quasi-bidimensional Hele-Shaw cell. During penetration, the intruder rotates in such a way that its final angular position is close to zero, i.e., its bottom surface parallel to the bottom of the container (this resembles what was observed for the cylindrical intrusions (no-ring) sinking into the agitated granular bed: after each half oscillation of the cell, they corrected their inclination). Similar situations were observed for different initial angles of the intruder, except for 45 degrees, where, on average, the angular position remained stable. We propose a phenomenological model based on resistive force theory (RFT) to describe its penetration and rotation dynamics under non-quasi-static conditions. The RFT is inspired by a set of rules related to the swimming of microorganisms at low Reynolds numbers and is a strong approximation for granular media that has been used mainly in quasi-static penetrations. It states that the drag force against the intruder motion is fairly well represented

by a simple superposition principle, and assumes that the friction of the granular tangential flow against the intruder surface contributes negligibly to the drag force. We have found that the RFT manages to quantitatively describe both, tilting and sinking motions, although with some punctual discrepancies.

The second part of the thesis includes another form of the fluidized matter: the granular flows. Most granular flows encountered in nature (from sand dunes, landslides, rock avalanches, to pyroclastic flows), and industry, are often classified as a liquid regime, where the material is dense but still flows as a fluid. This regime has received no little attention from the scientific community in the search for constitutive laws capable of reproducing the diversity of observed behaviors. However, one behavior in particular has been poorly studied: the transition from continuous to intermittent flows (CIT). If a granular material is poured from above on a horizontal surface between two parallel, vertical plates, a sand heap grows in time. For small piles, the grains flow smoothly downhill, but after a critical pile size X_c, the flow becomes intermittent: sudden avalanches slide downhill from the apex to the base, followed by an "uphill front" that slowly climbs up, until a new downhill avalanche interrupts the process. By means of experiments controlling the distance between the apex of the sandpile and the container feeding it from above, we show that X_c grows linearly with the input flux, but scales as the square root of the feeding height. We explain these facts based on a phenomenological model, and demonstrate that our controlled experiments allow to predict the value of X_c for the common situation in which the feeding height decreases as the pile increases in size. We also briefly discuss the transition from a situation like ours (a pile growing in time) to one of the most common and highly documented in the literature: the stationary pile. In addition, we identify that the proposed model accounts for the observed change in the shape of the fluid layer from one that is wedge-shaped as the pile grows to one whose thickness is constant along the surface.

Finally, the first steps in the photogrammetric study of a sand dune on one of the beaches of eastern Cuba are presented. This part discusses some of the advances in photogrammetry that have facilitated the reconstruction of three-dimensional models based on digital images. It also comments on the factors that affect the quality of model comparison over time, highlighting the need for the use of stable ground control points. On the other hand, estimates of the amount of eroded material between two points in time when data were acquired are presented. In spite of the fact that these preliminary study lacks precision, it is possibly the first attempt to study erosion in Cuban beach dunes by 3D modelling based on photogrammetry.

Résumé

Les milieux granulaires sont impliqués dans un grand nombre de processus industriels dans lesquels les problèmes liés à leur transport, leur stockage, leur écoulement et autres sont présentés quotidiennement. Leur présence dans la nature les rend très importants pour les sciences de la Terre car notre sol en est principalement composé. Les milieux granulaires forment une vaste famille composée de conglomérats de particules macroscopiques rigides, couvrant plusieurs matériaux, tailles et formes, qui interagissent principalement par friction et collision. Malgré une classification aussi simple, un milieu granulaire se comporte très différemment des solides, liquides ou gaz typiques, bien que pour certains cas, il soit possible de caractériser la matière granulaire selon les lois régissant ces états d'agrégation puisque, selon la façon dont elle est manipulée, elle se comporte comme un solide, un liquide ou un gaz.

Les comportements fluides et solides ont tendance à coexister dans l'état granulaire de la matière. Par exemple, la pénétration d'un intrus solide libéré dans un large lit granulaire peut être tout à fait régulière pendant la première partie de sa trajectoire, mais devient finalement fluctuante, jusqu'à ce que l'objet s'arrête complètement à une certaine profondeur dans le matériau. La première partie du mouvement peut ressembler à la pénétration d'une sphère dans un fluide visqueux, mais ensuite le milieu connaît une transition vers l'état de blocage, ce qui distingue le processus de tout comportement prévisible d'un liquide. Les scénarios de la vie réelle tels que les moulins/broyeurs à billes et les excavations près des murs impliquent des phénomènes complexes dont le traitement bénéficierait d'une meilleure compréhension de la façon dont les intrus pénètrent près des frontières dans la matière granulaire. Cependant, malgré les efforts de recherche importants consacrés à la compréhension de l'impact et de la pénétration de projectiles à basse vitesse dans des lits granulaires, les interactions intrus-mur ont rarement été documentées dans la littérature. Dans le premier chapitre de la thèse, il est décrit en détail la dynamique de pénétration d'un objet cylindrique dans un milieu granu-

laire quasi-2D. En suivant la trajectoire du cylindre lors de sa pénétration dans le lit granulaire, nous caractérisons deux types de mouvement distincts : son centre de masse s'éloigne horizontalement de la paroi latérale, et il tourne autour de son axe de symétrie. Alors que la répulsion est causée par la charge des chaînes de force entre l'intrus et la paroi, la rotation peut être associée aux forces de friction entre les grains et l'intrus. Enfin, nous montrons les analogies entre la sédimentation de deux intrus jumeaux libérés loin de toute frontière, et celle d'un intrus libéré près d'une paroi verticale.

La rotation d'intrus dans un milieu granulaire a été un autre sujet rarement documenté dans la littérature, sa raison peut être associée à l'intérêt d'établir des ponts entre le développement de la connaissance de la matière granulaire statique et son écoulement dynamique. Cela a conduit les études à se concentrer sur des situations de pénétration quasi-statiques où, en raison des limitations expérimentales, les intrus ne peuvent pas tourner. D'autre part, les lits granulaires secoués ont reçu un certain degré d'attention, en raison de l'intérêt croissant des ingénieurs et des géoscientifiques pour comprendre comment les structures artificielles telles que les bâtiments, et les roches massives reposant sur des sols granulaires répondent à la fluidification associée aux ondes sismiques. Cependant, la performance d'objets initialement posés sur la surface d'un lit granulaire soumis à une secousse latérale a été rarement étudiée. Dans ce sens, nous étudions le comportement d'objets cylindriques lorsqu'ils s'enfoncent dans un lit granulaire sec fluidisé par des oscillations latérales. De manière assez inattendue, il a été constaté que, dans une large gamme de puissances de secousses latérales, les cylindres à fond plat s'enfoncent verticalement, tandis que ceux qui ont une "fondation" consistant en un anneau peu profond attaché à leur fond, s'inclinent en plus de s'enfoncer. Ce dernier scénario semble dominer indépendamment de la nature de la fondation lorsque des vibrations latérales suffisamment fortes sont appliquées. Nous sommes en mesure d'expliquer le comportement observé par des simulations numériques quasi-2D, qui démontrent également l'influence du rapport d'aspect de l'intrus. La dynamique de la descente verticale est expliquée à l'aide d'une équation de mouvement newtonienne pour l'intrus. Nos résultats peuvent éclairer le comportement des bâtiments et autres constructions humaines pendant les tremblements de terre.

Afin d'avancer dans notre compréhension de la rotation exhibée par les intrus à fond plat, nous étudions une situation qui, bien que n'étant toujours pas quasi-statique, est plus simple que la pénétration dans le milieu granulaire agité. Nous avons donc étudié la pénétration d'un intrus cubique libéré à différents angles d'attaque à l'intérieur d'une cellule de Hele-Shaw quasi-bidimensionnelle. Pendant la pénétration, l'intrus tourne de telle manière que sa position angulaire finale est proche de zéro, c'est-à-dire que sa surface inférieure est parallèle au fond du récipient (cela ressemble à ce qui a été observé pour les intrusions

cylindriques (sans anneau) s'enfonçant dans le lit granulaire agité : après chaque demi-oscillation de la cellule, elles corrigeaient leur inclinaison). Des situations similaires ont été observées pour différents angles initiaux de l'intrus, sauf pour 45 degrés, où, en moyenne, la position angulaire est restée stable. Nous proposons un modèle phénoménologique basé sur la théorie de la force résistive (RFT) pour décrire la dynamique de sa pénétration et de sa rotation dans des conditions non-quasi-statiques. La RFT est inspirée d'un ensemble de règles liées à la nage des micro-organismes à faible nombre de Reynolds et constitue une approximation forte pour les milieux granulaires qui a été utilisée principalement dans les pénétrations quasi-statiques. Elle stipule que la force de traînée contre le mouvement de l'intrus est assez bien représentée par un simple principe de superposition et suppose que la friction du flux tangentiel granulaire contre la surface de l'intrus contribue de manière négligeable à la force de traînée. Nous avons constaté que le RFT parvient à décrire quantitativement les mouvements de basculement et d'enfoncement, bien qu'avec quelques divergences ponctuelles.

La deuxième partie de la thèse comprend une autre forme de la matière fluidisée : les écoulements granulaires. La plupart des écoulements granulaires rencontrés dans la nature (dunes de sable, glissements de terrain, avalanches de roches, écoulements pyroclastiques), et dans l'industrie, se situent dans le régime liquide, où la matière est dense mais s'écoule toujours comme un fluide. Ce régime a fait l'objet de peu d'attention de la part de la communauté scientifique dans la recherche de lois constitutives capables de reproduire la diversité des comportements observés. Cependant, un comportement en particulier a été peu étudié : la transition des écoulements continus aux écoulements intermittents (CIT). Si un matériau granulaire est versé par le haut sur une surface horizontale entre deux plaques parallèles et verticales, un tas de sable croît dans le temps. Pour les petits tas, les grains s'écoulent doucement vers le bas, mais à partir d'une taille de tas critique X_c, l'écoulement devient intermittent : des avalanches soudaines glissent vers le bas de l'apex vers la base, suivies d'un "front ascendant" qui remonte lentement, jusqu'à ce qu'une nouvelle avalanche descendante interrompe le processus. Au moyen d'expériences contrôlant la distance entre l'apex du tas de sable et le conteneur qui l'alimente par le haut, nous montrons que X_c croît linéairement avec le flux d'entrée, mais s'échelonne comme la racine carrée de la hauteur d'alimentation. Nous expliquons ces faits sur la base d'un modèle phénoménologique, et démontrons que nos expériences contrôlées permettent de prédire la valeur de X_c pour la situation courante dans laquelle la hauteur d'alimentation diminue lorsque la pile augmente en taille. Nous discutons également brièvement de la transition d'une situation comme la nôtre (une pile qui croît dans le temps) à l'une des situations les plus courantes et les plus documentées dans la littérature : la pile stationnaire. De plus, nous identifions que le modèle proposé explique le changement observé

dans la forme de la couche de fluide, qui passe d'une forme cunéiforme à une couche dont l'épaisseur est constante le long de la surface.

Enfin, nous montrons les premières étapes de l'étude par photogrammétrie d'une dune de sable sur une des plages de l'est de Cuba. Cette partie aborde certains des progrès de la photogrammétrie qui ont facilité la reconstruction de modèles tridimensionnels à partir d'images numériques. Elle commente également les facteurs qui affectent la qualité de la reconstruction, en soulignant la nécessité d'utiliser des points de contrôle et de géoréférencer les modèles. D'autre part, des estimations de la quantité de matériel érodé entre deux points dans le temps où les données ont été acquises sont présentées.

Table of contents

Introduction

Granular matter constitutes the most abundant form of matter on Earth: there are nearly as many grains of sand in our planet as there are stars in the universe –or at least that's what is believed. This state of matter composed of many parts has been deeply linked to the history of science to which its grains have served as a source of inspiration in many theories developed since classical Greece. On the other hand, grains have been part of the daily life of humankind since immemorial times –and our surroundings indicate that they will continue to be. As a result, it is estimated that in the interaction with these materials in their various forms (processing, storage and transportation) our species consumes approximately 10% of the energy produced on the planet. Unfortunately, due to their abundance, these materials are also associated with many of the catastrophic phenomena that often occur in nature and can cause considerable material and human damage.

Therefore, advances in the knowledge and understanding of the properties and phenomena that take place in granular matter will have a relevant impact in different fields of great value, ranging from industry to survival. In the following, a general introduction to the fundamental properties of granular matter will be presented.

Granular matter

In a simple and fairly comprehensive way, granular media can be described as assemblies of rigid and dissipative macroscopic particles whose shapes and materials

can be, and usually are, very varied. The diameter of the particles constituting them must be sufficiently large, usually greater than 100 μm, to consider them in a gravity-dominant regime rather than in a thermodynamic one, i.e., to reduce the interactions between them mainly to collision and friction [1, 2]. For particles of diameter between 1 μm and 100 μm, which constitute the domain of powders, other interactions such as van der Waals forces, humidity and air drag start to play an important role as well. And for those even smaller particles (colloids), with diameters of less than 1 μm, thermal agitation is no longer negligible [1]. Another important aspect is that, although their constituent particles are solid, granular matter can behave like solid, liquid or gas (it can even be found simultaneously in these three states, as it's the case for a pile of sand). To explain and find constitutive laws capable of reproducing the diversity of observed behaviors, fluid (hydrodynamics) and elastic mechanics have been employed.

In this dissertation the use of the term "granular materials" refers to dry granular materials, i.e., those whose interstitial space is occupied by a gas (air). When the interstitial fluid is a liquid these are commonly called "wet granular media" (or "suspensions") and their behaviors are usually quite different.

Impact of intruders into granular matter

Interest in the impact of objects in granular media probably dates back to the time when Galileo Galilei observed the Moon and wondered about the origin of its roughness. A significant amount of time has passed since then, however, much remains to be understood and developed about the fundamental concepts of impact physics. In this section a set of relevant concepts and results in the field of impact physics on granular beds are discussed with a general scientific background in order to favor the understanding of this thesis. These will concentrate only on one of the stages of impact dynamics: the penetration, leaving out the impact and collapse stages. A fairly large body of work has built up over the last years on these stages [2–8].

Although the physics of high and low velocity impacts may share certain aspects of cratering formation, they differ significantly in many others. Here, only the latter types of impacts are considered since the penetration stage dominates the

drag force dynamics at low velocities. These tend to be simpler since only the movement of the grains is important, as the stress generated by the impact is not capable of destroying them. In addition, if the target granular bed can be regarded as a continuum[1](which is usually the case), the comparison with conventional fluids can be carried out.

Many groups of researchers have been interested in deciphering the characteristics of the penetration into granular matter and several dependencies of granular drag force have been proposed on the basis of experimental results. One relevant case, was the study carried out by Lohse *et al.* in a light granular medium. An object consisted on a ping pong ball was released with zero initial velocity ($v_0 = 0$) onto the surface of a medium to which air was flowed through weakening its force chain structure (dry quicksand[2]). They found experimentally that the final penetration depth d, which is a key quantity when analyzing the granular drag force, depended linearly on the intruder mass ($d \propto m$) [9]. To explain this result they developed a simple force model assuming a Coulomb drag that increases linearly with depth $F_D = -kz$, with k constant. Others studies also found dependencies of F_D with the velocity, the intruder depth, etc.

In a rather controversial context, where many of the proposed models presented the granular drag force as the product of the powers of projectile depth and velocity [10]; linear in velocity [11]; constant, proportional to the initial impact velocity [12]; and proportional to depth [9]. Katsuragi *et al.* proposed a combination of inertial and frictional drags [13] representing the fluid-like and solid-like behaviors of granular matter, respectively.

Unified Drag Force Model

The equation of motion of an impacting sphere was written according to Newton's second law as follows:

$$m\frac{d^2z}{dt^2} = mg - \frac{m}{d}v^2 - kz \tag{1}$$

[1]If the large and rigid impactor case is considered $D_i/D_g >> 1$ (D_i is the diameter of the intruder and D_g of the grains)

[2]not to be confused with normal quicksand, which is a mixture of sand, clay and water

where d is a characteristic length scale.

This expression corresponds to a modified version of the Poncelet drag model ($\beta_d = 0$, $\alpha_d\gamma_d \neq 0$, see Eq. 2) for conventional fluids where the drag force equation can contain constant, inertial, and viscous terms and its general form can be written as:

$$m\frac{d^2z}{dt^2} = -\alpha_d v^2 - \beta_d v - \gamma_d \tag{2}$$

where α_d, β_d, and γ_d are parameters characterizing inertial, viscous, and constant (static) drag forces, respectively.

Although there are limits to the applicability of this law for cases where the impact is shallow (d and k are not constant) [14] and the solution of Eq. (1) tends to overestimate the penetration depth, there is very good agreement with the experimental results [13].

In Eq. (1), the term associated with viscous drag (linear with velocity) does not appear. In conventional fluids, the viscous effect dominates the drag force in the low Reynolds number (Re) regime, at low velocities. However, in granular matter this effect is relevant for penetrations at relatively high velocities as shown in studies by Goldman [15] and by de Bruyn [11]. In fact, according to Bagnold's scaling [16], the granular viscosity is proportional to the shear rate and, as in impact phenomena the main source of the shear rate is the penetration velocity v, the viscosity is proportional to v. This results in a viscous drag force proportional to v^2, similar to inertial drag, so the viscous and inertial drag forces could not be distinguished in granular impact.

During the first moments of impact, the inertial term of Eq. (1) dominates the drag force due to the momentum transfer from the intruder to the medium (the inertial term is usually associated with momentum transfer). As the intruder penetrates, its velocity decreases considerably and the frictional term becomes relevant during the late and deep stages. At this point, one would expect a shear component to the frictional term since friction usually acts tangentially at the interface. However, Brzinski *et al.* demonstrated experimentally that the frictional drag acts normal to the impactor surface [17]. The origin of this normal frictional drag is supposed to be related to the force chains scattered through the medium.

To appreciate the equation proposed by Katsuragi, the medium must be understood as a sort of continuum, but granular matter is inherently discrete, so Eq. (1) can only describe average behaviors. In fact, quite a few interesting features of granular penetration have been observed from direct measurement of the resistive force that cannot be explained by it. Goldman and Umbanhowar, for example, made measurements using an accelerometer and they found large fluctuations in acceleration that are also strongly dependent on the shape of the impactor [15]. According to Daniels *et al.* these fluctuations may be caused by the intermittency of the network of force chains generated by the intruder moving through the medium [18].

Clark *et al.* were able to study these fluctuations in the drag force [19]. To do this, they used particles made of a photoelastic material that allowed them to observe the force chains and found that its propagation occurred very intermittently. Furthermore, they found a clear correlation between the drag force fluctuation with the force chain propagation which indicates that the drag force fluctuation is intrinsic for the granular impact.

Despite its wide acceptance and use, the physical origins of this model (Eq. (1)), as well as the functional forms, are still under discussion. Recently Kang *et al.* modelled the resistance force to the quasi-static penetration and derived a linear relation between F_z and z, by considering only resistance forces normal to the intruder's surface [20]. They established that the force follows a modified Archimedes' law, with the resistance proportional to the intruding volume, and found that k (in Eq. (1)) depends only on the internal friction angle ϕ of the granular medium. Finally, they connected the initial transient nonlinear part of the force-depth relation with the development of a stagnant zone (SZ) ahead of the solid intruder (see Fig. 1). These results were later numerically confirmed, and visualized, by Feng *et al.* [21] who additionally investigated in detail the dynamics of SZ formation and growth and the dependence of this process on the properties of the medium.

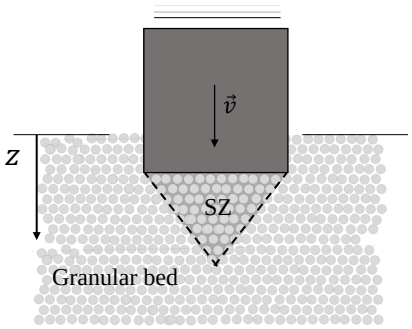

Figure 1: Stagnant zone (SZ). The system includes the intruder and a conical SZ ahead of it

Wall interactions

Aforementioned works have not taken into account other complex effects that sometimes play a crucial role in the dynamics of granular materials, as the finite container-size effects. Container walls are expected to modify the penetration dynamics, as it is usually the case for conventional fluids. Some works related to these influences have shown that the effects of a bottom wall, or a unilateral side wall, are not very significant if the intruder is far from them [22, 23]. In the case of the bottom wall, studies show that it is not relevant except when the intruders are a few millimeters away from it. For side walls, it has been observed that the impactor experiences a repulsion from them, decreasing its penetration depth as an oblique trajectory is produced [22]. In this case it was also found that the repulsion with respect to the wall depended on the initial separation and the size of the intruder, and its cause is associated with the loading of the force chains between it and the wall.

Dense granular flows

Most granular flows encountered in nature and industry are located in a "liquid" regime in which particles remain tightly packed and interact by both collision and long-lasting contacts (friction) through a continuously evolving network of contacts and forces [1]. From a phenomenological point of view, the granular

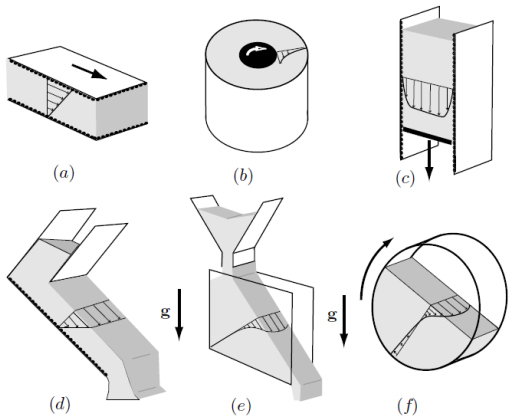

Figure 2: Configurations used to study dense granular flows: (a) plane shear, (b) the Couette cell, (c) a vertical silo, (d) an inclined plane, (e) heap flows and (f) a rotating drum. Image taken from [1].

medium flows like a liquid and, since flowing granular matter is capable of inducing various pattern formations similar to conventional fluids [24–31], the dynamics of granular flow are usually compared to fluid mechanics. In fact, the existence of steady uniform flows for wide ranges of flow thickness and inclinations makes the stresses in the medium to be shear-rate dependent as in conventional viscous fluids [1]. However, a non-negligible difference appears when, for example, a flow on an inclined plane surface stops for angles of inclination below a critical value [1].

During the last three decades or so there have been many studies on dense granular flows and much progress achieved in the understanding of this state of the granular matter. A significant part of the research has been concentrated on a set of configurations (see Fig. 2): flows confined between walls, such as in shear cells and silos; and free surface flows, such as flows down inclined planes, flows on a pile and rotating drum flows [32–34]. However, this section is focused on free surfaces flows, specifically on those over a static pile, in the so-called “granular heaps”.

A free surface flow on a pile is obtained when grains are poured at the top of a pile as sketched in figure 2(e). Unlike inclined planes, where the thickness of the flow over the surface and the inclination are fixed in experiments, in heaps, these parameters are chosen by the system itself and the mass rate of grains poured con-

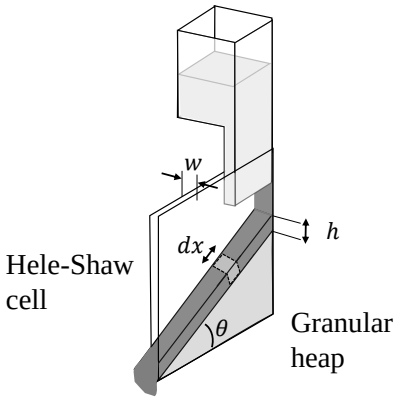

Figure 3: Sketch of an elementary slice of material.

stitutes the control parameter. Surface flows on heaps have been usually studied bounded between two vertical walls (Hele-Shaw cells) since in conical ones complex behaviors can appear making their modeling more complicated [35–37]. In particular, stationary flows are studied in piles whose bottom base has a constant length equal to the length of the cell, which can be open or closed, and which are usually modeled assuming a constant volume fraction uniform flow [38, 39]. For that, a slice of material of density ρ, length dx and height h, is considered between two smooth walls separated by a distance w, flowing over a static heap forming an angle θ with the horizontal direction (Fig. 3). Its balance of forces can be written as:

$$0 = \rho g h \sin\theta w dx - \mu(I(z))\rho g h \cos\theta w dx - \mu_w \rho g h^2 \cos\theta dx \tag{3}$$

The first term in Eq. (3) is the force due to gravity while the second is the tangential force that develops on the bottom face of the element due to the shear inside the material. $\mu(I(z))$ is a friction coefficient that depends on the inertial number $I = \dot{\gamma} d/\sqrt{P/\rho_p}$ [40]. The last term corresponds to the lateral friction forces due to the side walls. For smooth walls it is assumed that particles slip against the side walls and the induced stress is written as a pure solid friction with a constant coefficient of friction μ_w.

$$\tan\theta - \mu_w \frac{h}{w} = \mu(I(z)) \tag{4}$$

Eq. (4) can be used to explain the localization of the flow at the surface of the pile and the selection of the flow thickness [39, 41]. As h increases deeper in the pile, the second term of (4) increases. Consequently, the internal friction $\mu(I(z))$ must decrease to maintain equilibrium. However, it can only decrease to a finite critical value μ_1 when the value of I reaches zero[3], i.e. when the material is not sheared. The above implies that there exists a critical size h_{stop} for which the force of gravity, screened by lateral friction with the walls is not able to induce shear in the medium. The expression for the thickness is as follows:

$$h_{stop} = w\frac{\tan\theta - \mu_1}{\mu_w} \tag{5}$$

This configuration can be modeled using a viscoplastic description, by taking into account the lateral boundary conditions [42]. However, although the model is capable of making qualitative and quantitative predictions for the free surface velocity, it is not perfect. There are some experimental observations that are not well captured, as the transition from a continuous flow regime to an avalanche regime, that occurs when the flow rate Q decreases [42, 43].

Goals and organization of the thesis

Overall, this thesis aims at describing different phenomena not completely understood in granular media. Firstly, it focuses on the rotation described by intruders of different shapes when sinking in dry granular media under certain conditions. Secondly, it studies the transition from continuous to intermittent flow that occurs in surfaces flows for granular piles in a configuration with greater practical value than a stationary pile: a growing pile. The last goal is studying a methodology to characterize erosion of sand dunes in Cuban beaches for future phenomenological analysis.

The manuscript is composed of different research articles, some of them already published, whereas the others are in the process of scientific publication or are pending a first submission. It is organized in 5 chapters as follows: the first

[3]Small values of I ($I \to 0$) correspond to a quasi-static regime while large values of I ($I \gtrsim 1$) correspond to the rapid and dilute flow regime. The dense-flow regime lies in between

part (Chapters 1 to 3) concentrates on the penetration of intruders in granular media with particular attention to the rotation described during subsidence. It starts (Chapter 1) with the study of the influence of a vertical wall on the dynamics of a cylindrical intruder released at different separations from it in a light granular medium. Then, Chapter 2 discusses the influence of foundations on the subsidence of intruders initially resting on a granular bed that is shaken at different accelerations simulating an earthquake. Chapter 3 describes the dynamics of a square prism that is dropped at different initial angular orientations with special attention to its stability and its orientation at the end of the subsidence. The second part of the thesis is devoted to dense granular flows. Chapter 4 presents a study of the transition from continuous to intermittent flow that occurs in a growing granular pile in which the dependence of the size of its bottom base, for which the transition occurs, is obtained as a function of the control parameters of the experiment (the inflow of grains and the height of deposition). Finally, Chapter 5 describes the obtaining of digital elevation models of an actual sand dune in a Cuban beach for the subsequent study of its erosion over a period of time.

Bibliography of the current chapter

[1] B. Andreotti, Y. Forterre, and O. Pouliquen. *Granular media: between fluid and solid*. Cambridge University Press, 2013.

[2] H. Katsuragi. *Physics of Soft Impact and Cratering*. Springer Tokyo, 2016.

[3] JC Ruiz-Suárez. "Penetration of projectiles into granular targets". In: *Rep. Prog. Phys.* 76.6 (2013), p. 066601.

[4] G. Sánchez-Colina et al. "Note: "Lock-in accelerometry" to follow sink dynamics in shaken granular matter". In: *Review of Scientific Instruments* 85.12 (2014), p. 126101.

[5] E. Altshuler et al. "Settling into dry granular media in different gravities". In: *Geophysical Research Letters* 41.9 (2014), pp. 3032–3037.

[6] H. Askari and K. Kamrin. "Intrusion rheology in grains and other flowable materials". In: *Nature Mater* 15 (2016), pp. 1274–1279.

[7] Hu Zheng et al. "Intruder friction effects on granular impact dynamics". In: *Phys. Rev. E* 98 (3 2018), p. 032904.

[8] M. Espinosa et al. “Intruders cooperatively interact with a wall into granular matter”. In: *Granular Matter* 24.39 (2022), p. 2.

[9] D. Lohse et al. “Creating a dry variety of quicksand”. In: *Nature* 432 (7018 2004), p. 689.

[10] J. S. Uehara et al. “Low-Speed Impact Craters in Loose Granular Media”. In: *Phys. Rev. Lett.* 90 (19 2003), p. 194301.

[11] J. R. de Bruyn and A. M. Walsh. “Penetration of spheres into loose granular media”. In: *Canadian Journal of Physics* 82.6 (2004), pp. 439–446.

[12] M. Pica Ciamarra et al. “Dynamics of Drag and Force Distributions for Projectile Impact in a Granular Medium”. In: *Phys. Rev. Lett.* 92 (19 2004), p. 194301.

[13] H. Katsuragi and D. J. Durian. “Unified force law for granular impact cratering”. In: *Nature physics* 3.6 (2007), pp. 420–423.

[14] H. Katsuragi and D. J. Durian. “Drag force scaling for penetration into granular media”. In: *Phys. Rev. E* 87 (5 2013), p. 052208.

[15] D. I. Goldman and P. Umbanhowar. “Scaling and dynamics of sphere and disk impact into granular media”. In: *Phys. Rev. E* 77 (2 2008), p. 021308.

[16] R. A. Bagnold. “Experiments on a gravity-free dispersion of large solid spheres in a Newtonian fluid under shear”. In: *Proceedings of the Royal Society of London. Series A. Mathematical and Physical Sciences* 225.1160 (1954), pp. 49–63.

[17] T. A. Brzinski, P. Mayor, and D. J. Durian. “Depth-Dependent Resistance of Granular Media to Vertical Penetration”. In: *Phys. Rev. Lett.* 111 (16 2013), p. 168002.

[18] K. E. Daniels, J. E. Coppock, and R. P. Behringer. “Dynamics of meteor impacts”. In: *Chaos: An Interdisciplinary Journal of Nonlinear Science* 14.4 (2004), S4–S4.

[19] A. H. Clark and R. P. Behringer. “Granular impact model as an energy-depth relation”. In: *EPL (Europhysics Letters)* 101.6 (2013), p. 64001.

[20] Wenting Kang et al. “Archimedes’ law explains penetration of solids into granular media”. In: *Nature communications* 9.1 (2018), pp. 1–9.

[21] Yajie Feng, Raphael Blumenfeld, and Caishan Liu. “Support of modified Archimedes’ law theory in granular media”. In: *Soft Matter* 15 (14 2019), pp. 3008–3017.

[22] E. L. Nelson et al. “Projectile Interactions in Granular Impact Cratering”. In: *Phys. Rev. Lett.* 101 (6 2008), p. 068001.

[23] A. Seguin, Y. Bertho, and P. Gondret. "Influence of confinement on granular penetration by impact". In: *Phys. Rev. E* 78 (1 2008), p. 010301.

[24] F. Melo, P. B. Umbanhowar, and H. L. Swinney. "Hexagons, Kinks, and Disorder in Oscillated Granular Layers". In: *Phys. Rev. Lett.* 75 (21 1995), pp. 3838–3841.

[25] P. B. Umbanhowar, F. Melo, and H. L. Swinney. "Localized excitations in a vertically vibrated granular layer". In: *Nature* 382 (6594 1996), p. 793.

[26] D. J. Goldfarb, B. J. Glasser, and T. Shinbrot. "Shear instabilities in granular flows". In: *Nature* 415 (6869 2002), p. 302.

[27] S. L. Conway, T. Shinbrot, and B. J. Glasser. "A Taylor vortex analogy in granular flows". In: *Nature* 431 (7007 2004), p. 433.

[28] J. L. Vinningland et al. "Granular Rayleigh-Taylor Instability: Experiments and Simulations". In: *Phys. Rev. Lett.* 99 (4 2007), p. 048001.

[29] X. Cheng et al. "Towards the zero-surface-tension limit in granular fingering instability". In: *Nature Physics* 4 (3 2008), p. 234.

[30] J. R. Royer et al. "High-speed tracking of rupture and clustering in freely falling granular streams". In: *Nature* 459 (7250 2009), p. 1110.

[31] G. Prado, Y. Amarouchene, and H. Kellay. "Experimental Evidence of a Rayleigh-Plateau Instability in Free Falling Granular Jets". In: *Phys. Rev. Lett.* 106 (19 2011), p. 198001.

[32] GDR Midi. "On dense granular flows". In: *The European Physical Journal E* 14 (4 2004), p. 341.

[33] O. Pouliquen et al. "Flow of dense granular material: towards simple constitutive laws". In: *Journal of Statistical Mechanics: Theory and Experiment* 2006.07 (2006), P07020–P07020.

[34] Y. Forterre and O. Pouliquen. "Flows of Dense Granular Media". In: *Annu. Rev. Fluid Mech.* 40.1 (2008), pp. 1–24.

[35] N. Thomas. "Reverse and intermediate segregation of large beads in dry granular media". In: *Phys. Rev. E* 62 (1 2000), pp. 961–974.

[36] Ernesto Altshuler et al. "Sandpile formation by revolving rivers". In: *Phys. Rev. Lett.* 91.1 (2003), p. 014501.

[37] E. Altshuler et al. "Revolving rivers in sandpiles: From continuous to intermittent flows". In: *Phys. Rev. E* 77 (3 2008), p. 031305.

[38] D. V. Khakhar et al. "Surface flow of granular materials: model and experiments in heap formation". In: *J. of Fluid Mechanics* 441 (2001), pp. 255–264.

[39] P. Jop, Y. Forterre, and O. Pouliquen. "Crucial role of sidewalls in granular surface flows: consequences for the rheology". In: *J. of Fluid Mech.* 541 (2005), p. 167.

[40] Frédéric da Cruz et al. "Rheophysics of dense granular materials: Discrete simulation of plane shear flows". In: *Phys. Rev. E* 72 (2 2005), p. 021309.

[41] Nicolas Taberlet et al. "Superstable Granular Heap in a Thin Channel". In: *Phys. Rev. Lett.* 91 (26 2003), p. 264301.

[42] P. Jop, Y. Forterre, and O. Pouliquen. "A constitutive law for dense granular flows". In: *Nature* 441 (7094 2006), p. 727.

[43] P.-A. Lemieux and D. J. Durian. "From Avalanches to Fluid Flow: A Continuous Picture of Grain Dynamics Down a Heap". In: *Phys. Rev. Lett.* 85 (20 2000), pp. 4273–4276.

CHAPTER 1

Rolling away from the wall into granular matter

Published

V. Diaz-Melian et al. Physical Review Letter ***125****, 078002, 2020.*

doi: https://doi.org/10.1103/PhysRevLett.125.078002

Résumé (French abstract)

La sédimentation d'objets solides dans la matière granulaire près des frontières est un domaine de recherche presque vierge. Nous décrivons ici en détail la dynamique de pénétration d'un objet cylindrique dans un milieu granulaire quasi-2D. En suivant la trajectoire du cylindre lors de sa pénétration dans le lit granulaire, nous caractérisons deux types de mouvement distincts: son centre de masse s'éloigne horizontalement de la paroi latérale, et il tourne autour de son axe de symétrie. Alors que la répulsion est causée par la charge des chaînes de force entre l'intrus et la paroi, la rotation peut être associée aux forces de friction entre les grains et l'intrus. Enfin, nous montrons les analogies entre la sédimentation de deux intrus jumeaux libérés loin de toute frontière, et celle d'un intrus libéré près d'une paroi verticale.

Rolling away from the Wall into Granular Matter

V. L. Díaz-Melián, A. Serrano-Muñoz, M. Espinosa,
L. Alonso-Llanes, G. Viera-López, and E. Altshuler*
Group of Complex Systems and Statistical Physics,
Physics Faculty, University of Havana, 10400 Havana, Cuba

The sedimentation of solid objects into granular matter near boundaries is an almost virgin field of research. Here we describe in detail the penetration dynamics of a cylindrical object into a quasi-2D granular medium. By tracking the trajectory of the cylinder as it penetrates the granular bed, we characterize two distinct kinds of motion: its center of mass moves horizontally away from the lateral wall, and it rotates around its symmetry axis. While the repulsion is caused by the loading of force chains between the intruder and the wall, the rotation can be associated with the frictional forces between the grains and the intruder. Finally, we show the analogies between the sedimentation of twin intruders released far from any boundaries, and that of one intruder released near a vertical wall.

Fluid and solid-like behaviors tend to coexist in the granular state of matter. For example, the penetration of a solid intruder released into a wide granular bed may be quite smooth for the first part of its trajectory, but eventually becomes fluctuating, until the object completely stops at a certain depth inside the material. The first part of the motion may resemble the penetration of a sphere into a viscous fluid, but then the medium experiences a transition to the *jammed state* [1–5], which distinguishes the process from any expectable behaviour of a liquid. Real life scenarios such as balls mills [6] and excavations near walls [7] involve complex phenomena whose handling would benefit from a better understanding of how intruders penetrate near boundaries in granular matter.

However, in spite of the substantial research efforts devoted to understand the impact and penetration of low-velocity projectiles into granular beds [8–19], intruder-wall interactions have rarely been documented in the literature. A few authors have studied the effect of confinement in cylindrical containers where the intruder penetrates at the center. That is the case of Seguin *et al.* in 2008, who concludes that the final penetration depth of a sphere increases with the radius of the container, and that the effects of the walls decay within a distance of the order of the sphere's diameter [20]. In 2010, von Kann *et al.* studied the effect of the container radius on the shape and strength of sand jets occurring in loosely packed sand [21]. Katsuragi reported the quasistatic penetration of a spherical intruder into a cylindrical granular column, and found scaling laws relating the drag force and the wall pressures [22]. To our knowledge, the effect of a single vertical wall on the motion of an intruder has been studied only once: In 2008, Nelson *et al.* reported the horizontal repulsion of the intruder away from the wall by recording its landing position [12].

Here, we perform systematic penetration experiments of a cylindrical intruder into a quasi-2D granular medium, which reveal its detailed motion after being released at the free granular surface near a vertical wall. We observe two distinct phenomena during the sedimentation process: the intruder separates from the wall in the horizontal direction, and rotates around its symmetry axis. Further experiments suggest that the repulsion and rotation of one intruder released near a vertical wall is equivalent to substituting the wall by a second intruder released side by side with the original one.

Millimetric-sized expanded polystyrene spheres where deposited into a Hele-Shaw cell, as shown in Fig. 1(a). Cylindrical intruders were released from the surface of the granular bed, starting at different horizontal distances from the left (or right) wall of the cell by means of an electromagnetic device that minimized spurious vibrations

* ealtshuler@fisica.uh.cu

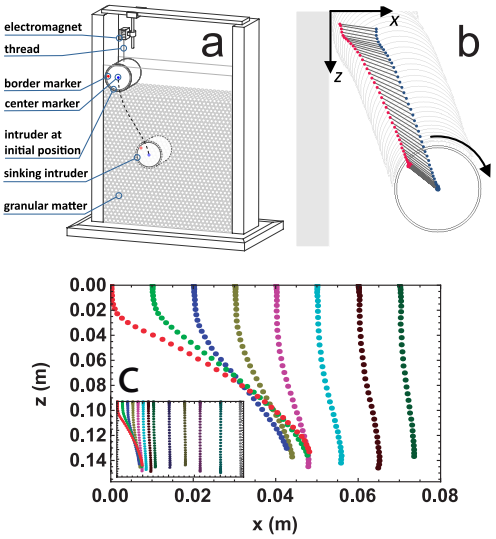

FIG. 1. Rolling away from the wall. (a) Cylinders are released into a Hele-Shaw cell at different initial distances x_0 from the left wall (the cylinder path is sketched for $x_0 = 0$). (b) Tracking of center (blue) and border (red) markers. The curved arrow indicates the rotation of the intruder in the clockwise direction. (c) From left to right: trajectories of an intruder released at $x_0 = 0$, 1, 2, 3, 4, 5, 6, and 7 cm, respectively (the inset includes $x_0 = 10$, 13, 16, 20, and 23.75 cm). Intruder mass and diameter were 0.255 kg and 7.5 cm, respectively. All trajectories were averaged over 10 measurements.

and torques on the intruder when released. The penetration process was followed using a digital camera that took videos through one of the large faces of the cell. Two colored dots situated at the center and near the border of one circular face of the cylinder [Fig. 1(b)] served as reference points for image analysis. Using them, the motion of the intruder's center of mass and its angle of rotation could be measured. Supplemental Material provided with this work explains in depth the experimental details. Some sample videos of three different experimental configuration are included.

Figure 1(c) shows the trajectories of the intruder after being released at different initial distances from the wall, x_0 (notice that the distance from the vertical wall has been plotted as the position of the left edge of the intruder relative to the boundary). Our results not only confirm that the intruder is laterally repelled by the wall (as suggested in [12], based on the final position of the object), but also reveal the details of the whole penetration process. For all values of x_0, the first stage of the penetration consists of an almost purely vertical plunge, after which the lateral motion away from the wall takes place. When the intruder is released relatively near the wall, the repulsion is smaller as the initial position of the cylinder, x_0 is larger. However, for even larger values of x_0 the sinking can be almost vertical, so the effect of the wall is no longer felt. Figure 1(c) also suggests that the final penetration depth does not depend substantially on x_0.

Figure 2(a) reports the time evolution of the net horizontal position of the intruder, confirming that it increases as x_0 decreases. The inset shows another interesting feature of the penetration process: the maximum lateral displacement from the wall is almost constant for small values of x_0, and then grows linearly starting approximately at $x_0 = 5$ cm. That behavior suggests that the interaction between the wall and the intruder decays significantly when the intruder is away from the wall a distance approximately equals to $l = 5$ cm. We will discuss the physical meaning of this value later on.

Figure 2(b) quantifies an entirely novel phenomenon: as the intruder moves away from the wall, it rotates around its symmetry axis. The graph shows that, if x_0 is small enough (i.e., 0 and 1 cm), the rotation is relatively large and clockwise, while it is smaller and counter-clockwise for $2\,\text{cm} < x_0 \leq 7\,\text{cm}$. After $x_0 \simeq 10$ cm, the rotation is negligible, as clearly shown in the inset, strongly suggesting that the repulsion and rotation effects are correlated. In the rest of the document, and also in the Supplemental Material, we will avoid using the terms clockwise and counterclockwise, since they depend on the side of the cell from which the intruder is released. Instead, we will call "normal" the rotational motion expected if the intruder was rolling down a solid ramp with friction while moving away from the wall. So, our experiments show that the cylinder describes "normal rotation" for

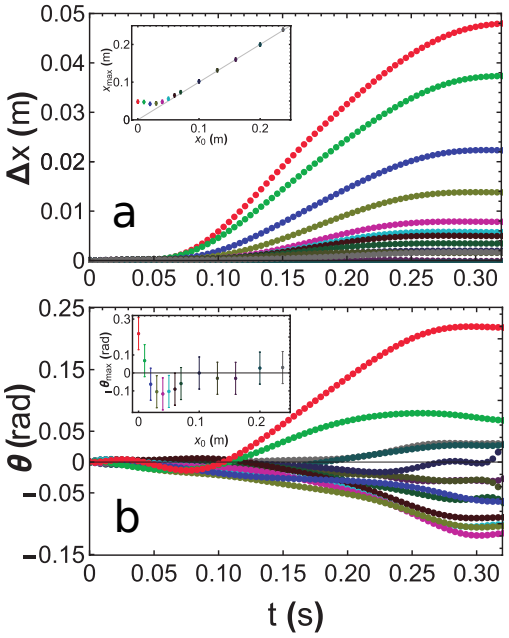

FIG. 2. Details of the horizontal and rotational motion seen in the experiments. (a) Time evolution of the lateral displacements ($\Delta x = x - x_0$) of the intruder for the x_0 values shown in Fig. 1(c). In the inset, the maximum lateral separation from the wall as a function of x_0 is shown (the line follows $x_{\max} = x_0$). (b) Time evolution of the angle rotated by the intruder (relative to its initial value). In the inset, the maximum angle of rotation as a function of x_0 is shown. Each curve in (a) and (b) are averaged over 10 repetitions of each experiment. Points in the insets are also averaged over 10 repetitions (error bars are the corresponding standard deviations). The color scale of both (a) and (b) is consistent with the one shown in Fig. 1.

$x_0 = 0$ and 1 cm, and "anomalous rotation" for 2 cm $< x_0 \leq 7$ cm.

Now, we discuss the physics behind the penetration process, with emphasis in repulsion and rotation phenomena. Figure 3(a) shows a snapshot from 2D discrete element simulations (DEM). It illustrates the presence of force chains underneath the intruder that are involved in the penetration dynamics. It is possible to see stronger force chains between the intruder and the wall than those at the opposite side of the intruder (simulation details can be found in Supplemental Material). It qualitatively confirms the speculation by Nelson *et al.* [12] related to the displacement along the x axis: "the motion of the projectile serves to load force chains between [intruder] and wall, which causes the repulsion".

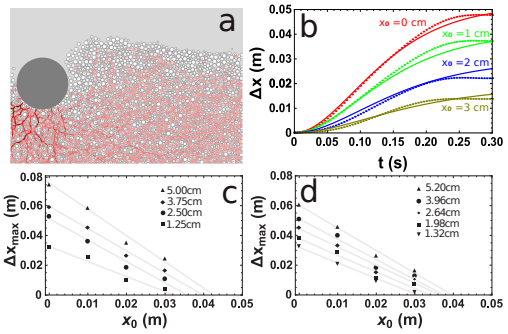

FIG. 3. DEM simulations and modeling of the repulsion. (a) Snapshot from a DEM simulation showing the force chains during the penetration of a disk-shaped intruder near a wall just after being released (darker red indicates bigger forces). (b) Horizontal motion vs. time for $x_0 = 0$: circles and lines represent experiment and the output of Eq. 1, respectively. (c) Maximum horizontal separation vs. x_0 for different cylinder radii: symbols and lines represent DEM simulations and linear fits, respectively. (d) Maximum horizontal separation vs. x_0 for different cell thicknesses: symbols represent DEM simulations.

Let us first try to understand the cause of the horizontal motion by analyzing our experimental data. Careful observation of the videos in slow motion shows that, immediately after the release of the intruder, partially jammed grains located between the cylinder and the vertical boundary "push" the intruder away from the wall. However, a short time afterwards, the grains are fully mobilized around the intruder, and the repulsive force substantially decays (see Supplemental Material for further details). We will assume that the pushing forces acting on the intruder are exerted by force chains of finite length showing an effective elastic behavior. We condense this picture into a simple 2D mechanical model: the intruder is assumed as a disk of radius R where linear springs with equilibrium length l are radially attached to its lower half. We do not consider any torsional effects on the springs,

so their only degree of freedom is associated with compression. If the springs are not touching any cell boundaries, they do not transmit any force from them to the intruder. So, if the intruder's left boundary is away from the vertical wall a distance $x > l$, it will not "feel" the presence of the wall, so the only horizontal force felt by the intruder will be a velocity-dependent drag. A similar analysis allows us to disregard the effect of the bottom wall. Assuming a continuum of finite springs for an intruder near the wall, and including a viscous-like force, we get the following equation of motion for the intruder's center of mass, x_c (see details of the derivation in Supplemental Material):

$$m\ddot{x}_c = k\Big\{[(l+R)^2 - x_c^2]^{1/2} - x_c \cos^{-1}\frac{x_c}{l+R}\Big\} - f(\dot{x}_c) \quad (1)$$

where R is the radius of the cylinder, $l = 5$ cm (see discussion above) and $f(\dot{x}_c) = \alpha\dot{x}_c(1+\beta\dot{x}_c)$, where $\alpha = 6\pi\eta R$ and $\beta = \frac{3}{8}\frac{\rho R}{\eta}$; ρ is taken as the granular density times the packing fraction. The remaining constants k and η were freely changed in the model to reproduce the averaged experimental results for the values of $x_0 = 0, 1, 2, 3$ cm. After fitting the data we obtained $k = 35$ N/m and $\eta = 5.0$ kg m^{-1} s^{-1}.

Notice that in Eq. 1, the first term at the right only holds for $0 \leq x_c \leq l + R$. The continuous lines in Fig. 3(b) show the solutions of Eq. 1 for $x_0 = 0, 1, 2$ and 3 cm (note that $\Delta x = x_c - R - x_0$). As can be seen, the model reproduces quantitatively the experimental curves within root-mean-square errors of 0.0214, 0.0483, 0.0514, and 0.0551 (normalized to the maximum value of each experimental curve) for $x = 0$, 1, 2, and 3 cm, respectively. The best accuracy is achieved especially for small values of x_0, where the repulsion is more evident. All in all, it can be said that the lack of symmetry of the force chains distribution around the intruder, their rapid decay, and a velocity-dependent "granular viscosity", are the key ingredients to explain the repulsion of the intruder by the wall.

Let us briefly discuss the physical meaning of our model parameters. Firstly, we assume that the breaking and building of force chains during the penetration process can be characterized by an elastic constant k which is much smaller than that expectable for grain-grain interactions, or even than that associated to linear chains of grains behaving elastically [23]. In fact, our "elastic interaction" cannot be taken literally, since the true repulsion mechanism is largely associated to irreversible plastic deformations of the granular system.

In our model, the springs have an average length, l. We speculate that it corresponds to the horizontal size of the stress field associated to the intruder (HSFI) [24]. In order to connect l with other lengths involved in our system, we have performed DEM simulations. The symbols in Fig. 3(c) correspond to simulated $\Delta x_{\max}$ vs. x_0 graphs for different diameters of the intruder, where $\Delta x_{\max}$ is the value of $x - x_0$ when the intruder stops. Based on them, we can make a rough estimation of l as the values of x_0 corresponding to $\Delta x_{\max} = 0$. As indicated by the linear fits represented by straight lines, l increases with the intruder's radius, which is consistent with the fact that the HSFI is reported to increase with the horizontal size of the intruder [24]. The symbols in Fig. 3(d) correspond to simulated $\Delta x_{\max}$ vs. x_0 graphs for different thicknesses of the Hele-Shaw cell (or, equivalently, to different heights of the cylindrical intruder). As can be seen, the maximum interaction distance also increases with the cell width within the range of our simulations.

Finally, let us comment on the "viscosity factor" that multiplies the velocity squared in Eq. 1. Its value $\alpha\beta = 0.09$ kg/m fits well our experimental data, but it is approximately 2$\sim$3 times larger than the equivalent parameter used by Pacheco *et al.* [14] to reproduce the vertical penetration of a spherical intruder into a cylindrical silo filled up with the same

kind of granular matter. This fact suggests that the granular viscosity term is not inertial in the hydrodynamic sense: the intruder collides with "grain clusters" defined by force chains [25, 26], so it is indirectly influenced by the specific geometry –and dimensionality– of the experiment.

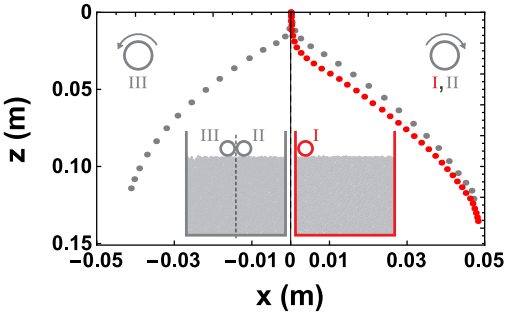

FIG. 4. Intruder-wall vs. intruder-intruder interactions. The red circles correspond to the trajectory of a single intruder released near the left wall ($x_0 = 0\,\mathrm{cm}$) while the gray ones correspond to the case of two intruders released at the center of the Hele-Shaw cell, far from the edges (see lower inset). The upper insets show the rotation direction of the intruders: clockwise for the trajectories at the right, and counter-clockwise for the one at the left. The points are averages over 10 repetitions of each experiment.

Now, we introduce some preliminary ideas to model the "normal" rotation. The comparison between Figs. 2(a) and 2(b) suggests that the normal rotation is caused by the horizontal motion. We also assume that non-zero frictional forces between the surface of the intruder and the surrounding grains are essential to get the rotational effect, which was corroborated by DEM simulations. As the intruder moves laterally with a velocity $\dot{x}(t)$, it experiences tangential frictional forces pointing to the wall that are stronger at the bottom than at the top, due to Janssen's effect (see Supplemental Material). We will assume that those forces are proportional to $(1 - e^{-z/\lambda})$, where λ is a characteristic length of the order of the width of the container [14] (5.3 cm in our case). Then, the difference between the bottom and top horizontal shear forces acting on an intruder whose center of mass is located at (x, z) scales as $F_{\mathrm{bottom}} - F_{\mathrm{top}} \sim \mu_{\mathrm{eff}} e^{-z/\lambda}$ where μ_{eff} is an effective friction that has been found proportional to the penetration velocity of an intruder into a fluidized granular bed [27], $\mu_{\mathrm{eff}} = \xi\dot{x}$. Then, the equation describing the rotational motion of the cylinder can be written as $\ddot{\theta} = k_r \dot{x} \exp(-z/\lambda) - f_\theta \dot{\theta}$ where k_r depends on the properties of the granular medium and the geometry of the experiment, and f_θ is proportional to the frictional torque exerted by the grains on the intruder. Using $k_r = 400\,\mathrm{m^{-1}s^{-1}}$ and $f_\theta = 32\,s^{-1}$ as free parameters, and inserting $x(t)$ taken from the experiments, the above equation of motion reproduces quite well the experimental θ vs. t dependence for $x_0 = 0$ (see Supplemental Material). However, this approach to explain the rotation is not able to reproduce properly the experimental results for $x_0 \geq 1\,\mathrm{cm}$, including the anomalous ones (interestingly, anomalous rotations cannot be reproduced by our DEM simulations, as stated in Supplemental Material). The anomaly may be caused by "quenched" effects, such as the inhomogeneous deposition of grains in the cell (especially near walls) associated to our filling protocol. But it can be also associated to "dynamical" effects, like the inversion of the effective tangential friction due to nontrivial flows of grains around the intruder when it is released farther from the wall –where force chains are less relevant. Such study will be the subject of future research.

We present a final experiment showing the parallelism between the motion of a single intruder released near a vertical wall, and two identical intruders released side by side far from any walls. Two cylinders identical to the one that produced all previous data were released side by side at the center of the Hele-Shaw cell, i.e., far from the lateral walls. As a result, they repel each other, producing two symmetrical trajectories represented by gray dots in Fig. 4 (this fact has been reported by Pacheco-Vázquez and Ruiz-Suárez in a purely 2D system [13], and earlier by Nelson *et al.* [12] by observing the endpoints of the two trajectories). In the same figure we have plotted a single intruder released at $x_0 = 0\,\mathrm{cm}$ from the left wall, represented by red circles. The very good coincidence between the red and right gray trajectories suggests that the evolution

of force chains between the two intruders is quite similar to the ones felt by the intruder at the right if the one at the left is substituted by a flat wall. This non-trivial fact resembles the method of images for electrical charges [28] and flow fields near boundaries in hydrodynamics [29] with recent applications to the case of microbial swimmers [30, 31].

In summary, we have fully characterized the horizontal repulsion of solid intruders when penetrating a quasi-2D granular bed near a wall, after being released on the free granular surface at a distance x_0 from a vertical boundary. Our experiments reveal that the interaction with the wall produces rotation of the intruder around its symmetry axis, which is normal or anomalous for small or large values of x_0, respectively. We are able to reproduce the motion along the x axis by assuming that the force chains associated with jammed grains between the wall and the intruder "push" it away from the wall while it is stopped by granular viscouslike forces. We assume that the non-zero frictional forces between the surface of the intruder and the surrounding grains are essential to get the rotational effect, which was corroborated by DEM simulations. Finally, we suggest that the repulsion and rotation of one intruder released near a vertical wall can be largely reproduced by substituting the wall by a second intruder released side by side with the original one.

We acknowledge D. J. Durian calling our attention to intruder-wall interactions as well as useful discussion with E. Clément, A. García and T. Shinbrot. This research was performed under the institutional project "Granular media: creating tools for the prevention of catastrophes".

[1] Liu, A. J. and Nagel, S. R. *Nature* **396**(6706), 21 (1998).
[2] Keys, A. S., Abate, A. R., Glotzer, S. C., and Durian, D. J. *Nat. Phys.* **3**(4), 260 (2007).
[3] Goodrich, C. P., Liu, A. J., and Sethna, J. P. *Proc. Natl. Acad. Sci. U. S. A.* **113**(35), 9745–9750 (2016).
[4] Jin, Y., Urbani, P., Zamponi, F., and Yoshino, H. *Sci. Adv.* **4**(12), eaat6387 (2018).
[5] Zhao, Y., Barés, J., Zheng, H., Socolar, J. E., and Behringer, R. P. *Phys. Rev. Lett.* **123**, 158001 (2019).
[6] Rajamani, R., Mishra, B., Venugopal, R., and Datta, A. *Powder Technology* **109**(1-3), 105–112 (2000).
[7] Yoo, C. *Journal of geotechnical and geoenvironmental engineering* **127**(3), 225–233 (2001).
[8] Mikkelsen, R., Versluis, M., Koene, E., Bruggert, G.-W., Van Der Meer, D., Van Der Weele, K., and Lohse, D. *Phys. Fluids* **14**(9), S14–S14 (2002).
[9] Uehara, J., Ambroso, M., Ojha, R., and Durian, D. J. *Phys. Rev. Lett.* **90**(19), 194301 (2003).
[10] Katsuragi, H. and Durian, D. J. *Nat. Phys.* **3**(6), 420 (2007).
[11] Goldman, D. I. and Umbanhowar, P. *Phys. Rev. E* **77**(2), 021308 (2008).
[12] Nelson, E., Katsuragi, H., Mayor, P., and Durian, D. J. *Phys. Rev. Lett.* **101**(6), 068001 (2008).
[13] Pacheco-Vázquez, F. and Ruiz-Suárez, J. *Nat. Commun.* **1**, 123 (2010).
[14] Pacheco-Vázquez, F., Caballero-Robledo, G., Solano-Altamirano, J., Altshuler, E., Batista-Leyva, A., and Ruiz-Suárez, J. *Phys. Rev. Lett.* **106**(21), 218001 (2011).
[15] Ruiz-Suárez, J. *Rep. Prog. Phys.* **76**(6), 066601 (2013).
[16] Brzinski III, T. A., Mayor, P., and Durian, D. J. *Phys. Rev. Lett.* **111**(16), 168002 (2013).
[17] Altshuler, E., Torres, H., González-Pita, A., Sánchez-Colina, G., Pérez-Penichet, C., Waitukaitis, S., and Hidalgo, R. *Geophys. Res. Lett.* **41**(9), 3032–3037 (2014).
[18] Sánchez-Colina, G., Alonso-Llanes, L., Martínez, E., Batista-Leyva, A., Clement, C., Fliedner, C., Toussaint, R., and Altshuler, E. *Rev. Sci. Instrum.* **85**(12), 126101 (2014).
[19] Bester, C. S. and Behringer, R. P. *Phys. Rev. E* **95**(3), 032906 (2017).
[20] Seguin, A., Bertho, Y., and Gondret, P. *Phys. Rev. E* **78**(1), 010301 (2008).
[21] von Kann, S., Joubaud, S., Caballero-Robledo, G. A., Lohse, D., and van der Meer, D. *Physical Review E* **81**(4), 041306 (2010).
[22] Katsuragi, H. *Phys. Rev. E* **85**(2), 021301

(2012).
[23] Andreotti, B., Forterre, Y., and Pouliquen, O. *Granular media: between fluid and solid*. Cambridge University Press, (2013).
[24] Kang, W., Feng, Y., Liu, C., and Blumenfeld, R. *Nature Communications* **9**, 1101 (2018).
[25] Takehara, Y., Fujimoto, S., and Okumura. *Europhys. Lett.* **89**, 012201 (2014).
[26] Clark, A. H., Petersen, A. J., and Behringer, R. P. *Phys. Rev. E* **92**(1), 44003 (2010).
[27] Harich, R., Darnige, T., Kolb, E., and Clément, E. *Europhys. Lett.* **96**(5), 54003 (2011).
[28] Jackson, J. D. *Classical electrodynamics*. AAPT, (1999).
[29] Blake, J. In *Math. Proc. Camb. Philos. Soc.*, volume 70, 303–310. Cambridge University Press, (1971).
[30] Lauga, E. and Powers, T. R. *Rep. Prog. Phys.* **72**(9), 096601 (2009).
[31] Altshuler, E., Miño, G., Pérez-Penichet, C., del Río, L., Lindner, A., Rousselet, A., and Clément, E. *Soft Matter* **9**(6), 1864–1870 (2013).

Supplemental Material for *Rolling away from the wall into granular matter*

V. L. Díaz-Melián, A. Serrano-Muñoz, M. Espinosa,
L. Alonso-Llanes, G. Viera-López, and E. Altshuler*
Group of Complex Systems and Statistical Physics,
Physics Faculty, University of Havana, 10400 Havana, Cuba

I. EXPERIMENTAL DETAILS

Expanded polystyrene spherical particles of density $14\pm 2\,\mathrm{kg/m^3}$ and diameter distributed between 2.0 and 6.5 mm, peaking at 5.8 mm were deposited into a Hele-Shaw cell of width 47.5 cm, height 48 cm and thickness 5.3 cm. The cell consisted in a three-piece aluminum frame and two glass plates. Cylindrical objects of height 5.2 cm and diameter 7.5 cm were used as intruders. The cylinders could be released from the surface of the granular bed, starting at different horizontal distances from the left (or right) wall of the cell by means of an electromagnetic device that minimized spurious vibrations and torques on the intruder when released. The penetration process was followed using a GoPro camera with a resolution of 720×1280 pixels, at 120 frames per second, that took videos through one of the glass faces.

Two colored dots situated at the center and near the border of one circular face of the cylinder served as reference points for image analysis. Using them, the motion of the intruder's center of mass could be tracked within an uncertainty of 0.16 mm, and the angle of rotation of the intruder around its symmetry axis could be measured within an uncertainty of 0.005 rad. For each initial separation from the left wall, 10 experiments where performed. Between experiments, the granular material was removed from the cell, and then it was refilled using a precise protocol: using a specially designed funnel with a rectangular cross-section of 2.5×19.5 cm, the granular material was gently deposited from the bottom to a height of approximately 40 cm inside the cell, as the funnel was slowly elevated. This resulted in a packing fraction of 0.65 ± 0.01.

We underline that in order to achieve reproducibility of the rotational effect, it is crucial to guarantee an excellent parallelism between the vertical walls of the cell and between the flat faces of the intruder, as well as avoiding any granular particles to get trapped between the glass walls and the flat faces of the intruder (in our case, the maximum difference in the separation between the two glass plates was of 1 mm between the bottom and top of the cell, equivalent to 0.3 mm between the initial and final positions of the intruder). Releasing the intruder without applying any undesired torque is also relevant –so the magnetic release system is essential.

II. DERIVATION OF THE EQUATION OF MOTION ALONG THE HORIZONTAL AXIS

Assuming a continuum of finite springs around the intruder, we get:

$$m\ddot{x}_\mathrm{c} = k \int_0^{\theta_\mathrm{max}} \left(l + R - \frac{x_\mathrm{c}}{\cos\theta}\right) \cos\theta d\theta \quad (1)$$

where $x_\mathrm{c} = x + R$, $l = 0.05\,\mathrm{m}$ and m , R are the intruder's mass and radius respectively. k is a free parameter associated with the characteristics of the granular particles. θ denotes the angle formed between the x axis and the direction of the spring. Note that we have not taken into account interactions with the opposite vertical wall (or the floor) because springs are assumed far enough to avoid contact. For θ_max (maximum θ of the springs that touch the wall) we have

$$\theta_\mathrm{max} = \cos^{-1}\left(\frac{x_\mathrm{c}}{l+R}\right). \quad (2)$$

* ealtshuler@fisica.uh.cu

Springs with higher values of θ are not involved in the dynamics because they do not reach the vertical wall. Substituting Eq. 2 into Eq. 1 we directly obtain:

$$m\ddot{x}_{\rm c} = k\{[(l+R)^2 - x_{\rm c}^2]^{1/2} - x_{\rm c}\cos^{-1}\frac{x_{\rm c}}{l+R}\}. \quad (3)$$

If we add a viscous-like force term to the right member of the equation above [1–3] (for which we assume a hydrodynamic approach using the corresponding Reynolds number to differentiate between linear and quadratic velocity-dependencies [4]), we get Eq. 1 of the main text.

Fig. 1 (a) shows the net horizontal force on the intruder by differentiating twice the x vs. t experimental graphs corresponding to $x_0 = 0\,$cm, multiplying the result by the mass of the intruder, and smoothing out the final values. Fig. 1 (a) shows that the repulsive force decays shortly after reaching its peak value, as stated in the main the text. The force continues to decline in time until it gets to zero at the end of the experiment. We mimic that behavior with the function of x_c shown in Eq. 3, that accounts for the repulsive (positive) force acting on the intruder. This term decreases with x_c in an approximately linear fashion, until it becomes zero after the intruder separates from the wall a distance $l = 0.05\,m$. To achieve the negative net force in the horizontal axis a viscous-like force term was added to the equation.

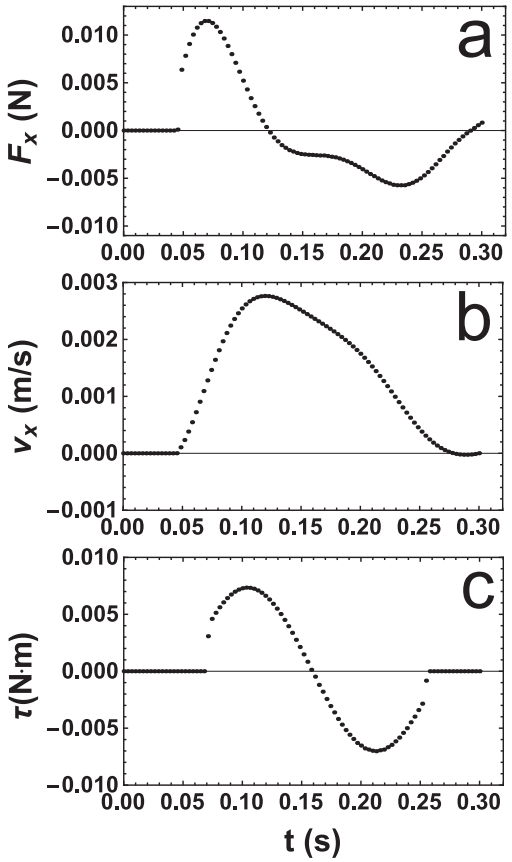

FIG. 1. Time evolution of some parameters extracted from experimental data (a) Net horizontal force on the intruder force (b) Intruder's horizontal velocity (c) Net torque on the intruder.

III. PRELIMINARY MODELING OF THE ROTATIONAL MOTION

Fig. 2 (a) shows a sketch of the shear forces acting on the intruder which are, in principle, responsible for its rotational motion.

One of the hypothesis to reach the rotational equation of motion presented in the main text of the article is that the torque on the intruder is correlated to the velocity along the horizontal axis. We have calculated the net torque on the intruder by differentiating twice the θ vs. t experimental graphs for $x_0 = 0$, multiplying by the moment of inertia of the intruder, and smoothing out the result.

Fig. 1(b,c) shows the strong correlation between the velocity along the horizontal axis and the resulting torque on the intruder. With the increase of $\dot{x}$, the exponential term in the equation of motion (representing the shear forces acting on the intruder) increases, while the frictional forces are negligible, resulting in a positive (or "normal") net torque on the intruder. The torque increases until it reaches a peak that occurs almost at the same moment when $\dot{x}$ also reaches its peak, as expected from our equation of motion. As the horizontal velocity decreases, the first term at the right hand of the equation of motion decreases, so the frictional forces dominate the dynamics, until the motion finally stops.

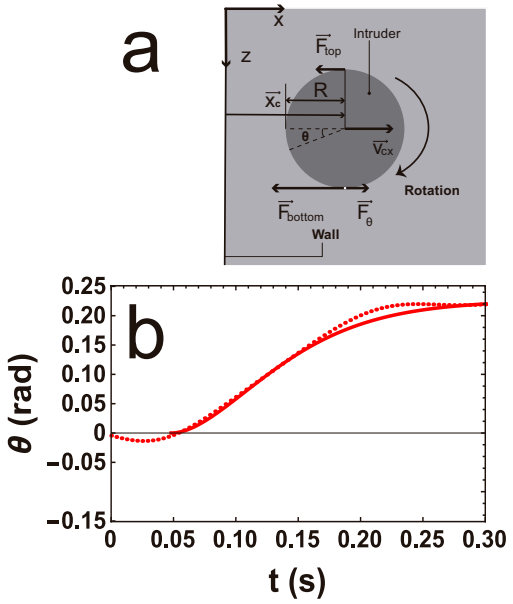

FIG. 2. Preliminary modeling of rotation. (a) Sketch representing the main parameters and forces involved in modeling the intruder's rotation. (b) Rotation vs time for $x_0 = 0$ cm: circles and line represents experiment and the output of the equation $\ddot{\theta} = k_r \dot{x} \exp(-z/\lambda) - f_\theta \dot{\theta}$ (see main text for details).

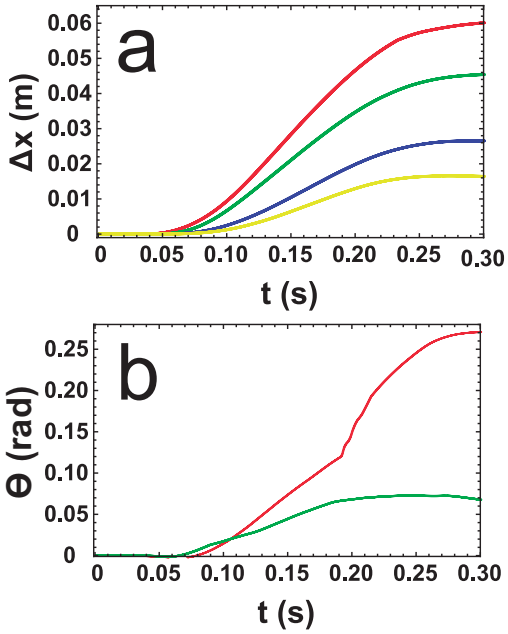

FIG. 3. Basic experimental results reproduced by DEM simulations. (a) Simulated graphs equivalent to the experimental results displayed in Fig. 2(a) of the main text. The difference between simulations and experimental values is always less than a 20 percent in the vertical axis. (b) Simulated graphs equivalent to the experimental results displayed in Fig. 2(b) of the main text, for $x_0 = 0$ cm and $x_0 = 1$ cm. The difference between simulations and experimental results is always under 15 percent in the vertical axis.

Fig. 2(b) presents the experimental points corresponding to rotation for $x_0 = 0$ cm, and the solution of the equation of motion $\ddot{\theta} = k_r \dot{x} \exp(-z/\lambda) - f_\theta \dot{\theta}$ under the conditions described in the main text.

IV. DEM SIMULATIONS

Figure 3(a), in the main text, shows a snapshot from a 2D DEM simulations using LAMMPS [8]. Particles were set as spheres with movement restricted to one plane. Mass, density and dimensional values are the same as in the experimental setup. The interaction between particles is ruled by a Hertzian model. The frictional force between two granular particles is described as in [5], [6] and [7]. The restitution and friction coefficients were set at 0.1 and 0.5, respectively. The Poisson Ratio was set at 2.0/7.0 and Young's Modulus was selected as $10^7\, N/\mathrm{m}^2$. The simulation included 6000 particles. The granular bed was prepared following the experimental process: slowly lifting a 2D funnel containing the particles followed by a wiggle of the cell.

Using the bi-dimensional components of the acceleration of the center of mass of every particle, we could compute the force between each pair. Figure 3(a) of the main text shows the force-chain diagram of these forces, normalized using the maximum force found in the whole simulation. The color intensity of each *force link* is proportional to that normalized force.

While LAMMPS[8] allowed an easy visualization of the force chains, 3D DEM simulations based on CHRONO Project[9] demonstrated to reproduce in a faster way the penetration dynamics of the intruder in 3D. Those simulations were developed using the same pa-

rameters as in LAMMPS with the corresponding changes due to the extension of the simualtion to 3D. The separation of the walls were taken as the experimental value of 0.053 m, and the number of particles were between 52000 and 54000, with a fixed height of the granular bed at the experimental value of 0.40 m. The intruder was reproduced as a cylindrical particle with the experimental dimensions. The granular bed was prepared using a uniform random pour in sets of 1400 particles until 61600 particles were deposited. Particles with a height exceeding 0.40 m were removed from the simulation. The intruder was released after a fixed "cooling time" of 50 ms.

Fig. 3 shows that the DEM simulations based on CHRONO Project are able to reproduce the horizontal motion of the intruder away from the wall (a), as well as its "normal" rotation (b) (interestingly, anomalous rotations could not be reproduced by our DEM simulations). Figure 3(c,d) of the main text shows CHRONO Project DEM simulations that allow to find the relation between l and both, the intruder radius and cell width. Finally, it is worth mentioning that changing the friction coefficient between the intruder and the back/front walls has a negligible influence in the penetration process.

[1] Katsuragi, H. and Durian, D. J. *Nat. Phys.* **3**(6), 420 (2007).

[2] Pacheco-Vázquez, F., Caballero-Robledo, G., Solano-Altamirano, J., Altshuler, E., Batista-Leyva, A., and Ruiz-Suárez, J. *Phys. Rev. Lett.* **106**(21), 218001 (2011).

[3] Altshuler, E., Torres, H., González-Pita, A., Sánchez-Colina, G., Pérez-Penichet, C., Waitukaitis, S., and Hidalgo, R. *Geophys. Res. Lett.* **41**(9), 3032–3037 (2014).

[4] Landau, L. and Lifshitz, E. *Theoretical Physics, vol. 6, Fluid Mechanics*. Pergamon, London, (1987).

[5] Brilliantov, N. V., Spahn, F., Hertzsch, J.-M., and Pöschel, T. *Physical review E* **53**(5), 5382 (1996).

[6] Silbert, L. E., Ertaş, D., Grest, G. S., Halsey, T. C., Levine, D., and Plimpton, S. J. *Physical Review E* **64**(5), 051302 (2001).

[7] Zhang, H. and Makse, H. *Physical Review E* **72**(1), 011301 (2005).

[8] Plimpton, S. Technical report, Sandia National Labs., Albuquerque, NM (United States), (1993).

[9] Project Chrono. `http://projectchrono.org`. Accessed: 2016-03-07.

CHAPTER 2

Sink vs. tilt penetration into shaken dry granular matter

Published

L. Alonso-Llanes et al. Physical Review E ***105****, 024903, 2022.*

doi: https://doi.org/10.1103/PhysRevE.105.024903

Résumé (French abstract)

Nous étudions le comportement d'objets cylindriques lorsqu'ils s'enfoncent dans un lit granulaire sec fluidisé par des oscillations latérales. De manière quelque peu inattendue, nous avons constaté que, dans une large gamme de puissances d'oscillation latérale, les cylindres à fond plat s'enfoncent verticalement, tandis que ceux dont la "fondation" consiste en un anneau peu profond attaché à leur fond, s'inclinent en plus de s'enfoncer. Ce dernier scénario semble dominer indépendamment de la nature de la fondation lorsque des vibrations latérales suffisamment fortes sont appliquées. Nous sommes en mesure d'expliquer le comportement observé par des simulations numériques quasi-2D, qui démontrent également l'influence du rapport d'aspect de l'intrus. La dynamique de pénétration vertical est expliquée à l'aide d'une équation de mouvement newtonienne pour l'intrus. Nos résultats peuvent éclairer le comportement des bâtiments et d'autres constructions humaines pendant les tremblements de terre.

Sink vs. tilt penetration into shaken dry granular matter: the role of foundation

L. Alonso-Llanes,[1,2,*] G. Sánchez-Colina,[1] A. J. Batista-Leyva,[1,3]
C. Clément,[2] E. Altshuler,[1] and R. Toussaint[2,4,†]

[1] *Group of Complex Systems and Statistical Physics, Physics Faculty, University of Havana, 10400 Havana, Cuba*
[2] *Université de Strasbourg, CNRS, Institut Terre et Environnement de Strasbourg, UMR7063, 67000 Strasbourg, France*
[3] *Instituto Superior de Tecnologías y Ciencias Aplicadas (InSTEC). University of Havana, 10400 Havana, Cuba*
[4] *SFF PoreLab, The Njord Centre, Department of Physics, University of Oslo, P.O. Box 1074 Blindern, 0316 Oslo, Norway*

We study the behavior of cylindrical objects as they sink into a dry granular bed fluidized due to lateral oscillations. Somewhat unexpectedly, we have found that, within a large range of lateral shaking powers, cylinders with flat bottoms sink vertically, while those with a "foundation"consisting in a shallow ring attached to their bottom, tilt besides sinking. The latter scenario seems to dominate independently from the nature of the foundation when strong enough lateral vibrations are applied. We are able to explain the observed behavior by quasi-2D numerical simulations, which also demonstrate the influence of the intruder's aspect ratio. The vertical sink dynamics is explained with the help of a Newtonian equation of motion for the intruder. Our findings may shed light on the behavior of buildings and other man-made constructions during earthquakes.

I. INTRODUCTION

The Kocalei earthquake occurring on August 17, 1999 affected in various ways many constructions in the city of Adapazari, Turkey. Following observers, some buildings sank vertically into the soil, others tilted, and some even suffered lateral translation over the ground [1–3]. This case illustrates well the diversity of damage that earthquake fluidization of soils may cause to man-made structures [4].

Liquefaction in the ground may be triggered dynamically by waves emitted during earthquakes, generating cyclic shear stresses that lead to the gradual build-up of pore water pressure [5, 6]. The shaking produced by seismic events is a trigger for extensive liquefaction, as was observed recently in Belgium [7]. Ground fluidization [8, 9] has been investigated in different kinds of media like sand [9], dry granular soils [10] and sediments [11]. Of immediate interest for engineering and for the geosciences is to understand how man-made structures such as buildings, and massive rocks laying on granular soils respond to fluidization associated to seismic waves.

Granular matter itself displays a variety of puzzling phenomena [12–25], but during the last decade or so, our understanding of the dynamics of objects penetrating into granular media has advanced quickly [26–43]. While laterally shaken granular beds have received a certain degree of attention [44, 45], the performance of objects initially laying on the surface of a granular bed submitted to lateral shaking has been rarely studied [46–50].

In this paper we perform systematic experiments associated to the latter scenario, which may help understanding the performance of human constructions and rocks laying on granular beds during earthquakes. In particular, using a cylinder as a simplified model, we study its settling dynamics on a granular bed submitted to lateral vibrations. Somewhat unexpectedly, we have found that, within a large range of lateral shaking powers, cylinders with flat bottoms sink vertically, while those with a "foundation"consisting in a shallow ring attached to their bottom, tilt besides sinking. The latter scenario seems to dominate independently from the nature of the foundation

* lalonso@fisica.uh.cu
† renaud.toussaint@unistra.fr

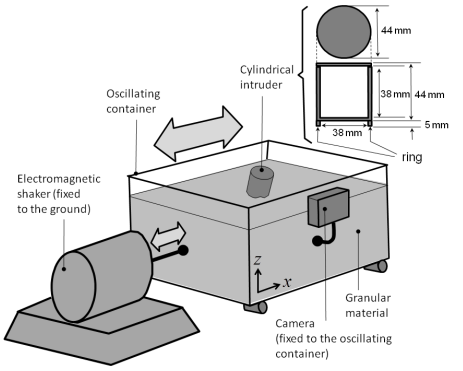

FIG. 1. Experimental setup. At the upper right, we have illustrated the intruder consisting in a cylinder with ring.

when strong enough lateral vibrations are applied. Quasi-2D simulations mimicking the experiments were also performed. The settling dynamics of the simulated intruders, with or without foundation, reproduces the corresponding experimental results. Our simulations also reveal how the difference in force-chain distributions between flat and non-flat bottom cylinders produces different torques justifying the two types of penetration. In addition, we present a simple phenomenological model that reproduces well the sinking dynamics and helps understanding how the tilting process influences the sinking one.

II. EXPERIMENTAL

The penetration experiments were performed on a granular bed contained in a test cell of approximately $25 \times 25 \times 25$ cm^3 filled with Ugelstad spheres of non expanded polystyrene with a bulk density 1050 kg/m^3, and diameter 140 μm (monodisperse within a 1 percent), type Dynoseeds ©, produced by Microbeads, Norway. The box was horizontally shaken at different amplitudes of motion (A), and a frequency (f) of 5.0 Hz (a value commonly found in seismic waves), using a TIRA ©TV51120-M shaker, see figure 1. By controlling the voltage of the shaker input signal we varied the amplitude of the oscillations up to a maximum value corresponding to a peak ground acceleration of $A(2\pi f)^2 \approx 12.2$ m/s^2 [51]. This acceleration range covers most potentially damaging earthquakes, from weak to strong [52], though there has been reports of larger peak ground accelerations [53]. The time the shaker needs to reach the steady state depends on the dimensionless acceleration, being longer for larger accelerations. The time intervals can range from one (0.2 s) to three periods.

Two types of intruders were used in the experiments: (a) a hollow 3D printed cylinder of 44 mm diameter, 44 mm height h_c (external dimensions), and 5 mm thick walls, and (b) the same cylinder with a ring of 5 mm height and 3 mm thickness glued to its bottom (illustrated in the upper right corner of Fig. 1). Intruders (a) and (b) will be called "No-ring"and "Ring", respectively, from now on. Their masses were adjusted with ballast in such a way that their densities matched the average effective density of the granular medium, which was measured as 430 kg/m^3. As far as the ballast used has a density near the effective density of the granular material, it was almost evenly distributed inside the cylinder. Note that, using a flat bottom cylinder and a ring-like bottom cylinder, we are modifying the "foundation"of our intruder.

A digital camera *Hero 2* made by GoPro © was fixed to the electromagnetic shaker, in such a way that it could take a video of the sinking process from an oscillating reference frame locked to the test cell, as proposed in [48]. This method allowed a much better quality of the cylinder's images, and made easier their digital processing. Videos were taken at a maximum rate of 120 frames per second, with a resolution of 1920×1080 pixels.

The images were processed as follows. We first converted the videos to image sequences in *.jpg format, and cropped each picture, excluding irrelevant space. Then, the images were binarized through an appropriate threshold. Using the tool *regionprops* from *MatlabR2014a* ©, we identified and assigned coordinates to several bright marks we had glued to certain points of the cylindrical intruder. The coordinates of the marks were used to calculate the position of the intruder's geometrical center and inclination relative to the vertical

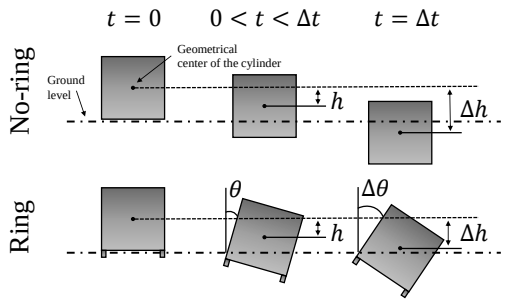

FIG. 2. Sketch of sinking and tilting processes. The top row illustrates the sinking process of a No-ring cylinder in three moments during the experimental interval from $t = 0$ to a final time $t = \Delta t$. The bottom row shows the same temporal sequence for a Ring cylinder, which tilts in addition to sink.

in each picture. In some experiments where the sinking was particularly big, it was difficult to obtain the tilt angle, since part of the marks sank below the level of the sand surface, and they were impossible to follow. In such cases the upper border of the cylinder was identified using the Matlab's tools *find* and *bwtraceboundary*, and then fitted to a polynomial using the function *polyfit*. The fit was used to find the inclination. In the case of experiments ending in a very inclined position, the reference to calculate the inclination was the cylinder's corner above the sand surface, that was identified as the intersection of the two polynomial fits of the upper and one lateral borders of the cylinder.

As the cylinder oscillates due to the vibration of the box, it is difficult to determine the final position, particularly when there is a big tilting. Then, in order to determine the sinking depth and tilting, we observe in the videos the onset of a cyclic movement of a reference point in the cylinder. Then, the final position could be measured in the frames filmed after the shaker was stopped.

The experimental protocol can be described as follows: (I) preparing the granular medium by stirring it evenly with a long rod, (II) gently depositing the cylinder in the upright position on the free surface of the granular bed, (III) turning ON the camera, (IV) switching ON the shaker after setting the desired frequency and amplitude (V) turning OFF the shaker and the camera after the penetration process had visibly finished.

In Fig. 2 we define the main parameters describing the sinking process of a No-ring cylinder (upper row), and the tilting and sinking of a Ring cylinder (bottom row), during the experimental lapse, defined as Δt. As the figure indicates, in the following we will call h the penetration of the geometrical center at a time t and Δh the final penetration at time $t = \Delta t$. Note that both magnitudes are defined as the vertical displacement of the geometrical center of the cylinder (without taking the ring into account). In the same way we will call θ the inclination of the intruder at time t and $\Delta\theta$ the final inclination at $t = \Delta t$.

We also explored the phenomenology through numerical simulations. They were based on a discrete element method code (DEM) for the computation of granular systems [20, 22, 24, 49, 50, 54, 55]. We modeled a quasi-2D granular medium, made of finite-sized hard spheres with radii between 1.0 and 1.5 mm, to avoid the crystallization effect. The medium contains 4000 particles and is prepared by placing the latter randomly in a space 30 cm wide and 25 cm high and then allowing them to settle under the action of gravity $g = 9.81$ m/s^2. Once the medium reaches equilibrium, it occupies a virtual space 30 cm wide and about 8 cm high, laterally delimited by flat walls that define the Hele-Shaw cell. The simulation box used was created narrow in order to have a single plane of particles in the direction perpendicular to the images shown in Figures 3 and 4. The components of the velocities and forces along this direction are set to zero at each time step. To mimic the experimental conditions, we simulate particles of density 1050 kg/m^3.

The two intruders are made of cohesive particles. One is a square of 40 mm side, made of $N = 1681$ particles with diameter 1 mm, placed in a quasi-2D square arrangement, which simulates the No-ring intruder of the experiments. The second one is also a square of 40 mm side to which two ″small feet″are attached. Each foot has a size of 4.5 $\times$ 2.7 mm^2, so the simulated Ring intruder

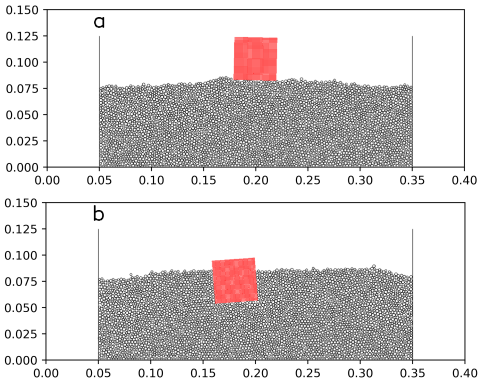

FIG. 3. (color online) Snapshots of the initial (a) and final (b) positions of a No-ring intruder in a typical quasi-2D simulation using a shaking frequency of 5 Hz.

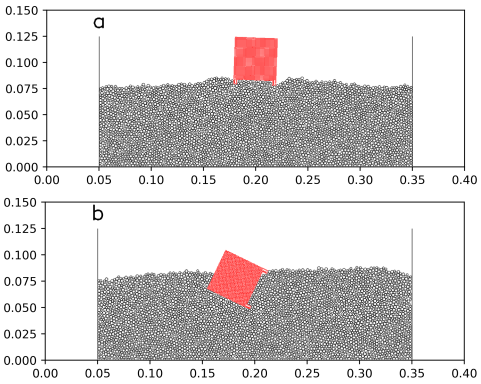

FIG. 4. (color online) Snapshots of the initial (a) and final (b) positions of a Ring intruder in a typical quasi-2D simulation using a shaking frequency of 5 Hz.

contains a total of $N = 1705$ particles. The density of the spheres ρ_p which form the intruders is adjusted so that the bulk density of the rigid body matches the effective density of the granular medium. The latter is calculated once the medium has settled down and is stable, and was always found to be around $\rho_m = 566$ kg/m^3. Then, the density of the particles forming the intruder is obtained as $\rho_p = \rho_m V_i/NV_p$, where V_i is the volume of the intruder and V_p the volume of a sphere.

Once our granular medium is created, we place the intruder 1 mm above the medium, with its bottom parallel to the horizontal direction. We release it, under the action of the force of gravity, and wait until the whole system becomes motionless (i.e. its total kinetic energy reaches a value under 10^{-7} J). Then, we apply horizontal oscillations of different amplitudes and a frequency of 5 Hz ($\Delta t \approx 8$s) to the walls of the cell and compute the time evolution of the position and tilting angle of the intruder. The amplitudes were chosen in such a way that the dimensionless acceleration $\Gamma = A(2\pi f)^2/g$ had the values of 0.16, 0.25, 0.5, 1.0, 1.25 and 1.5.

The contact between spheres was modeled as a linear spring-dashpot $F_{ij} = (k_n \delta \mathbf{n}_{ij} - m_{eff}\gamma_n \mathbf{v}_n) - (k_t \Delta \mathbf{S}_t + m_{eff}\gamma_t \mathbf{v}_t)$ [54, 56], where k and γ are the elastic and viscoelastic damping constants, $\delta \mathbf{n}_{ij}$ is the overlap distance along the line connecting the centers of the two spheres, and $\mathbf{v}$ their relative velocity. $\Delta \mathbf{S}_t$ is the tangential displacement vector between two spheres, which is truncated to satisfy a frictional yield criterion, and $m_{eff} = m_i m_j/(m_i + m_j)$ is the effective mass of two spheres of mass m_i and m_j. We considered normal (n) and tangential (t) forces components between the particles and, in order to model hard spheres that interact on contact (i.e. spheres whose deformation during collisions is less than a small fraction of their radii), we used the following parameter values: $k_n = 1.2 \times 10^7$ N/m, $k_t = 2/7 k_n$, $\gamma_n = 12$ s^{-1} and $\gamma_t = 0.1\gamma_n$. The interaction force between the walls and the particles touching them is the same as the corresponding for two particles but considering the wall of infinite radius and mass (flat wall). The microscopic friction coefficient between spheres, and between spheres and boundaries, was taken as $\mu = 0.3$. The time step dt was chosen to guarantee that there are at least 50 steps during one characteristic time of a collision $dt = t_c/50$, where $t_c = \pi/\sqrt{(k_n/m_{eff}) - \gamma_n^2}$.

Figures 3 and 4 show the initial and final positions of both types of intruders in two typical runs. Fig. 3 indicates that the No-ring cylinders are slightly inclined, while in Fig. 4 the large inclination of the Ring one becomes obvious.

We also performed an additional set of simulations aimed at elucidating the influence of

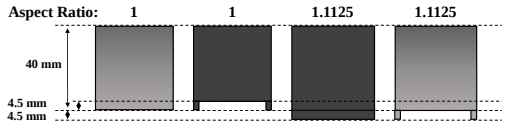

FIG. 5. Comparison of the geometry of the intruders used to test the influence of the aspect ratio. In light gray the intruders previously described and in dark gray the new ones.

the intruder's aspect ratio in the sink - tilt behaviour. Two intruders, one No-ring with aspect ratio 1.125, and a Ring with aspect ratio 1 (see Fig. 5), were submitted to the same range of dimensionless accelerations. Note that the new intruders (in dark gray in Fig. 5) have the same dimensions of the former ones (in light gray) but the geometry of the bottom is interchanged.

The new intruders are also rigid bodies made of 1 mm diameter cohesive particles and their bulk densities also correspond to that of the granular medium. The new Ring intruder is composed by $N = 1498$ particles forming a 40 mm wide and 35.5 mm high rectangle to which two 4.5×2.7 mm^2 feet were added. Note that the size of these feet and those of the Ring intruder are the same. The new No-ring is a rectangle of 40 mm wide and 44.5 mm high composed of $N = 1845$ particles.

III. RESULTS AND DISCUSSION

A. Sink *vs.* tilt penetration in experiments

Figure 6(a) shows the time variation of the sinking depth for selected values of the dimensionless acceleration $\Gamma = A(2\pi f)^2/g$ (where $g = 9.81$ m/s^2 is the gravitational acceleration and $A(2\pi f)^2$ is the horizontal peak acceleration of the sand box) for No-ring cylinders. It is easy to see that the penetration of the No-ring cylinders follows a common pattern for all the accelerations. A first process of fast sinking is followed by a slow creep. Only the penetration depth increases with Γ. In this figure we do not show the total creep process,

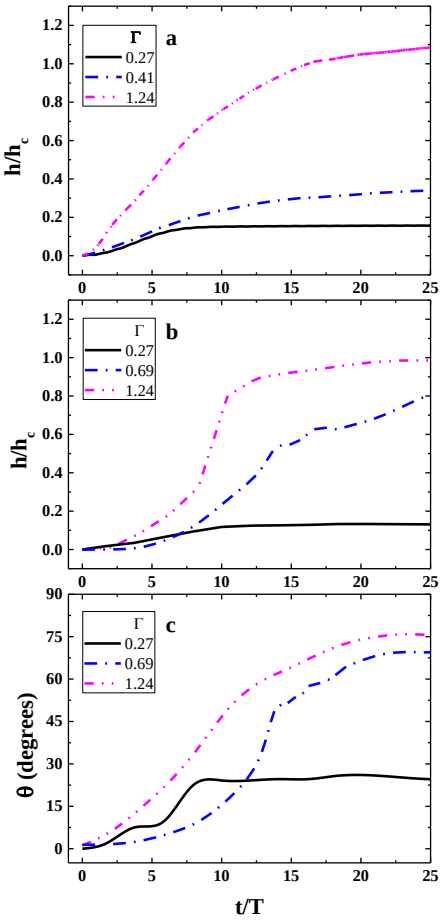

FIG. 6. (color online) Experiments. Time evolution of penetration depths and tilt angles. Time dependence of the penetration depth of a No-ring cylinder (a), the penetration depth of a Ring cylinder (b) and the tilting angle of a Ring cylinder (c), for different dimensionless accelerations. The long-time creep process is not completely shown. The tilting angle of No-ring cylinders is not displayed, due to the fact that it oscillates around angles not larger than 5° relative to the vertical direction.

due to its long duration. As the height of the cylinder is $h_c = 44$ mm, it is possible to check from Fig. 6(a) that, for a dimensionless accelerations of 1.24, the cylinder sinks completely. An important characteristic of the sinking process in this type of cylinder is that the intruder penetrates the granular medium with almost

no tilting, and a final inclination smaller than 5°.

Figure 6(b) is similar to the previous one, but measurements were performed with Ring cylinders. The general features of both graphics are similar, but there is a difference, that will be better observed in the following figures: the dimensionless acceleration at which the cylinder sinks completely in the medium is bigger for the Ring cylinders than for the No-ring ones.

Figure 6(c) presents the time evolution of the tilting angle for a Ring cylinder, a process that occurs simultaneously with the sinking. The sinking and tilting dynamics of Ring cylinders is more irregular than that of the No-ring ones. This is illustrated in Fig. 6(b) and (c), even after being submitted to a moving average process, to get a smoother graph.

No-ring cylinders tend to sink vertically as the granular soil is fluidized by horizontal shaking, while cylinders with rings tend to tilt. Figure 7 quantifies the differences between the initial and final stages of the process, for almost all the range of accelerations our experimental setup was able to reach.

Figure 7(a) shows sink data for No-ring cylinders. As can be seen, for dimensionless accelerations up to $\Gamma = 0.27$, there was no significant penetration of the intruder into the granular bed. Vertical penetrations started to increase significantly above this acceleration, reaching a plateau around $\Gamma \approx 0.7$. At the plateau, the cylinder has sunk completely, but stays "floating" into the fluidized granular medium, as expected for an object isodense relative to it, so there is no further sinking.

In Fig. 7(b) the sinking process of the Ring cylinders is summarized. Though the low acceleration part is similar to Fig. 7(a), now the plateau is not observed for the range of accelerations recorded. Notice that from the depth reached at $\Gamma \approx 1.2$, approximately the height of the cylinder h_c, it would not sink any further, and that from this value of Γ onwards a plateau would appear.

Figure 7(c) shows the tilt data for Ring cylinders. No significant tilting is observed for Γ smaller than approximately 0.25. With the increase of the dimensionless accelerations, the cylinder significantly tilts, increasing abruptly

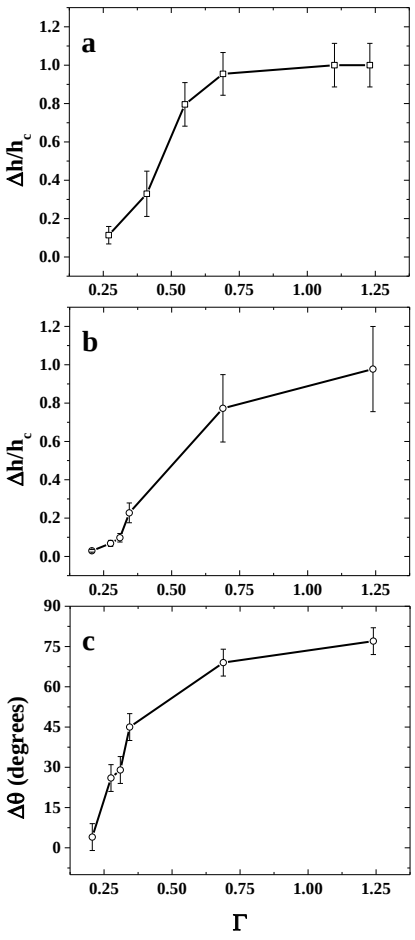

FIG. 7. Experiments. Sinking and tilting: heights and angles for different dimensionless accelerations Γ. Final sink heights for No-ring cylinders (a) and for Ring cylinders (b). Final tilt angles for Ring cylinders (c). Tilt angles of No-ring cylinders are not shown for the same reasons of the previous figure.

the tilting angle with Γ, until it slows down at $\Gamma \approx 0.7$. We do not show the tilting angle of No-ring cylinders, because it is always smaller than 5°, with a random distribution of values around the vertical direction.

Figures 7(b) and (c) are closely related, because they are two descriptions of the same process: the motion of Ring cylinders into the granular medium, that includes both sinking and tilting. The fact that at the accelerations

shown in this figure the plateau in the sinking depth is not reached while for the tilting angle at higher values of Γ the inclination almost saturates, could be explained by the increase of the friction of the intruder with the granular medium when the tilting angle increases. At $\Gamma \approx 0.7$ the intruder has reached a large inclination, but is not completely submerged into the medium. An increase in the acceleration does not increase significantly the angle, because the resulting torque has diminished due to the influence of both sinking and tilting, but the increase in fluidization helps further sinking, until most of the cylinder is submerged.

The sinking process can be understood taking the experimental results in Ref. [46] into account. When the system is submitted to lateral shaking, a fluidized layer appears in the upper part of the granular cell. This layer reaches a depth h_f that depends on the dimensionless acceleration Γ. Below this layer exists a "solid" layer. For accelerations in the range spanned in our experiments, h_f varies almost linearly with Γ (see Fig. 3(a) in Ref. [46]), so we can write

$$h_f(\Gamma) = \alpha(\Gamma - \Gamma^*); \Gamma > \Gamma^* \qquad (1)$$

where Γ^* is the onset of fluidization and α is the slope of the linear dependence. If $\Gamma \leq \Gamma^*$ the depth of the fluidized layer is zero.

Then, at low values of Γ the granular medium is not fluidized, and the cylinder almost does not sink (merely 5 mm at $\Gamma = 0.27$; see Fig. 7(a)). For accelerations above the fluidization threshold, the cylinder sinks until it gets in contact with the solid layer. The larger is the acceleration, the deeper is that layer, so the bigger is Δh. But as soon as the solid layer appears at a depth larger than the cylinder's height, it does not sink further: instead, it "floats" due to isodensity with the sand, so a plateau is reached.

According to reference [57], Γ^* can be taken as proportional to the friction coefficient μ between the cylinder and the granular medium. In these experiments we can approximate $\mu \approx 0.3$, which is the value we use in the simulations. The authors also conclude that the final depth of intrusion depends on isostasy, and on the severity of shaking. It can be entirely determined by isostasy, when the shaking completely unjam the medium and suppresses the average friction around the intruder [50].

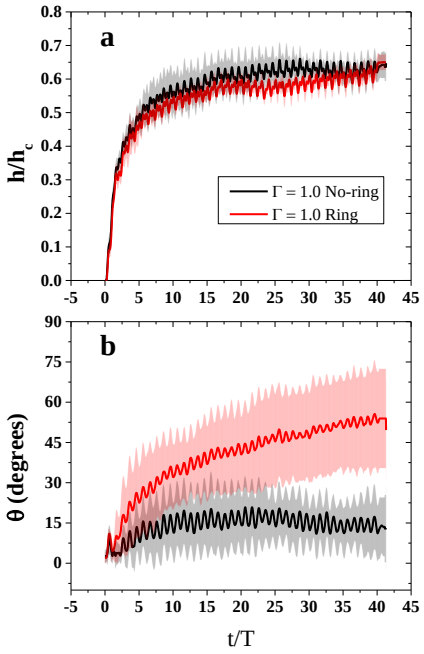

FIG. 8. (color online) Simulations. Time dependence of sinking depth (a) and tilting angle (b) for both types of intruders with $\Gamma = 1.0$. The central lines are the average of six simulations, while the colored bands cover $\pm 1\sigma$.

To better understand the differences in the dynamics of both types of intruders, we performed numerical simulations and their results are described below.

B. Sink vs tilt in quasi-2D numerical simulations

Figure 8 shows the time dependence of the penetration depth (a) and tilting angle (b) for both types of intruders at the dimensionless acceleration $\Gamma = 1.0$. In both figures the thick curves represent the average value of six repetitions varying the initial conditions and the surrounding zone represents ± 1 standard deviation.

Regarding the vertical sinking in Fig. 8(a),

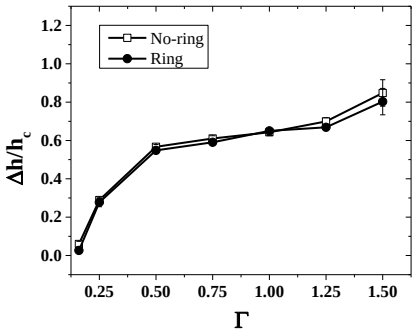

FIG. 9. (color online) Simulations. Final depth reached for No-ring (squares) and Ring (circles) cylinders as a function of the dimensionless acceleration. Symbols represent the average of six experiments and the error bars $\pm\sigma$.

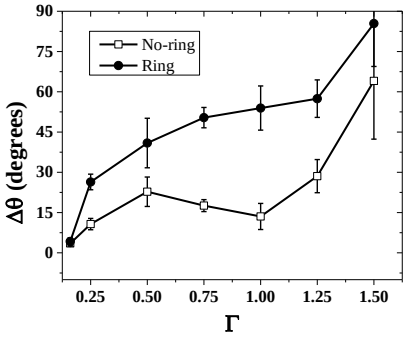

FIG. 10. (color online) Simulations. Maximum tilting angle reached for No-ring and Ring cylinders as a function of the dimensionless acceleration. Symbols represent the average of six simulations and the error bars $\pm\sigma$.

we do not observe major changes between Ring and No-ring intruders; both types of intruders sink less than in the experiments. This may be related with the lower dimensionality of the simulations relative to the real experiment. Quasi-2D granular media allow less choices of readjustment than in 3D: they are easily jammed, which makes it more difficult for an object to sink. Moreover, the size ratio of the intruder over the particles is 8 times smaller in the simulations than in the experiments (experiments: 44 mm/0.140 mm $\approx$ 300; simulations: 40 mm/1 mm= 40), which means that if one particle is stuck under the intruder during the simulations, it will slow down the intruder significantly more than if the particle were 8 times smaller.

Figure 8(b) indicates that the presence of a foundation at the bottom of the intruder causes a large tilting. Indeed, for the shaking with no ring, the intruder tilting angle is around 10°, but during the shaking with ring, the intruder tilts fast, reaching an angle around 50°. This resembles what happens in the experiments (see Fig. 4): the intruder almost ends up lying on one of its sides. Of course, the tilting is also limited by the diminished dimensionality in the quasi 2D simulations.

Figure 9 compares the penetration depth reached for both types of cylinders at different values of Γ. The conclusions obtained from Fig. 8 are valid for all the dimensionless accelerations used in the simulations: there are no significant differences in the final sinking depth between both types of intruders.

In Fig. 10, on the contrary, the difference in tilting angles between the two types of intruders is clearly seen. For all the values of Γ the simulated Ring intruder tilts more than the No-ring one. For Γ=1.50, the No-ring tilts up to an angle that is closer to the Ring's one, corresponding to preliminary observations found in experiments with frequencies above 5 Hz for dimensionless accelerations Γ >1.25.

According to our simulations, the difference in tilting between intruders lies in that one type of intruder, the No-ring one, is somehow more capable of rectifying its rotation during sinking, while the other, the Ring intruder, is not. This rectification can be understood as the process of returning to, or recovering, the initial rotation angle once one oscillation of the cell has concluded and, as can be seen in the temporal evolution of θ (Fig. 11(a)), the difference in the rotation angles between the No-ring and Ring intruders is produced by a non-rectifying cumulative process taken by the latter.

To understand why the tilting dynamics is affected by the presence of the legs, which makes the No-ring intruder able to further rectify its rotation – at least for the values of gamma between 0.25 and 1.25–, we calculate

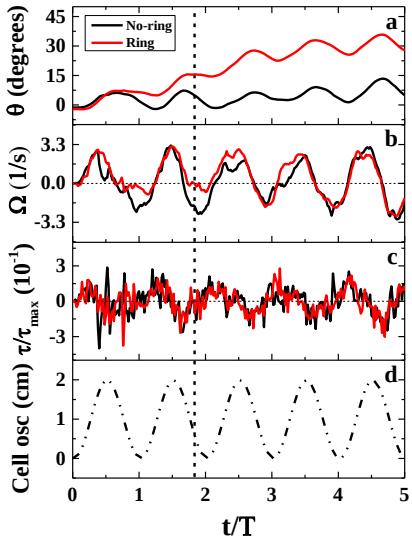

FIG. 11. (color online) Simulations. Temporal evolution of the calculated magnitudes for the intruders during the first second of a simulation using $\Gamma = 1.0$. From top to bottom: the evolution of the rotation θ (a), the angular velocity Ω (b), the torque about the center of mass τ (c) and finally, the position of the cell (d) showing the oscillation described by it. The vertical line indicates the instant $t = 1.84$ T. τ_{max} is maximum torque on a non-tilting but horizontally accelerated No-ring intruder.

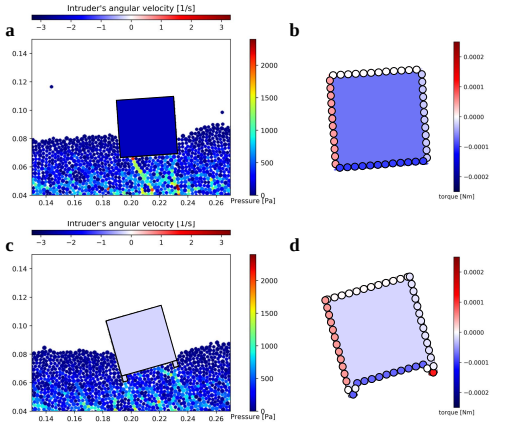

FIG. 12. (color online) Simulations. Pressure field in the granular medium represented as a jet color map for No-ring (a) and Ring (c) intruders. The color of the intruders represents their angular velocity using a seismic color map. In (b) and (d) the outer segments of the intruders are represented as a whole with a color corresponding to the resulting torque about the center of mass that is generated on all grains belonging to them. Notice that for the Ring intruder each leg is divided into 3 segments. The grains in these segments are magnified for better viewing. The resulting torque about the center of mass is represented as the interior color of the intruder. For both angular velocity and torque, blue color represents clockwise.

from the simulations the torque about the center of mass and the angular velocity.

Fig. 11 shows the time evolution of θ, the angular velocity, the torque about the center of mass and the oscillation of the cell for the two types of intruders in a simulation with $\Gamma = 1.0$. Focusing on the θ curve, the difference in tilting can be noticed during the first second of the simulation (as in Fig. 8 (b) for the averaged values) as well as the aforementioned Ring intruder non-rectification process. Unexpectedly, the values of the torques shown in Fig. 11 (c) are very similar for the two intruders, contradicting the intuitive idea that the sole presence of the legs would produce higher torques about the Ring intruder's center of mass making it rotate more. However, the slight differences may affect, to a greater or lesser extent, the rotational movement of the latter with respect to the No-ring intruder (see Fig. 11 (b)).

In general, during the first half of a cell oscillation, both intruders rotate in the same direction –counterclockwise due to the fact that the granular bed moves from left to right–. But, during the second half, some forces appear in the bottom and/or the inside of the Ring intruder's right leg that do not allow it to rotate in the same way as the No-ring does. In some cases, these forces completely prevent it from rotating clockwise, as in both first oscillations shown in Fig. 11. This process is prone to occur in each of the oscillations during the simulation and its repetition causes the differences in inclination observed for the two intruders after 8 simulated seconds (see Fig. 10).

Fig. 12 illustrates in more detail what is described above. In (a) and (c) it shows the pressure field in the granular medium at $t = 1.84$ T (time indicated in Fig. 11 by the vertical line), where the force chains are represented using a

sequential color map. In them, the color of the intruders represents their angular velocity, which in turn is displayed as a diverging color map where blue indicates clockwise rotations. Figures 12 (b) and (d) show the contribution to the torque about the center of mass of each of the intruder segments as a result of the forces acting on them. In this case, the color of the intruders is associated with the resulting torque about the center of mass. Note that all the grains of each outer edge in (b) and (d) are represented with one color corresponding to the resulting torque about the center of mass obtained from the torques of all the particles on this same edge, though only the parts of the edge in contact with the granular medium are effectively interacting. These figures help identify what type of torque, clockwise or counterclockwise, is generated in each part of the intruders (including the legs), how it is generated, and how representative it is for the resulting torque about the center of mass. In this particular case, it is observed for the Ring intruder that the force associated with the lower part of the right leg is responsible for almost canceling the torque about the center of mass. Therefore, the Ring intruder remains inclined while the No-ring one rotates back to its original position.

Those forces acting on the Ring intruder's legs could be associated with the grain jamming between them. Fig 13 shows that almost all the blue grains that were initially in the region between the legs remain there throughout the simulation. Furthermore, it can be seen that some of the grains (cyan) around the Ring intruder accumulate between its legs: this is because during the first part of the oscillations these grains tend to move towards the legs, however, they cannot leave them during the second part. In contrast, grains in the region below No-ring intruders have more freedom to exit. The previous process suggests that the Ring intruder along with the grains between the legs could be treated as a No-ring intruder with increased friction at the bottom. This increase in friction will make the grains underneath more likely to get stuck, preventing them from coming out and thus creating force chains capable of stopping the clockwise rotation (restoring towards vertical position)

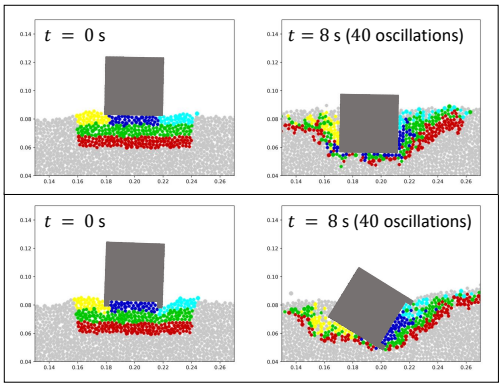

FIG. 13. (color online) Simulations. Grain tracking. Initial (left) and final (right) positions of the No-ring (top) and Ring (bottom) intruders as well as the grains of the granular medium next to them. The grains right below the intruders are represented in blue while the yellow and cyan colors represent the grains initially at the left and right side of the intruders, respectively. Note that for the Ring intruder, the blue grains initially located between the legs remain in the same region until the end of the simulation

.

of the intruder.

A final observation from the simulations for dimensionless accelerations of $\Gamma = 1.5$ is that the No-ring intruder rotates almost 90 degrees in a 100% of the cases where it reached 45 degrees, doing so in an abrupt way. The Ring intruders, however, show a constant growth up and, in some cases (after reaching 90 degrees), increase the slope reaching values of up to 180 degrees. It is worth noting that once Ring intruders turn 90 degrees they begin to resemble No-ring ones as the presence of the legs loses importance in the penetration dynamics. Behaviors such as those described before were not observed experimentally since the Γ values used in the experiments did not exceed 1.24 due to technical limitations of the shaker used.

The experimental findings are explained not only by the numerical simulations, but also by a Newtonian model developed in the Appendix 1. This model is based in the force balance on a cylinder sinking in a granular medium. The forces considered in the 1D model are gravity, a frictional force proportional to velocity

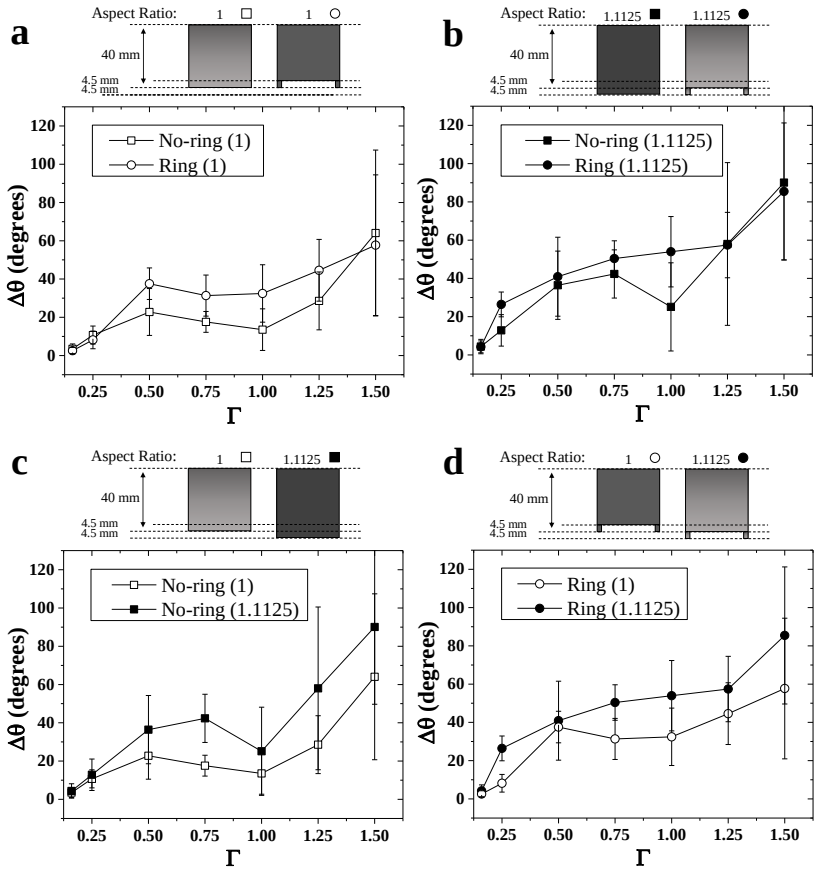

FIG. 14. Simulations. Final tilt angles at different Γ for two intruders with (a) aspect ratio 1 and different foundations; (b) aspect ratio 1.1125 and different foundations; (c) a flat bottom and different aspect ratios and (d) a ring at the bottom and different aspect ratios.

and a pressure like force, proportional to the depth h, as expressed in Eq. (A.13). Though this model does not include the degree of freedom associated with tilting, the consideration of its influence in the lineal and surface dimensions of the intruder is enough to explain why a tilted intruder reaches a final depth smaller than that reached by a non tilted intruder for a given Γ.

Now, we examine the influence of the intruder's aspect ratio on the penetration dynamics. The results of the simulations performed with the intruders of different aspect ratios are summarized in Fig. 14. Fig. 14(a) compares the dependence of the final tilt of two intruders with the same aspect ratio (1), one with legs and the other with a flat bottom. With the exception of the smaller values of Γ where no noticeable differences are apparent, the intruder with legs always tilts more. This behavior is repeated in the results of Fig. 14(b) for a larger aspect ratio (1.1125): again the intruder with legs has a final tilt larger than the one with a flat bottom. Therefore, the above suggests that the presence of a ring at the bottom of the intruder causes a higher final tilt, although it might become less important with increasing aspect ratio. Figures 14(c) and (d) compare intruders with the same foundation and different aspect ratios. Both figures lead to the same conclusion: the larger the aspect ratio, the larger the tilt angle. Summarizing the results of Fig. 14, the intruder with higher aspect ratio and ring placed on

the bottom has the largest tilt angle for all dimensionless accelerations, and the intruder with flat bottom and lower aspect ratio has the smallest tilt angle. Interestingly, the other two intruders show approximately equal final tilt angle values for equal values of Γ.

IV. CONCLUSIONS

We have studied the behavior of cylindrical objects as they sink into a dry granular bed fluidized by horizontal oscillations, as a model system to understand the effects of earthquake-related fluidization of soils on human constructions and other objects like rocks.

We have found that, within a relatively large range of lateral shaking amplitudes at a frequency of 5 Hz, cylinders with flat bottoms sink vertically, while those with a "foundation"consisting in a shallow Ring attached to their bottom, tilt laterally besides their vertical sinking.

We have been able to mimic the above described behaviors by quasi-2D numerical simulations. With their help we found that these differences are not necessarily due to the sole existence of the legs that generate bigger torques about the center of mass. Instead, they can be associated with the jamming of the particles in the region between the legs, which can increase the friction at the bottom of the Ring intruder generating force chains capable of preventing the total recovery of its initial angle of rotation. Numerical experiments also helped to clarify the influence of the intruder aspect ratio on the tilt dynamics: of two intruders with the same foundation, the one with higher aspect ratio will have a larger tilt angle. So, the aspect ratio and the foundation type cooperate to establish the penetration dynamics of the intruder.

We have also reproduced the vertical sink dynamics of cylinders with a flat base using a Newtonian equation of motion for an object penetrating a fluidized layer of granular matter, where the granular effective density increases with depth, eventually reaching a solid phase. The same model allows to understand the sinking even in the present of tilting (Appendix 1).

Finally, it is worth noting that preliminary experimental data and quasi-2D numerical simulations suggest that, when strong enough lateral shaking is applied, the tilting scenario tends to dominate regardless the nature of the intruder's foundation.

ACKNOWLEDGMENTS

L. A. thanks the Photovoltaic Research Lab of the University of Havana for allowing the use of its facilities. E. A. drew inspiration from the late M. Álvarez-Ponte. We acknowledge support from Project 29942WL (Fonds de Solidarité Prioritaire France-Cuba), from the EU ITN FlowTrans, and from the INSU. We thank the SCAC of the French Embassy in Havana and the University of Strasbourg for their support. RT acknowledges the support of the Research Council of Norway through its Centres of Excellence funding scheme, Project No. 262644. We thank Mustapha Meghraoui, Einat Aharonov, Knut Jørgen Måløy, Eirik G. Flekkøy, for fruitful discussions. This research was made in the frame of the University of Havana's institutional project "Medios granulares: creando herramientas para prevenir catástrofes".

Appendix

1. Sink dynamics: a phenomenological Newtonian model

The model to be formulated should account for two related processes, the sinking in the vertical direction and the oscillations perpendicular to it. But as was shown above, the No-ring intruders have only small oscillations that end fast, being the overall sinking process almost vertical. Regarding the Ring intruders, though they strongly oscillate, the tilting process ends first, so we will consider only the equation controlling the vertical sinking, figuring out how the tilting angle affects the sinking dynamics.

In order to formulate a model to describe analytically the sinking process, let us consider

the forces acting on the cylinder. As soon as the shaking starts, if the dimensionless acceleration is above threshold, the upper part of the granular bed is fluidized, and the intruder sinks.

Let us assume that the cylinder just sinks vertically, and let us name the vertical downward axis as z. The force balance on the intruder can be written as

$$m\vec{a} = m\vec{g} + \int (-P)\hat{n}dS + \int \sigma_s \cdot \hat{n}dS \quad \text{(A.1)}$$

where P is the pressure, σ_s the shear stress tensor, $\hat{n}$ is the vector normal to the intruder's surface, and the integrals run over the boundary of the intruder that is inside the granular material. Assuming a hydrostatic pressure profile, we can write:

$$P = \int_0^h \rho(z')gdz' \quad \text{(A.2)}$$

where h, as previously, is the depth reached by the cylinder below the surface of the granular medium. In Eq. (A.2) we have made explicit that the density of the material varies with depth. Let us assume that it varies as a power law between zero and the density of the solid layer, ρ_{sl}, that is reached at a depth h_f:

$$\rho(z') = \rho_{sl}\Big(\frac{z'}{h_f}\Big)^p \quad \text{(A.3)}$$

where $p \in [0, 1]$. The selection of the value of p is discussed below (see also Appendix 2).

By combining (A.3) and (A.2) and integrating, we find the hydrostatic buoyancy force acting on the cylinder with a length h under the (average) level of the granular bed, as:

$$\int (-P)\hat{n}dS = -\frac{\rho_{sl}Sg}{(p+1)h_f^p}h^{p+1}\hat{h} \quad \text{(A.4)}$$

where S is the characteristic area of the intruder cross section, and $\hat{h}$ is a unit vector pointing downwards. It is easy to see that the buoyancy force depends on the volume submerged into the granular medium.

Neglecting the inertial forces, which according to our simulations is typically two orders of magnitude smaller than the contact forces, the shear stress component goes as

$$\int \sigma_s \cdot \hat{n}dS = -D\gamma v\hat{h} \quad \text{(A.5)}$$

where γ has the dimensions of a viscosity, D is the characteristic size of the cross section of the intruder and v is its sinking speed [58, 59]. By substituting Eq. (A.4) and Eq. (A.5) into Eq. (A.1), and only recovering the modular values, we get:

$$m\frac{d^2h}{dt^2} + D\gamma\frac{dh}{dt} + \frac{\rho_{cs}Sg}{(p+1)h_f^p}h^{p+1} = mg \quad \text{(A.6)}$$

Before solving Eq. (A.6) we will assume that the sink velocity is constant, which follows quite well the behavior during the fast sink regime, as seen in Fig. 15 (*i.e.*, we neglect the inertial term). So,

$$\frac{dh}{dt} + \frac{\rho_{sl}Sg}{D\gamma(p+1)h_f^p}h^{p+1} = \frac{mg}{D\gamma} \quad \text{(A.7)}$$

which can be written as

$$\frac{dh}{dt} + ah^{p+1} = b \quad \text{(A.8)}$$

The definitions of a and b are easily deduced by comparing Eqs. (A.7) and (A.8).

Equation (A.8) has analytical solutions if $p = 0$ or $p = 1$, which correspond to the extreme cases of constant density and a linear density profile with depth, respectively. The solutions are

$$h(t) = \frac{b}{a}(1 - e^{-at}) \quad \text{(A.9)}$$

if $p = 0$, and

$$h(t) = \sqrt{\frac{b}{a}}\tanh(\sqrt{ab}t) \quad \text{(A.10)}$$

if $p = 1$.

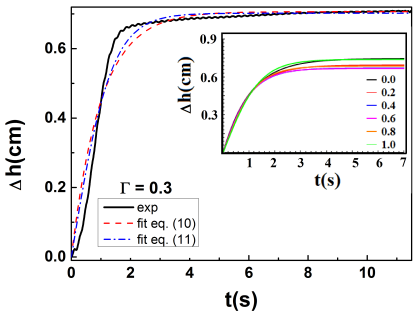

FIG. 15. (color online) Time dependence of sinking depth for the No-ring cylinder from experiment, compared with that determined from Eqs. (A.9, A.10). The inset shows the solutions of Eq. (A.6) for different values of p (see text).

It is easy to see that both expressions correspond to an exponential growth that saturates.

Figure 15 shows the experimental results (continuous line) obtained for a dimensionless acceleration $\Gamma \simeq 0.3$. It is possible to see in more detail the initial fast sinking process, followed by the slow creep. Fig. 15 also shows the fitting of equations (A.9, A.10) to experimental data. Both solutions reproduces well the main features of the sinking process.

It is almost impossible to determine experimentally the exact density profile. But we do not need to know it in order to validate our model, if we use the following rationale. Firstly, we fit Eqs. (A.9, A.10) to the experimental data and obtain the values of a, b that correspond to $p = 0$ $(a(p = 0), b(p = 0))$ and $p = 1$ $(a(p = 1), b(p = 1))$. Let us assume that a and b vary linearly with p between the extremes values which were obtained from the fitting process. For an intermediate value of p (say, p_1) we can calculate the corresponding values of $a(p_1)$ and $b(p_1)$. With them, we can in turn determine the constants of Eq. (A.6). Then, we solve this equation numerically. This procedure is repeated for values of p between 0 and 1, with a step of 0.1.

The inset in Fig. 15 shows some of the numerical solutions for the values of p in the legend. The main conclusion is that the density profile has small influence on the first (and most important) part of the sinking process. Of course, the final depth is influenced by the value of p, but due to experimental uncertainties, it is almost impossible to choose any particular value.

Let us now study the influence of the values of p in the quality of the fit of the solution of Eq. (A.6) to the experimental data. For doing this we notice that the values of a and b in Eq. (A.9) can be easily obtained from the experiments. Considering Eq. (A.8) in the first moments of motion, as h is small, $h'(t) \simeq b$, so b can be evaluated as the initial slope. As at large times $h(t) \sim h_{eq}$ ($h_{eq} = \Delta h$ if $h(0) = 0$) then $a = b/h_{eq}^{p+1}$. Then solving Eq. (A.6) for a given value of $b, p, a(p)$ and naming the result h_{mod}, the best value of p arises from the minimization:

$$p_{opt} = \arg\min \sum_{i=1}^{N} [h_{mod}(t_i, p) - h_{exp}(t_i)]^2 \tag{A.11}$$

where $h_{exp}(t)$ are the experimental values of h.

The result for $\Gamma \leq 1.0$ is indifferent to p: the fit is equally good no matter which is the value of $p \in [0, 1]$. For $\Gamma = 1.24$ there are differences in the quality of the fits for various values of p, but Eq. (A.11) gives a minimum for $p = 0$, so, we will use $p = 0$ in the following (Appendix 2 supports the selection of p from the simulations). Then, Eq. (A.6) becomes:

$$m\frac{d^2h}{dt^2} + D\gamma\frac{dh}{dt} + \frac{\rho_{sl} S g}{h_f} h = mg \tag{A.12}$$

that can be taken as the simplest equation of motion describing the vertical sink dynamics of our cylinders. It is worth noticing that Eq. (A.12) reproduces quite closely the results reported in Fig. 15, and can be used to qualitatively describe the vertical sinking of Ring-cylinders while tilting, as we will see below. It is possible to demonstrate that Eq. (A.12), developed for a granular bed fluidized by shaking, is closely related with that proposed in [30] to describe the penetration of an intruder into ultra-light granular material that eventually behaves like a fluid medium even in the absence of shaking.

In order to understand the influence of the tilting dynamics in the sinking process, it is useful to note that, when applying Eq. (A.12) to a tilted cylinder, the values of both D and S change. The reason is that when we calculate the surface integrals, the result will be proportional to the cylinder's immersed volume. As the cylinder tilts, both the immersed surface and linear dimensions increase more than in the case of sinking without tilting, so the drag force is bigger in the former case. Considering, for instance, the situation represented in the lower row of Fig. 2, when the cylinder sinks a distance Δh, the surface and linear dimensions increase as the inverse of $\cos\theta$ (of course, other intruder geometries may follow different laws).

To test it, let us assume a simplified model: the increase factor of S and D is proportional to the characteristic size of the cross section of the cylinder projected on the horizontal plane, i.e., it is proportional to the inverse of $\cos\theta$. Then, instead of D and S, we will solve Eq. (A.12) using $D/\cos\theta(t)$ and $S/\cos\theta(t)$, where $\theta(t)$ is a function that grows from zero to the maximum angle θ_{max} reached by the cylinder, mimicking Fig. 6(c), i. e. with the same time constant.

The consequences can be seen in Fig. 16. While in the beginning the sinking process in all situations occurs with the same dynamics, as the cylinder approaches the final angle, the behavior changes, being the final depth larger for the situations corresponding to low tilting.

The upper curve, calculated for $\theta = 0$ coincides with the upper curve in the inset of Fig. 15 (calculated for $p = 0$). Subsequent curves are calculated for values of θ_{max} varying in steps of $\pi/15$, the lowermost curve corresponds to $\theta_{max} = \pi/3$. As the inclination of the cylinder increases, both the buoyancy and the viscous drag do. The effect of these factors on the sinking process of Ring cylinders was already noted in Fig. 6(b): an immediate consequence is the decrease of the sinking depth (for a given Γ), compared with that of the No-ring ones, which can be easily observed in the experiments. From the inset it is possible to deduce that, for the larger angles, a small decrease in the depth is observed.

In spite of the simplifications assumed, it is worth noting that one of the basic differences between Fig. 7 (a) and (b) –for a given Γ the No-ring cylinders sink deeper than the Ring ones– could be qualitatively described by our model.

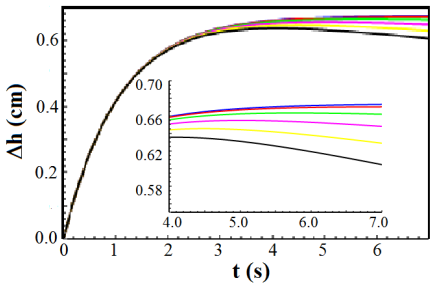

FIG. 16. (color online) Time dependence of sinking depth as calculated solving numerically Eq. (A.12) considering the variation of S and D provoked by tilting (see text). Upper curve is for $\theta_{max} = 0$ while the lower one is for $\theta_{max} = \pi/3$. Between them, θ_{max} varies in steps of $\pi/15$. The inset shows the last three seconds.

Finally, there is another element that was neither considered by us: as the container shakes horizontally, it produces a horizontal drag that changes periodically its direction. According to [60], it creates an additional lift force, and also a dependence of the drag force with depth, which, of course, must influence the detailed penetration dynamics of the Ring cylinders. The results of Li et al [40] also support these ideas.

2. Density profile of the granular medium

At each time step the simulation box is subdivided into a fixed number of rectangles for which the density is calculated as $\rho = m/V$, where m is the sum of the masses of all the particles of the granular medium within each rectangle and V is the volume of the rectangle calculated as its area multiplied by the average diameter of the particles of the medium inside it.

The density profile for each dimensionless acceleration Γ is obtained by calculating the average of the density profile at each time step. The latter is obtained by averaging the profiles

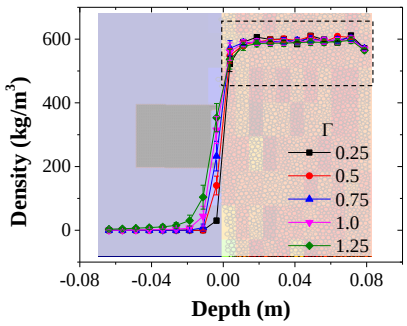

FIG. 17. (color online) Density profiles for the different values of dimensionless acceleration Γ obtained from the simulations. The background shows the subdivision of the simulation box where the color of each rectangle goes sequentially from blue to red and represents its density. The intruder is represented in light gray.

of a set of rectangle columns near the intruder. These columns are chosen avoiding the presence of the intruder in them in order not to affect the density profile since only the particles that compose the granular medium are taken into account in its calculation.

Figure 17 shows the density profiles as a function of depth for the different values of Γ. As can be seen in the region of the graph enclosed by dashed lines, the density of the medium saturates rapidly with increasing depth for all dimensionless accelerations. This fact supports from the simulations the use of $p = 0$ in expression A.3 of Appendix 1.

[1] J. D. Bray, J. P. Stewart, M. B. Baturay, T. Durgunoglu, A. Önalp, R. B. Sancio, J. P. Stewart, D. Ural, A. Ansal, J. B. Bardet, and et. al., Damage patterns and foundation performance in adapazari, Earthquake Spectra **16**, 163 (2000).

[2] R. B. Sancio, J. D. Bray, J. P. Stewart, T. L. Youd, H. T. Durgunoglu, A. Önalp, R. B. Seed, C. Christensen, M. B. Baturay, and T. Karadayılar, Correlation between ground failure and soil conditions in adapazari, turkey, Soil Dynamics and Earthquake Engineering **22**, 1093 (2002).

[3] R. B. Sancio, J. D. Bray, T. Durgunoglu, and A. Önalp, Performance of buildings over liquefiable ground in adapazari, turkey, in *Proc., 13th World Conf. on Earthquake Engineering* (Canadian Association for Earthquake Engineering Vancouver, Canada, 2004).

[4] N. Ambraseys, Engineering seismology: Part i, Earthquake Engineering & Structural Dynamics **17**, 1 (1988).

[5] S. Ben-Zeev, L. Goren, S. Parez, R. Toussaint, C. Clément, and E. Aharonov, The combined effect of buoyancy and excess pore pressure in facilitating soil liquefaction, in *Poromechanics VI* (2017) pp. 107–116.

[6] S. Ben-Zeev, E. Aharonov, R. Toussaint, S. Parez, and L. Goren, Compaction front and pore fluid pressurization in horizontally shaken drained granular layers, Physical Review Fluids **5**, 054301 (2020).

[7] K. Vanneste, M. Meghraoui, and T. Camelbeeck, Late quaternary earthquake-related soft-sediment deformation along the belgian portion of the feldbiss fault, lower rhine graben system, Tectonophysics **309**, 57 (1999).

[8] N. R. Council, *Liquefaction of Soils During Earthquakes* (The National Academies Press, Washington, DC, 1985).

[9] J. Berrill and R. Davis, Energy dissipation and seismic liquefaction of sands: revised model, Soils and foundations **25**, 106 (1985).

[10] E. Clement and J. Rajchenbach, Fluidization of a bidimensional powder, EPL (Europhysics Letters) **16**, 133 (1991).

[11] C. Wang and M. Manga, *Earthquakes and Water* (Springer-Verlag Berlin Heidelberg, 2009).

[12] H. M. Jaeger, S. R. Nagel, and R. P. Behringer, Granular solids, liquids, and gases, Reviews of modern physics **68**, 1259 (1996).

[13] T. Shinbrot and F. J. Muzzio, Reverse buoyancy in shaken granular beds, Phys. Rev. Lett. **81**, 4365 (1998).

[14] E. Altshuler, O. Ramos, E. Martínez, A. J. Batista-Leyva, A. Rivera, and K. E. Bassler, Sandpile formation by revolving rivers, Phys. Rev. Lett. **91**, 014501 (2003).

[15] I. S. Aranson and L. S. Tsimring, Patterns and collective behavior in granular me-

dia: Theoretical concepts, Reviews of modern physics **78**, 641 (2006).

[16] B. Andreotti, Y. Forterre, and O. Pouliquen, *Granular media: between fluid and solid* (Cambridge University Press, 2013).

[17] E. Altshuler, R. Toussaint, E. Martínez, O. Sotolongo-Costa, J. Schmittbuhl, and K. J. Måløy, Revolving rivers in sandpiles: From continuous to intermittent flows, Phys. Rev. E **77**, 031305 (2008).

[18] J. Boudet, Y. Amarouchene, B. Bonnier, and H. Kellay, The granular jump, Journal of Fluid Mechanics **572**, 413 (2007).

[19] J. L. Vinningland, Ø. Johnsen, E. G. Flekkøy, R. Toussaint, and K. J. Måløy, Granular rayleigh-taylor instability: Experiments and simulations, Phys. Rev. Lett. **99**, 048001 (2007).

[20] Ø. Johnsen, R. Toussaint, K. J. Måløy, and E. G. Flekkøy, Pattern formation during air injection into granular materials confined in a circular hele-shaw cell, Phys. Rev. E **74**, 011301 (2006).

[21] Ø. Johnsen, R. Toussaint, K. J. Måløy, E. G. Flekkøy, and J. Schmittbuhl, Phys. Rev. E **77**, 011301 (2008).

[22] M. J. Niebling, E. G. Flekkøy, K. J. Måløy, and R. Toussaint, Sedimentation instabilities: impact of the fluid compressibility and viscosity, Phys. Rev. E **82**, 051302 (2010).

[23] M. J. Niebling, E. G. Flekkøy, K. J. Måløy, and R. Toussaint, Mixing of a granular layer falling through a fluid, Phys. Rev. E **82**, 011301 (2010).

[24] M. J. Niebling, R. Toussaint, E. G. Flekkøy, and K. J. Måløy, Dynamic aerofracture of dense granular packings, Phys. Rev. E **86**, 061315 (2012).

[25] S. Turkaya, R. Toussaint, F. K. Eriksen, M. Zecevic, G. Daniel, E. G. Flekkøy, and K. J. Måløy, Bridging aero-fracture evolution with the characteristics of the acoustic emissions in a porous medium, Frontiers in Physics **3**, 70 (2015).

[26] J. Uehara, M. Ambroso, R. Ojha, and D. J. Durian, Low-speed impact craters in loose granular media, Phys. Rev. Lett. **90**, 194301 (2003).

[27] J. Boudet, Y. Amarouchene, and H. Kellay, Dynamics of impact cratering in shallow sand layers, Phys. Rev. Lett. **96**, 158001 (2006).

[28] H. Katsuragi and D. J. Durian, Unified force law for granular impact cratering, Nature physics **3**, 420 (2007).

[29] D. I. Goldman and P. Umbanhowar, Scaling and dynamics of sphere and disk impact into granular media, Phys. Rev. E **77**, 021308 (2008).

[30] F. Pacheco-Vázquez, G. Caballero-Robledo, J. Solano-Altamirano, E. Altshuler, A. Batista-Leyva, and J. Ruiz-Suárez, Infinite penetration of a projectile into a granular medium, Phys. Rev. Lett. **106**, 218001 (2011).

[31] L. Kondic, X. Fang, W. Losert, C. O'Hern, and R. Behringer, Microstructure evolution during impact on granular matter, Phys. Rev. E **85**, 011305 (2012).

[32] H. Torres, A. González, G. Sánchez-Colina, J. Drake, and E. Altshuler, Impact dynamics in "hard" and "soft" granular matter, Revista Cubana de Física **29**, 1 (2012).

[33] A. H. Clark and R. P. Behringer, Granular impact model as an energy-depth relation, EPL (Europhysics Letters) **101**, 64001 (2013).

[34] J. Ruiz-Suárez, Penetration of projectiles into granular targets, Reports on Progress in Physics **76**, 066601 (2013).

[35] T. A. Brzinski, P. Mayor, and D. J. Durian, Depth-dependent resistance of granular media to vertical penetration, Phys. Rev. Lett. **111**, 168002 (2013).

[36] E. Altshuler, H. Torres, A. González-Pita, G. Sánchez-Colina, C. Pérez-Penichet, S. Waitukaitis, and R. Hidalgo, Settling into dry granular media in different gravities, Geophysical Research Letters **41**, 3032 (2014).

[37] S. Joubaud, T. Homan, Y. Gasteuil, D. Lohse, and D. van der Meer, Forces encountered by a sphere during impact into sand, Phys. Rev. E **90**, 060201 (2014).

[38] R. Harich, T. Darnige, E. Kolb, and E. Clément, Intruder mobility in a vibrated granular packing, EPL (Europhysics Letters) **96**, 54003 (2011).

[39] É. Kolb, J. Cviklinski, J. Lanuza, P. Claudin, and É. Clément, Reorganization of a dense granular assembly: The unjamming response function, Phys. Rev. E **69**, 031306 (2004).

[40] C. Li, T. Zhang, and D. I. Goldman, A terradynamics of legged locomotion on granular media, science **339**, 1408 (2013).

[41] J. Aguilar and D. I. Goldman, Robophysical study of jumping dynamics on granular media, Nature Physics **12**, 278 (2016).

[42] W. Kang, Y. Feng, C. Liu, and R. Blumenfeld, Archimedes' law explains penetration of solids into granular media, Nature communications **9**, 1 (2018).

[43] V. L. Díaz-Melián, A. Serrano-Muñoz, M. Espinosa, L. Alonso-Llanes, G. Viera-López,

and E. Altshuler, Rolling away from the wall into granular matter, Phys. Rev. Lett. **125**, 078002 (2020).

[44] M. Medved, H. M. Jaeger, and S. R. Nagel, Modes of response in horizontally vibrated granular matter, Europhysics Letters **52**, 66 (2000).

[45] C. A. Kruelle, Physics of granular matter: pattern formation and applications, Rev. Adv. Mater. Sci **20**, 113 (2009).

[46] S. Tennakoon, L. Kondic, and R. Behringer, Onset of flow in a horizontally vibrated granular bed: Convection by horizontal shearing, EPL (Europhysics Letters) **45**, 470 (1999).

[47] L. Liu and R. Dobry, Seismic response of shallow foundation on liquefiable sand, Journal of geotechnical and geoenvironmental engineering **123**, 557 (1997).

[48] G. Sánchez-Colina, L. Alonso-Llanes, E. Martinez, A. Batista-Leyva, C. Clement, C. Fliedner, R. Toussaint, and E. Altshuler, Note:"lock-in accelerometry" to follow sink dynamics in shaken granular matter, Review of scientific instruments **85**, 126101 (2014).

[49] C. Clément, R. Toussaint, and E. Aharanov, Shake and sink: liquefaction without pressurization, arXiv preprint arXiv:1802.04391 (2018).

[50] C. Clément, R. Toussaint, M. Stojanova, and E. Aharonov, Sinking during earthquakes: Critical acceleration criteria control drained soil liquefaction, Phys. Rev. E **97**, 022905 (2018).

[51] The maximum oscillation amplitude that the shaker can generate is 13 mm. For a frequency of 5.0 Hz, the maximum possible acceleration is 12.83 m/s^2.

[52] U.S. Geological Survey, Shakemap scientific background, `https://earthquake.usgs.gov/data/shakemap/background.php`, accessed: 2021-11-5.

[53] H. Goto, Y. Kaneko, J. Young, H. Avery, and L. Damiano, Extreme accelerations during earthquakes caused by elastic flapping effect, Scientific Reports **9**, 1117 (2019).

[54] P. A. Cundall and O. D. Strack, A discrete numerical model for granular assemblies, Geotechnique **29**, 47 (1979).

[55] S. Parez, E. Aharonov, and R. Toussaint, Unsteady granular flows down an inclined plane, Phys. Rev. E **93**, 042902 (2016).

[56] A. P. Thompson, H. M. Aktulga, R. Berger, D. S. Bolintineanu, W. M. Brown, P. S. Crozier, P. J. in 't Veld, A. Kohlmeyer, S. G. Moore, T. D. Nguyen, R. Shan, M. J. Stevens, J. Tranchida, C. Trott, and S. J. Plimpton, Lammps - a flexible simulation tool for particle-based materials modeling at the atomic, meso, and continuum scales, Computer Physics Communications **271**, 108171 (2022).

[57] R. Toussaint, C. Clément, C. Fliedner, M. Stojanova, E. Aharonov, G. Sanchez, E. Altshuler, A. Batista, and E. Grude Flekkoy, Soil liquefaction: how the granular medium evolves, macroscale and microscale study, in *EGU General Assembly Conference Abstracts* (2014) p. 12539.

[58] J. R. de Bruyn and A. M. Walsh, Penetration of spheres into loose granular media, Canadian Journal of Physics **82**, 439 (2004).

[59] M. Hou, Z. Peng, R. Liu, Y. Wu, Y. Tian, K. Lu, and C. Chan, Projectile impact and penetration in loose granular bed, Science and Technology of Advanced Materials **6**, 855 (2005).

[60] X. Zhang, D. Sheng, G. P. Kouretzis, K. Krabbenhoft, and S. W. Sloan, Numerical investigation of the cylinder movement in granular matter, Phys. Rev. E **91**, 022204 (2015).

CHAPTER 3

Rotation of square prisms into granular matter

Pending submission
L. Alonso-Llanes et al..

Résumé (French abstract)

Nous étudions la pénétration d'un intrus cubique libéré à différents angles d'attaque à l'intérieur d'une cellule de Hele-Shaw quasi-bidimensionnelle remplie d'un milieu granulaire. Pendant la pénétration, l'intrus tourne de telle manière que sa position angulaire finale est proche de zéro, c'est-à-dire que sa surface inférieure est parallèle au fond du récipient. Ce phénomène intéressant a été observé pour différents angles initiaux de l'intrus, sauf pour 45 degrés, où la position angulaire est restée stable. Nous proposons un modèle phénoménologique basé sur la théorie de la force résistive (RFT) pour décrire sa dynamique de pénétration et de rotation dans des conditions non-quasi-statiques. Nous constatons que la RFT parvient à décrire quantitativement les mouvements d'inclinaison et d'enfoncement, bien que ces derniers présentent certaines divergences.

Controlling sedimentation by tilting: penetration of prisms into granular matter

L. Alonso-Llanes,[1,2,*] M. Espinosa,[1] R. Toussaint,[2,3] and E. Altshuler[1,†]

[1] *Group of Complex Systems and Statistical Physics, Physics Faculty, University of Havana, 10400 Havana, Cuba*
[2] *Université de Strasbourg, CNRS, Institut Terre et Environnement de Strasbourg, UMR7063, 67000 Strasbourg, France*
[3] *PoreLab, The Njord Centre, Department of Physics, University of Oslo, P.O. Box 1074 Blindern, 0316 Oslo, Norway*

The penetration of solids into granular matter is relevant for many natural and industrial processes. However, controlled studies have mostly tackled the case where the intruder is released on the granular surface along one of its symmetry axes. Here, we study the penetration into a granular medium of a square prism intruder released at different angles of attack inside a quasi-bidimensional Hele-Shaw cell. During penetration, the intruder rotates in such a way that its final angular position relative to the horizontal is close to zero, i.e., its bottom surface ends up parallel to the bottom of the container. This behavior was observed for different initial angles of the intruder, except for 45 degrees, where the average angular position remained stable. We propose a phenomenological model based on the resistive force theory (RFT) to describe its penetration and rotation dynamics under non-quasistatic conditions. We find that the RFT is capable of semi-quantitatively describe both tilting and sinking motions observed in experiments.

I. INTRODUCTION

Over the last decades, the scientific community has been quite interested on granular materials, not only because they show phenomena from other fields of physics but also because they are attractive on their own. The penetration of intruders into granular beds has not been exempt of this interest and has received substantial attention very recently [1–18]. By taking into account similarities and differences between flowing matter and fluids, a few models to calculate the forces acting on intruders moving through granular matter have been proposed [19–26]. One theory that has shown to be very effective, despite its simplicity, is the resistive force theory (RFT) which assumed that the resistive forces against the motion of intruder surfaces is well represented by a superposition principle.

In this paper we investigate experimentally the penetration of a square prism intruder into granular matter released at the free surface at different angles relative to the horizontal. Our results reveal that both the shape of the trajectory and the rotation of the intruder can be controlled by the released angle. Surprisingly, the observed results can be reproduced at least semi-quantitatively by the RFT model, extending its application boundaries into uncharted territory.

II. EXPERIMENTAL RESULTS

Experiments took place inside a quasi-2D Hele-Shaw cell 47.5 cm wide and 48.0 cm high consisting in two vertical glasses separated by a gap of 5.3 cm with walls at the bottom and sides (Fig. 1(a)) [13]. The cell was filled up with expanded polystyrene spherical beads of a bulk density 14 ± 2 kg/m^3 and diameter distributed between 2.0 mm and 6.5 mm.

An intruder consisting in a rectangular parallelepiped of $5.2 \times 6.9 \times 6.9$ cm^3 with a bulk density of 986 kg/m^3, was released on the free surface of the granular medium from the center of the cell at different orientation angles (attack angles relative to the horizontal direction). The release of the intruders is made by means of an electromagnetic device eliminating undesired linear or angular initial velocities. After each experiment, the polystyrene beads are removed and then gently deposited

* laciel.alonso@gmail.com
† ealtshuler@fisica.uh.cu

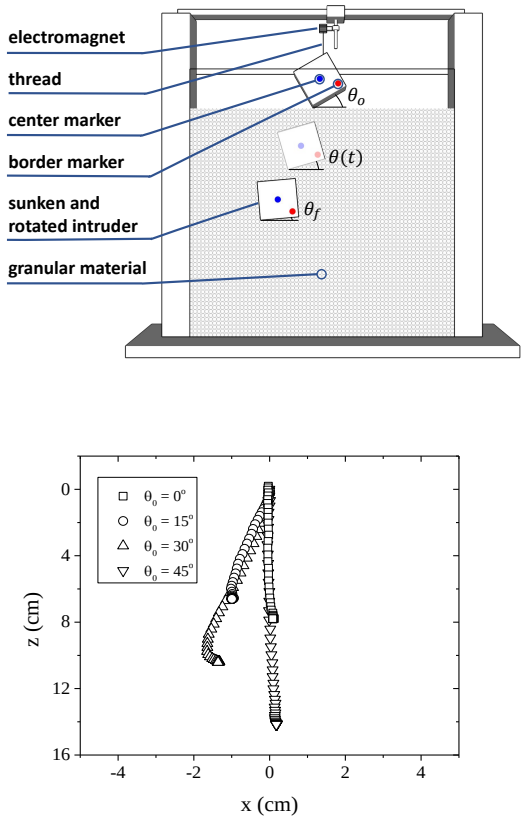

FIG. 1. (a) Experimental setup. (b) Average trajectories followed by intruders released at different initial angles relative to the horizontal.

back into the cell using a specially designed funnel to help ensure reproducibility of the preparation [13]. Finally, the cell is shaken horizontally, flattening the free surface of the granular medium to a height of about 40 cm. The intruder is then placed in such a way that its lower extreme is gently touching the free granular surface, and released. The presence of markers on the intruder (see Fig. 1(a)) makes it possible to follow its sinking and tilting dynamics from videos recorded by a camera at 1080p@120fps where at least 10 repetitions was performed for each angle of attack. All the video processing was made using a python library [27] from which the rotation of the intruder and the trajectories of its center of mass were obtained.

III. RESULTS AND DISCUSSIONS

Figure 1(b) shows the average trajectories described by the intruder released at different orientation angles. It is noteworthy how intruders with initial rotation angles of 15 and 30 degrees describe similar trajectories during their sinking, as if they were sliding down an inclined plane. For their part, the released intruders with attack angles of 0 and 45 degrees nearly followed a vertical trajectory, also shared for the most part, with very little displacement along the x direction.

Figure 2(a) shows the time evolution of the angle between the bottom side of the intruder and the horizontal direction, for each of the initial orientations under study. Here, the correlation between rotation and displacement in the x direction, early mentioned in Fig. 1(b), can be seen: only intruders with 15 and 30 degrees rotated and displaced considerably. The displacement can be understood by analyzing the normal drag forces acting on the intruder surfaces which, having horizontal components, push the square prism to the side. Interestingly, these intruders show a correction in their orientation as they sink (they decrease their rotation with respect to the horizontal direction), moving to the most stable orientation (i.e., with one face parallel to the bottom of the cell). This correction is directly associated with the geometry of the intruder and the depth dependence of the resistive forces, which are larger on the surface regions that are deeper inside the granular medium, thus producing torques that act as "rotation rectifiers". On average, at angles of attack of 0 and 45 degrees, the intruder ends up its motion with the same orientation, since the resulting torque due to the forces on its surfaces is close to zero. Nevertheless, at 45 degrees, relatively large deviations in the final orientation are observed, making it an unstable initial orientation, therefore 0 degrees emerges as the most stable orientation during sinking. For similar reasons, the differences in vertical displacement shown in Fig. 2(b) appear, since the vertical components of the resistive forces normal to the intruder surfaces are larger for orientations near 0 degrees and smaller for those near 45 degrees.

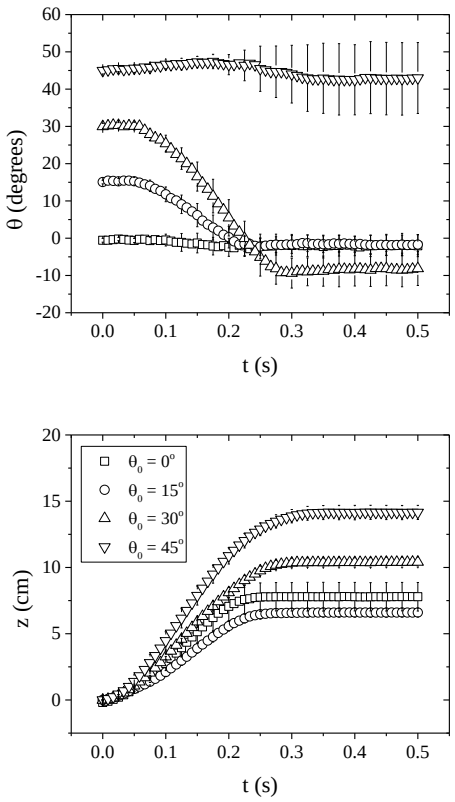

FIG. 2. Time evolution of the (a) the orientation angle and (b) of the vertical displacement z of intruders released at different attack angles.Each curve shown is averaged over 10 repetitions and bars represent standard deviation from the mean.

A. Interpretation of the results in terms of the Resistive Force Theory (RFT)

The granular resistive force theory (RFT) is inspired by a related rule-set for swimming microorganisms at low Reynolds numbers and states that the total resistive force acting on a quasi-2D intruder moving in the xz-plane can be obtained as the sum of the resistive forces (f_x,f_z) on each of its boundary surfaces (or surface elements) [4]. These forces depend only on the position, orientation and direction of motion of the surface in consideration, with no cross-correlation with the rest of them, which can be approximated by:

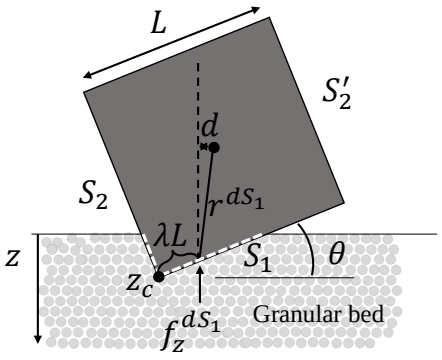

FIG. 3. Sketch used to derive model equations.

$$(f_x, f_z) = \int_S (\alpha_x(\theta,\gamma), \alpha_z(\theta,\gamma)) z H(z) dS \quad (1)$$

where S represents the surface of the intruder, θ the orientation angle of the differential surface element, and γ the intrusion angle, both measured with respect to the horizontal direction, as shown in Fig. 3. The term $zH(z)$, where H is the Heaviside function, avoids the existence of resistive forces on the surface elements outside the granular medium and increases the resistance linearly with the depth z.

The key ingredient of RFT is the choice of α_x and α_z which has to be done based on the experiments. As mentioned above, RFT makes use of the superposition principle, so the square-faced cuboid can be separated into several surfaces in the xz-plane. For a complete description of the dynamics the surfaces S_1 and S_2, are the only ones taken into account, since they are the ones in contact with the granular bed. The surface $S_2^{'}$ is included through boundary conditions.

To solve Eq. (1) we will first consider that the motion of the intruder is confined to the z-direction, that is, $f_z >> f_x$ and $v_z >> v_x$ along its entire path, which makes $\gamma = \pi/2$ and reduces the analysis to one dimension. We then consider that the drag force on the surface elements is symmetric about $\theta = 0$ degrees; larger for small values of the orientation angle, and zero for $\theta = \pi/2$. Taking into ac-

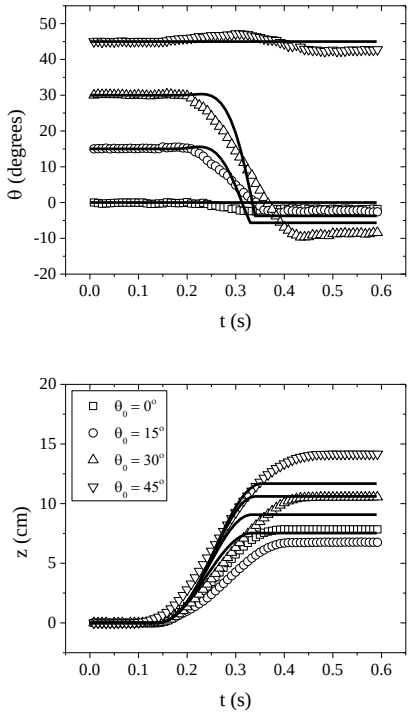

FIG. 4. Temporal evolution of (a) the orientation and (b) the vertical displacement for the initial angles under study. Lines represent the model output.

count all of the aforementioned, an expression for α_z is proposed, where c_1 is a constant free parameter with pressure dimensions:

$$\alpha_z(\theta) = c_1 \cos^2\theta \tag{2}$$

Finally, we set the net force F_z equal to zero when the intruder stops its penetration, i.e., when v_z becomes zero for the first time after the release, since the intruder's stopping is discontinuous in terms of acceleration [21]. This constraint is used to avoid the bouncing of the intruder if f_z becomes bigger than Mg (where M is the intruder's mass and g the acceleration of gravity) which is not seen in experiments. Once the intruder stops, the frictional support provided by the distribution of the force chains is such that it compensates the effect of the force of gravity acting on the intruder: $|f_z|$ decreases sharply from a value above Mg to a value equal to Mg at the end of the trajectory.

In our model only the action of the gravity force and the forces generated on the surfaces were considered. The viscous drag force (i.e., a linear relation between drag force and velocity) was not taken into account because, unlike ordinary fluids, viscosity is not dominant for penetrations at relatively low velocities [22]. All these elements are represented by the following equation for the vertical force:

$$F_z = Mg - f_z(S_1) - f_z(S_2) = M\ddot{z} \tag{3}$$

where:

$$\begin{aligned} f_z(S_1) &= c_1 L \cos^2\theta \int_0^{f_1(\theta,z)} (z_c - \lambda L \sin\theta) d\lambda \\ f_z(S_2) &= c_1 L \sin^2\theta \int_0^{f_2(\theta,z)} (z_c - \lambda L \cos\theta) d\lambda \end{aligned} \tag{4}$$

with

$$\begin{aligned} f_1(\theta, z) &= min(1, z/(L\sin(\theta)) \\ f_2(\theta, z) &= min(1, z/(L\cos(\theta)) \end{aligned} \tag{5}$$

For the net torque we have:

$$\vec{\tau} = \vec{\tau}(S_1) + \vec{\tau}(S_2) = \frac{1}{6} M L^2 \ddot{\theta} \tag{6}$$

where

$$\begin{aligned} \tau(S_1) &= c_1 L^2 \cos^2\theta \int_0^{f_1(\theta,z)} (z_c - \lambda L \sin\theta)(\lambda\cos\theta - 1/2(\cos\theta - \sin\theta)) d\lambda \\ \tau(S_2) &= c_1 L^2 \sin^2\theta \int_0^{f_2(\theta,z)} (z_c - \lambda L \cos\theta)(\lambda\sin\theta + 1/2(\cos\theta - \sin\theta) - I(\theta)\cos(\theta)) d\lambda \end{aligned} \tag{7}$$

Magnitude	Value
M	0.237 kg
g	9.81 m/s^2
L	0.068 m
c_1	900 N/m^2

TABLE I. Parameters used in the model. The first three are directly taken from the experiment, while the third is a fitting parameter.

with $I(\theta) = (1/2)\,\mathrm{sign}\,\theta(\mathrm{sign}\,\theta - 1)$ is used to take into account the role exchange between S_2 and $S_2^{'}$ when $\theta < 0$.

Eqs. (3) and (6) are solved for the values shown in Table I where all parameters were directly extracted from the experiment, and c_1 was taken as a fitting parameter. Fig. (4) shows the results obtained for both tilt and vertical displacement as a function of time. Note that the analytical model is able to reproduce the average behaviors for angular orientation and vertical penetration. However, some discrepancies are noticeable in the fits for both the time evolution and the final values. The largest ones are observed for the vertical penetration with $\theta_0 = 15^o$ and $\theta_0 = 45^o$,while for the tilt it is $\theta_0 = 30^o$. Furthermore, the model brings out equilibrium orientations of the system, $\theta_0 = 0^o$ and $\theta_0 = 45^o$, similar to what was observed in experiments. The increase in vertical penetration with θ_0 is also observed.

Fig. 5(a) summarizes the performance of the model in quantitatively reproducing the total intruder rotation for all orientations used. It also clearly shows how the intruders during this non-quasi-stationary sinking tend to rectify the initial rotation they possess, with the exception of those orientations where hardly any resulting torque is generated.

From Fig. 5 (b) we can conclude that the model manages to quantitatively reproduce the experimental results, with the exception of the vertical displacement for $\theta_0 = 15^o$ and $\theta_0 = 45^o$ which shows relatively small deviations (20%). This suggests that RFT could be useful to explain also non-quasistatic penetration in granular media and highlights the importance in analytical modeling of a force linearly dependent on depth of penetration. On the other hand, it confirms that non-quasistatic penetration in granular media should not be modeled using continuous resistive forces, since there is no elastic contribution in the granular impact drag force and the rebound obtained by solving the equation of motion, when $v = 0$, is not observed experimentally. This is due to the nature of force chains: they do not "push" the intruder up; rather, they offer resistance to penetration in the form of "barriers" whose stability increases with depth. The intruder stops when it reaches a "barrier" that it cannot "pass through".

IV. CONCLUSIONS

We have systematically studied the penetration of a square prism intruder released at different angles of attack inside a quasi-dimensional Hele-Shaw cell. During penetration, the intruder rotates in such a way that its final angular position is close to zero, i.e., its bottom surface parallel to the bottom of the container. Similar behaviors were observed for all the different initial angles of the intruder, except for 45 degrees, where the average angular position remained unchanged. We proposed a phenomenological model based on resistive force theory (RFT) to describe its penetration and rotation dynamics under non-quasistatic conditions, showing that RFT theory is capable of quantitatively describe both tilting and sinking motions.

ACKNOWLEDGMENTS

We thank the support provided by the French Embassy in Havana through its Cooperation and Cultural Action Service (SCAC), Campus France, the ITES and the University of Strasbourg. We also thank to the INSU ALEAS program, the International Associate Laboratory France-Norway on Deformation Flow and fracture of disordered Materials LIA D-FFRACT and the Research Council of Norway through its Centres of Excellence funding scheme, project number 262644.

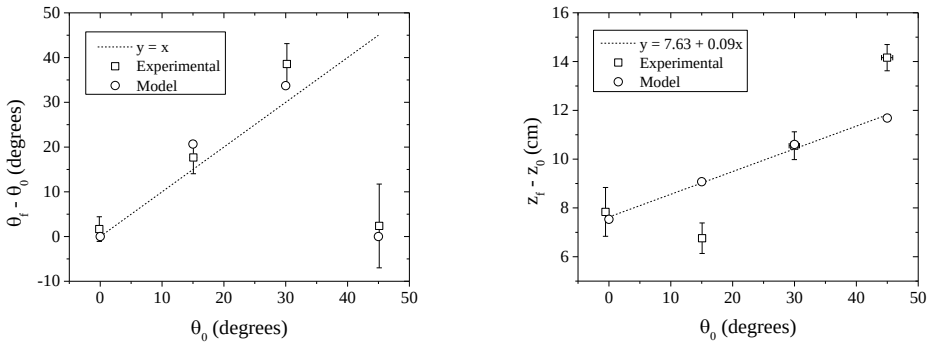

FIG. 5. Total (a) rotation and (b) sinking as function of the angle of attack.

[1] J. Ruiz-Suárez, Penetration of projectiles into granular targets, Rep. Prog. Phys. **76**, 066601 (2013).

[2] G. Sánchez-Colina, L. Alonso-Llanes, E. Martínez, A. J. Batista-Leyva, C. Clement, C. Fliedner, R. Toussaint, and E. Altshuler, Note: "lock-in accelerometry" to follow sink dynamics in shaken granular matter, Review of Scientific Instruments **85**, 126101 (2014).

[3] E. Altshuler, H. Torres, A. González-Pita, G. Sánchez-Colina, C. Pérez-Penichet, S. Waitukaitis, and R. Hidalgo, Geophys. Res. Lett. **41**, 3032 (2014).

[4] H. Askari and K. Kamrin, Intrusion rheology in grains and other flowable materials, Nature Mater **15**, 1274 (2016).

[5] W. Kang, Y. Feng, C. Liu, and R. Blumenfeld, Archimedes' law explains penetration of solids into granular media, Nature communications **9**, 1 (2018).

[6] H. Zheng, D. Wang, D. Z. Chen, M. Wang, and R. P. Behringer, Intruder friction effects on granular impact dynamics, Phys. Rev. E **98**, 032904 (2018).

[7] M. Harrington, H. Xiao, and D. J. Durian, Stagnant zone formation in a 2d bed of circular and elongated grains under penetration, Granular Matter **22**, 10.1007/s10035-019-0981-8 (2019).

[8] S. Kumar, M. Dhiman, and K. A. Reddy, Magnus effect in granular media, Phys. Rev. E **99**, 012902 (2019).

[9] C.-P. Liu, S. Bai, and L. Wang, Resistance forces on an intruder penetrating partially fluidized granular media, Phys. Rev. E **99**, 012903 (2019).

[10] T. Hossain and P. Rognon, Drag force in immersed granular materials, Phys. Rev. Fluids **5**, 054306 (2020).

[11] K. Huang, D. Hernández-Delfin, F. Rech, V. Dichtl, and R. C. Hidalgo, The role of initial speed in projectile impacts into light granular media, Scientific Reports **10**, 10.1038/s41598-020-59950-z (2020).

[12] S. Shah, C. Cheng, P. Jalali, and L. Kondic, Failure of confined granular media due to pullout of an intruder: from force networks to a system wide response, Soft Matter **16**, 7685 (2020).

[13] V. L. Díaz-Melián, A. Serrano-Muñoz, M. Espinosa, L. Alonso-Llanes, G. Viera-López, and E. Altshuler, Rolling away from the wall into granular matter, Phys. Rev. Lett. **125**, 078002 (2020).

[14] S. Agarwal, A. Karsai, D. I. Goldman, and K. Kamrin, Efficacy of simple continuum models for diverse granular intrusions, Soft Matter **17**, 7196 (2021).

[15] S. Agarwal, A. Karsai, D. I. Goldman, and K. Kamrin, Surprising simplicity in the modeling of dynamic granular intrusion, Science Advances **7**, eabe0631 (2021).

[16] M. Espinosa, V. Diaz-Melian, A. Serrano-Munoz, and E. Altshuler, Intruders cooperatively interact with a wall into granular matter, Granular Matter **24**, 2 (2022).

[17] L. Alonso-Llanes, G. Sánchez-Colina, A. J. Batista-Leyva, C. Clément, E. Altshuler, and R. Toussaint, Sink versus tilt penetration into shaken dry granular matter: The role of the

foundation, Phys. Rev. E **105**, 024903 (2022).

[18] A. Seguin, Forces on an intruder combining translation and rotation in granular media, Phys. Rev. Fluids **7**, 034302 (2022).

[19] M. Pica Ciamarra, A. H. Lara, A. T. Lee, D. I. Goldman, I. Vishik, and H. L. Swinney, Dynamics of drag and force distributions for projectile impact in a granular medium, Phys. Rev. Lett. **92**, 194301 (2004).

[20] M. A. Ambroso, R. D. Kamien, and D. J. Durian, Dynamics of shallow impact cratering, Phys. Rev. E **72**, 041305 (2005).

[21] H. Katsuragi and D. J. Durian, Unified force law for granular impact cratering, Nature physics **3**, 420 (2007).

[22] D. I. Goldman and P. Umbanhowar, Scaling and dynamics of sphere and disk impact into granular media, Phys. Rev. E **77**, 021308 (2008).

[23] F. Pacheco-Vázquez, G. A. Caballero-Robledo, J. M. Solano-Altamirano, E. Altshuler, A. J. Batista-Leyva, and J. C. Ruiz-Suárez, Infinite penetration of a projectile into a granular medium, Phys. Rev. Lett. **106**, 218001 (2011).

[24] H. Katsuragi and D. J. Durian, Drag force scaling for penetration into granular media, Phys. Rev. E **87**, 052208 (2013).

[25] A. H. Clark and R. P. Behringer, Granular impact model as an energy-depth relation, EPL (Europhysics Letters) **101**, 64001 (2013).

[26] T. A. Brzinski, P. Mayor, and D. J. Durian, Depth-dependent resistance of granular media to vertical penetration, Phys. Rev. Lett. **111**, 168002 (2013).

[27] A. Reyes, G. Viera-Lopez, J. Morgado-Vega, and E. Altshuler, yupi: Generation, tracking and analysis of trajectory data in python, arXiv preprint arXiv:2108.06340 (2021).

Rotation of intruders into granular matter: DEM simulations and experiments

In the previous article we studied experimentally the rotation of a square prism intruder which is dropped with different attack angles and proposed a RFT model for describing it. Here we try to reproduce the experimental results obtained using DEM simulations. We also compare these results to simulations and new experiments of an intruder with the same shape than the previous one and with foundations attached to its bottom, as shown in the Fig. 1. These intruders are equivalents to the intruders studied in Chapter 2 for a cell under shaking. We will refer to them as no-legs and two-legs intruders, respectively.

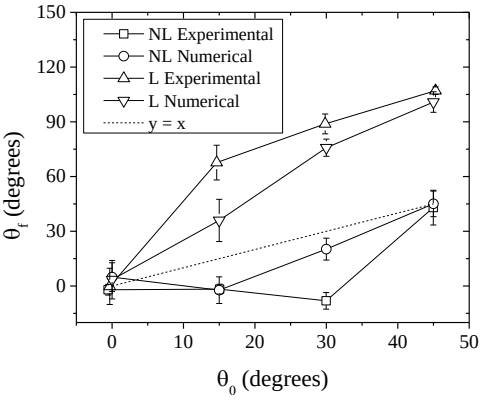

FIG. 2. Final orientation θ_f of the studied intruders released with different attack angles θ_0.

I. DEM SIMULATIONS

Two-dimensional DEM simulations were performed using the Large-scale Atomic/Molecular Massively Parallel Simulator (LAMMPS) [1]. In these, all the geometrical parameters corresponding both to the intruder and the cell were set as in the experimental setup. Similarly, for the particles composing the granular medium we used randomly distributed diameter values within the experimental range; their bulk density also coincided with the real one.

No-legs intruders were created as rigid bodies composed of several particles whose bulk density was set so that the intruder sinks were comparable to those obtained experimentally. The diameter of its particles was chosen small enough such that the edges of the intruder mimicked a smooth surface for the medium. Two-legs intruders were created by adding more grains at the bottom of no-legs intruders to create the foundations. Both intruders have same size than the experimental ones.

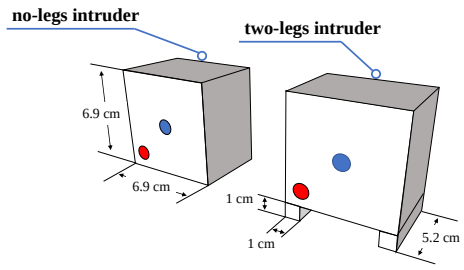

FIG. 1. Intruders with their dimensions indicated. (a) no-legs intruder (b) two-legs intruder.

The granular bed is prepared by the random generation of particles inside an small region that moves vertically until the height of the medium is approximately 40 cm, as in the experiments performed. This manner of depositing the grains ensures a quick relaxation of the medium. Since DEM simulations are deterministic, in order to achieve reasonable statistics we prepared different media varying the seed of the random generator.

Once the medium is created the intruder is placed at the horizontal center of the cell and at a vertical position 5 mm higher than the maximum y-coordinate of the particles below it. Then, it is released with an acceleration of $g = 9.8$ m/s^2. Simulation stops once the

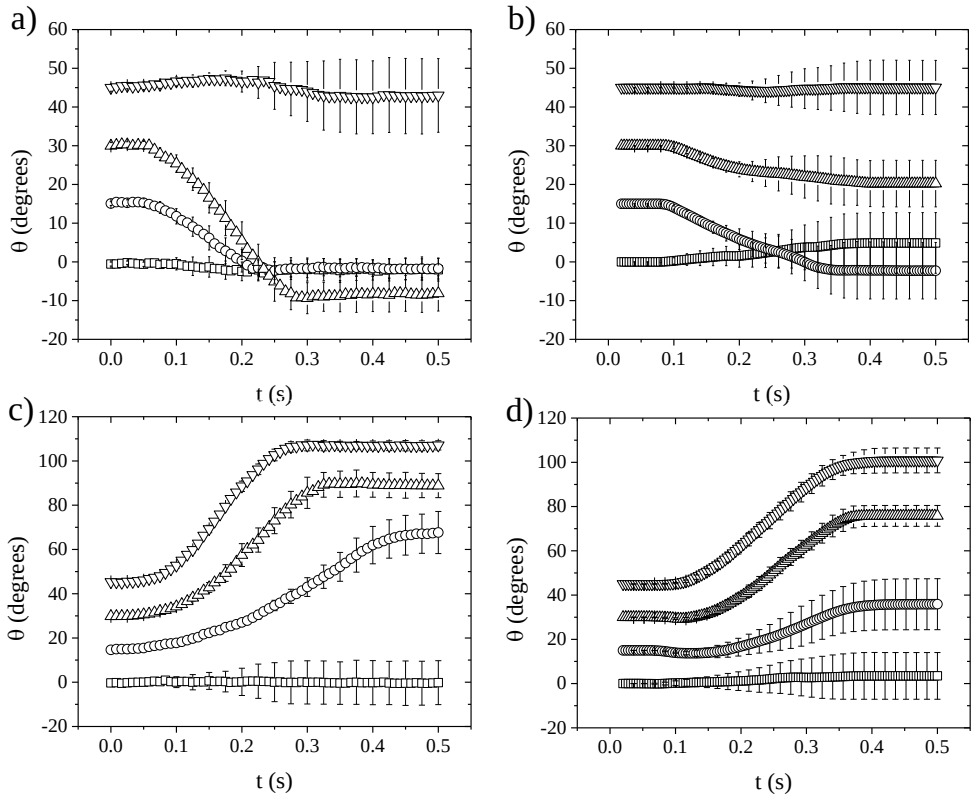

FIG. 3. Rotation with different initial orientation angles. Time evolutions, (a) experimental and (b) numerical for no-legs intruders and (c) experimental and (d) numerical for two-legs intruders. θ is measured from the horizontal. Each curve shown is averaged over 10 repetitions and bars represent its standard deviations.

total kinetic energy of the grains reach a value under 10^{-7} J.

For all the interactions, grain-grain, grain-wall and grain-intruder, we used a Hertzian contact model with friction and restitution coefficients of 0.5 and 0.1 respectively. For the elastic properties of the material we used a Young's modulus of 10^7 Pa and Poisson ratio of 2/7. The effective stiffness k_n was defined in terms of the shear modulus of the grains G and the Poisson ratio, as stated in [2].

II. RESULTS AND DISCUSSION

The final orientation angle as function of the initial angle obtained for the two different intruders is shown in Fig. 2. It is observed that the quasi-2D simulations capture the essence of the phenomenon. The first feature worth noting is the difference in the sense of rotation of the two types of intruders: two-legs intruders rotate counterclockwise while no-legs intruders rotate clockwise. This difference is closely related to the results discussed in Chapter 2 of the present thesis when it was observed that no-ring intruders rectified the rotation produced by the cell oscillation while ring intruders were inclined to high values of angles during sinking into the granular bed. The origin of this difference is undoubtedly due to the foundations, i.e., the presence of the legs.

Compared to the intruder without legs, the presence of the left leg has a reducing effect on the value of the rectifying torque (clockwise,

in this case) generated in the deepest part of the intruder, where the force exerted by the medium is greater. Here, the moment arm is smaller since the presence of the legs hardly shifts the intruder's center of mass due to their low density. On the other hand, the presence of the right leg increases the torque generated, counterclockwise, due to the jamming of the grains with it, similar to what occurred for a ring intruder.

Simulations reproduce the experimental results quite well for no-legs intruders. The only significant discrepancy is for the attack angle of 30 degrees, where the simulation underestimates the value of the rotation by a factor of 3.8. For two-legs intruders, the results differ more, although the same qualitative behavior is observed between simulations and experiments and the deviation between both point curves decreases as the angle of attack increases. Figure 3 shows the time evolution of the tilting angles for the two intruder types.

As discussed in Fig. 2 and in the main article, it can be seen how the no-legs intruder corrects its inclination during penetration (see Fig. 3(a) for the experimental and (b) numerical results). Only for the 45 degree case this correction is not appreciable, however, the relatively large statistical dispersion of the final orientation for this angle of attack reveals that 45 degrees is an unstable orientation for the intruder. Any perturbation during sinking will cause the intruder to move to lower or higher angles.

The rotational symmetry of order 4 possessed by the no-legs intruder reduces the entire analysis to angles between 0 and 90 degrees. However, those angle intervals between (0° - 45°) and (45° - 90°) have reflection symmetry with respect to a plane that passes through the geometric center of the intruder and is perpendicular to the base of the cell. Therefore, when the intruder departs from 45 degrees, towards upper or lower angles, it always tends to an orientation in which one of its sides is parallel to the bottom of the cell, which makes the orientations $k\pi/2$ (with $k = 0, 1, 2, 3$) stable points of the system. In order to confirm the above statement, simulations with angles of attack around 45 degrees were performed. Figure 4 shows the final orientations of no-legs intruders released with angles between 32 and 58 (or -32) degrees. Here it can be appreciated the symmetry of the system that was mentioned before. Despite that static granular matter exhibits history dependence (history-dependent grain network structure determines how force is scattered by force chains) simulations show expected average behaviors. Once the intruder deviates from the 45-degree orientation, there is an unbalance between the torques generated on surfaces, being greater on the one whose rotation with respect to the horizontal is smaller (the intrusion angle is considered equal to 90 degrees, as in the RFT model) since the resistance generated by the surface is greater the closer its angular orientation is to 0 [3]. If, on the contrary, a slight inclination with respect to 45 degrees is given initially, on average the intruder will tend to continue to move away from 45 degrees.

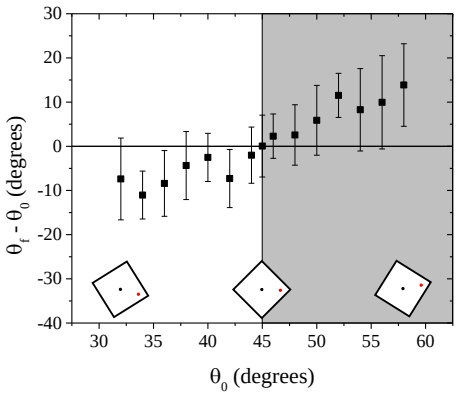

FIG. 4. Rotation of no-legs intruders released at different attack angles close to 45 degrees, specifically from 32 to 58 (or -32). Points represent average values over 10 repetitions and error bars its standard deviations.

Two-legs intruders do not have stable orientations for the angles of attack tested. For these intruders, the stable orientation must be at 180 degrees where again, one flat surface of the intruder will tend to be parallel to the base of the cell. An inclination of 90 degrees does not constitute a stability point since the presence of the legs slightly moves the center of mass of the intruder, therefore, with this orientation and as a result of the jamming of

the grains between the legs, a counterclockwise torque must be generated.

III. CONCLUSIONS

We have numerically analyzed the penetration of a square prism intruder released at different angles of attack inside a quasi-dimensional Hele-Shaw cell by qualitatively reproducing the experimental results. We confirmed that the 45 degree orientation is an unstable point for the intruder which moves away from it with small perturbations or small relative initial rotations. We have also performed experimental and numerical analyses of the rotation in square prism intruders with two legs as foundations and compared them with the previous ones.

[1] S. Plimpton, Fast parallel algorithms for short-range molecular dynamics, Journal of Computational Physics **117**, 1 (1995).

[2] H. P. Zhang and H. A. Makse, Jamming transition in emulsions and granular materials, Phys. Rev. E **72**, 011301 (2005).

[3] H. Askari and K. Kamrin, Intrusion rheology in grains and other flowable materials, Nature Mater **15**, 1274 (2016).

CHAPTER 4

Continuous to intermittent flows in growing granular heaps

Published

L. Alonso-Llanes et al. Physical Review E, ***106****, 014904, 2022.*

doi: https://doi.org/10.1103/PhysRevE.106.014904

Résumé (French abstract)

Si un matériau granulaire est versé par le haut sur une surface horizontale entre deux plaques parallèles et verticales, un tas de sable se développe avec le temps. Pour les petits tas, les grains s'écoulent doucement vers le bas, mais à partir d'une taille critique Xc du tas, l'écoulement devient intermittent : des avalanches soudaines glissent vers le bas de l'apex vers la base, suivies d'un front montant qui remonte lentement, jusqu'à ce qu'une nouvelle avalanche descendante interrompe le processus. Au moyen d'expériences contrôlant la distance entre l'apex du tas de sable et le conteneur qui l'alimente par le haut, nous montrons que X_c croît linéairement avec le flux d'entrée, mais s'échelonne comme la racine carrée de la hauteur d'alimentation. Nous expliquons ces faits sur la base d'un modèle phénoménologique, et démontrons que nos expériences contrôlées permettent de prédire la valeur de X_c pour la situation courante dans laquelle la hauteur d'alimentation diminue lorsque la pile augmente en taille.

Continuous to intermittent flows in growing granular heaps

L. Alonso-Llanes,[1,2,*] E. Martínez,[3,*] A. J. Batista-Leyva,[1,4] R. Toussaint,[2,5,†] and E. Altshuler[1,‡]

[1] *Group of Complex Systems and Statistical Physics, Physics Faculty, University of Havana, 10400 Havana, Cuba*
[2] *Université de Strasbourg, CNRS, Institut Terre et Environnement de Strasbourg, UMR7063, 67000 Strasbourg, France*
[3] *Department of Physics, NTNU, NO-7491 Trondheim, Norway*
[4] *Instituto Superior de Tecnologías y Ciencias Aplicadas (InSTEC), University of Havana, 10400 Havana, Cuba*
[5] *SFF PoreLab, The Njord Centre, Department of Physics, University of Oslo, P.O. Box 1074 Blindern, 0316 Oslo, Norway*

If a granular material is poured from above on a horizontal surface between two parallel, vertical plates, a sand heap grows in time. For small piles, the grains flow smoothly downhill, but after a critical pile size X_c, the flow becomes intermittent: sudden avalanches slide downhill from the apex to the base, followed by an "uphill front" that slowly climbs up, until a new downhill avalanche interrupts the process. By means of experiments controlling the distance between the apex of the sandpile and the container feeding it from above, we show that X_c grows linearly with the input flux, but scales as the square root of the feeding height. We explain these facts from a phenomenological model based on the experimental observation that the flowing granular phase forms a "wedge" on top of the static one, differently from the case of stationary heaps. Moreover, we demonstrate that our controlled experiments allow to predict the value of X_c for the common situation in which the feeding height decreases as the pile increases in size.

I. INTRODUCTION

Granular matter is known to exhibit many unexpected behaviors [1–15] since, depending on the way it is handled, it behaves as a solid, a liquid or a gas [16, 17]. Most granular flows encountered in nature, and industry, are located in the liquid regime, where the material is dense but still flows as a fluid. This regime has received no little attention from the scientific community in the search for constitutive laws capable of reproducing the diversity of observed behaviors [18–24]. However, one behavior in particular has been poorly studied, and it constitutes the focus of our paper: the transition from continuous to intermittent flows (CIT).

The phenomenon was first described in the so-called rotating drum geometry, i.e., for a cylinder partially filled with granular matter rotating around its axis of symmetry, which lies in a plane perpendicular to the force of gravity. If this device rotates slowly enough, the particle flow near the free surface is intermittent producing avalanches. However, for higher rotational velocities, the particles establish a continuous flow such that the free surface shows a stationary profile, as reported by Rajchenbach [25].

Shortly after, Lemieux and Durian showed the existence of a continuous to intermittent transition in the flow of glass beads down a stationary heap, confined between plane-parallel walls, as the input flux decreased [26], which was corroborated by Jop *et al.* when studying the role of confinement in this type of geometry [21].

Altshuler and co-workers [27] also observed a CIT in narrow sand rivers moving through conical piles in various configurations: by increasing the pile base size, grown with constant input flux, or by varying the input flux in both open and closed piles with a constant size base. In another study by this group, they observed that the transition was maintained after reducing the pile dimension by confining it in a Hele-Shaw cell [28].

* These two authors contributed equally
† renaud.toussaint@unistra.fr
‡ ealtshuler@fisica.uh.cu

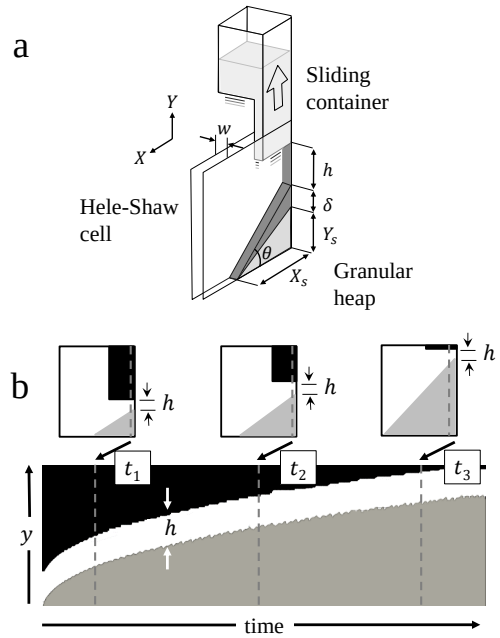

FIG. 1. Experimental setup. (a) Sketch of the experimental setup, where the sliding container allows to control the value of the grain feeding height, h (the darker color indicate the mobile grains) (b) Diagram showing three stages of the heap growth at constant h, corresponding to times t_1, t_2 and t_3. The upper side shows a lateral view of the Hele-Shaw cell including a vertical line of pixels that allows to construct the spatial-temporal diagram shown in the bottom panel. The diagram, which corresponds to a real experiment, illustrates the constancy of h.

More recently, Fischer *et al.* [29] found that for a given range of rotational speeds, rotating drums exhibit a progressive transition of flow by temporal intermittency, where spontaneous and erratic changes from one regime to another occur.

Here we study the CIT in a growing granular heap where the drop height of the grains is controlled in addition to the input flux. Our experiments reveal that the horizontal size of the pile where the CIT takes place, X_c, depends linearly on the input flux and varies as the squared root of the dropping height. We explain those scalings in terms of a model based on previous knowledge on dense granular flows. On the other hand, we show that it is possible to predict X_c without controlling the dropping height, based on the data obtained by controlling it.

II. EXPERIMENTAL

A sand heap is grown into a Hele-Shaw cell of width $w = 12$ mm consisting in two vertical glass plates perpendicular to a flat horizontal surface of 28-cm long. One of the thin vertical sides of the cell is closed by a glass wall, and the opposite one is open. A thin stream of sand is dropped through a modifiable rectangular slit made in the bottom of a parallelepiped-shaped container held on top of the cell, so the sand enters parallel and near the thin, closed vertical wall of the Hele-Shaw cell. As a result, a sand heap forms that grows from the closed vertical wall to the open wall, as depicted in Fig. 1(a). The input flux F_{in} is obtained by processing images taken with a camera at a capture rate of 30 fps and a resolution of 1024×768 pixels: the total pile area is computed in each frame and F_{in} is determined as the slope of its dependence with time. F_{in} is defined as Q_{in}/w, where Q_{in} is the volumetric input flux. We used sand with a high content of silicon oxide and an average grain size of $d = 100$ μm from Santa Teresa (Pinar del Río, Cuba) [7, 27, 28].

A feature that distinguishes this setup from most of the ones reported in the literature is the fact that the distance between the point of delivery of the sand and the upper part of the heap, h, can be held constant in time (within a range from 1 cm to 15 cm) due to the vertical movement of the sand container, see Fig. 1 (b). This is particularly important for growing heaps since this distance changes during the experiments if the point of delivery is fixed, which is not the case in the commonly studied stationary heaps. The control of the deposition height is achieved thanks to a feedback system: when a laser light is interrupted by the growing tip of the heap, a signal is sent to a motor that rises the position of the sand container until a new laser beam is detected [30, 31]. The constancy of h is illustrated in the spatial-temporal diagram shown

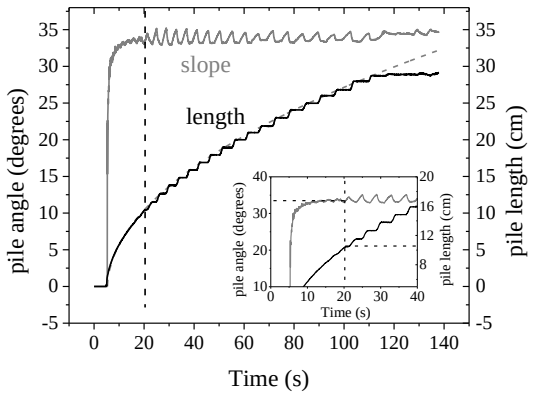

FIG. 2. Quantifying the continuous to intermittent flow transition. The gray continuous line corresponds to the temporal evolution of the average slope of the pile, while the black continuous line represents its horizontal length very near the bottom of the Hele-Shaw cell. The light gray line (dashed) is a fit following the law $x \sim t^{1/2}$. The transition occurs at $X_c \approx 10.3$ cm, $t_c \approx 20$ s and with a repose angle of $\theta_s \approx 33.5^\circ$, as clearly seen in the zoom shown in the inset. The data represented in the graphs correspond to a fixed input flux of $F_{in} = 2.68$ cm^2/s and a constant deposition height of $h \approx 1.5$ cm.

in Fig. 1(b) taken along a vertical line near the taller side of the heap. If the container is kept at a fixed height relative to the laboratory, the heap grows in a "conventional way", i.e., with h decreasing as the height of the pile increases, which may be more interesting for engineering applications.

III. RESULTS AND DISCUSSION

A. Presentation of the continuous to intermittent transition

As the piles grow, a transition between continuous to intermittent behavior is observed. From the time the first grains hit the floor of the Hele-Shaw cell, up to a certain horizontal length X_c of the bottom of the heap, the flow of grains is continuous: grains flow down the heap forming a fluid layer next to the free surface of the pile, which is approximately straight. As the horizontal length of the pile grows above X_c, an intermittent regime is reached: an "avalanche" of grains slides down the hill from the upper side of the pile all the way to the lower side and stops, forming a step-front that moves uphill as new grains are fed into the pile. Once the uphill step-front is within a few inches of the top of the pile, a new downhill avalanche takes place, and so on. The continuous to intermittent flow transition occurring at $X = X_c$ was originally reported for experiments in which h was not controlled [28], and has been recently seen by us for controlled height experiments [31].

For all combinations of deposition heights and fluxes studied, the transition can be visualized as in Fig. 2, which is based on a measurement using a fixed input flux of 2.68 cm^2/s and a constant deposition height $h \approx 1.5$ cm. The first quantity plotted is the length of the base along the horizontal axis near the bottom of the Hele-Shaw cell [32] as time goes by. We have plotted the temporal evolution of the average angle of the free surface relative to the horizontal. Both curves complement each other to extract the transition coordinates, as the vertical dashed line suggests.

The horizontal length of the pile grows as mass conservation dictates and stops for the first time after reaching a value of about 10.3 cm, from which it continues as steps. On the other hand, the average slope of the pile describes a similar behavior: it grows in time and then starts to oscillate around an average angle of approximately 33.5 degrees. Note that shortly before the onset of the oscillations the average slope has some noisy oscillations with relatively small amplitude that may be associated with a transient in which spontaneous transitions occur between both regimes as observed in rotating drums [29]. Both changes in behavior occur about 20 s after the beginning of the experiment (see vertical dashed line). That is just the moment when the growth of the horizontal length of the heap goes from a continuum to an intermittent regime: the horizontal steps correspond to the time intervals during which a step-front climbs uphill after each downhill avalanche, keeping constant the length of the pile. This feature is also seen in the curve of the angle where an increase in its value

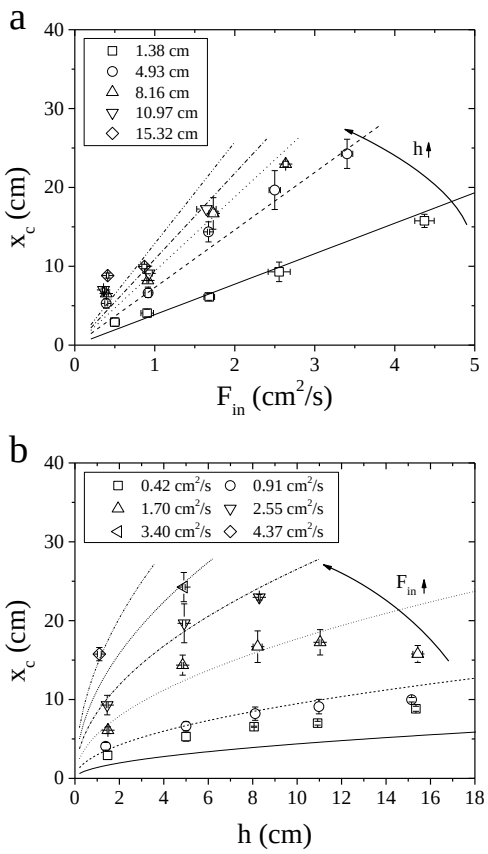

FIG. 3. Dependencies of the transition length on the input flux and deposition height. Transition length as a function of (a) the input flux, for different deposition heights and (b) the deposition height, for different input fluxes. Symbols represent experimental data while the lines the theoretical expression proposed in Eq. (3). Note that the bottom of the cell has a finite size of 28 cm, thus for certain parameter values the base of the pile reaches the open edge of the cell before transition occurs. This leads to some curves shown having fewer data points than others.

represents the climb of the step-front while a decrease represents the occurrence of one avalanche. Notice that after $t \approx 110$ s the pile bottom reaches the outlet, turning into a system widely studied in the literature (a stationary heap) which we do not discuss here.

B. Dependence of the transition coordinates on the input flux and deposition height

Fig. 3 shows the dependence of the pile transition lengths (X_c) on the input flux (F_{in}) and the deposition heights (h). Fig. 3(a) indicates that the dependence on the transition length is linear with the input flux. On the other hand, Fig. 3(b) shows that the transition length scales as the square root of the deposition height. These dependencies can be understood by means of a simple model of the growing heap explained in detail in the Appendix, see Fig. 7. Fig. 7(a) shows an image that reveals the geometry of the flowing layer during the continuous regime. The experiment was performed on silica sand with average diameter 1.5 mm, and a video was taken with a fast camera at 1000 fps. Note that, differently from the case of stationary heaps, the flowing layer is wedge-shaped in growing piles, where the wedge point is at the lower end of the pile. Fig. 7(b) shows a schematic based on the observed geometry, showing all the parameters used in our model.

Let us consider an incompressible flow of grains (ρ = constant) on the free surface of a growing heap during the continuous regime. Inside a control volume that moves with velocity $v_\perp$ to include only the fluid layer, the equations of mass and linear momentum (in the x-direction) conservation of the flowing grains are as follows:

$$\begin{aligned} \rho\frac{\partial\delta}{\partial t} + v_\parallel\frac{\partial\delta}{\partial x} &= -v_\perp \\ \rho\frac{\partial\left(v_\parallel\delta\right)}{\partial t} + \rho v_\parallel^2\frac{\partial\delta}{\partial x} &= -\frac{\partial\left(\delta\tau_{xx}\right)}{\partial x} + \tau_{yx} + \tau_{zx}\frac{\delta}{w} + \rho g\delta\sin\theta + (\rho v_x v_\perp)|_{y=0} \end{aligned} \tag{1}$$

In these equations δ is the thickness of the flowing layer of grains, and w its width,$v_\parallel$ =

$\frac{1}{\bar{\delta}w}\int_0^w\int_0^\delta v_x dzdy$ is the averaged velocity down the heap, where v_x is considered constant along the fluid layer as it is suggested by experimental measurements [21, 26]. τ_{xx} is the normal stress while τ_{yx} and τ_{zx} are the shear stresses at the interface between the flowing and static layers, and at the walls, respectively.

We make some other assumptions to simplify the equatios in (1). The normal stress τ_{xx} is considered as the dynamic pressure, equal to $\frac{1}{2}\rho v_\parallel^2$, and its variation in the flow direction (x) is neglected since changes in the layer thickness are small. The shear stresses $\tau_{yx} = \rho g\delta\cos\theta\tan\theta_s$ and $\tau_{zx} = \mu_w\rho g\delta\cos\theta$ are assumed as Coulomb's frictional stresses where $\tan\theta_s$ is the static friction of the pile μ_s and μ_w the dynamic friction coefficient of the grains with the walls. τ_{zx} is taken as suggested in [21]. $v_x|_{y=0}$ is expected to be equal or close to 0, so, $\rho v_x v_\perp$ is neglected. The quasi-steady solution of the obtained equations, the one in which a quasi-steady flow is considered where the time variations of δ and $v_\parallel$ are approximately equal to 0, gives (see the Appendix A for details),

$$L_x = \frac{3Q_{in}\alpha\sqrt{2gh}\sin\theta}{2g\bar{\delta}\cos\theta\left(-\tan\theta+\mu_w\frac{\bar{\delta}}{w}+\tan\theta_s\right)w} \tag{2}$$

Here $\bar{\delta} = (1/L_x)\int_0^{L_x}\delta dx$ and $Q_\perp = Q_{in} = v_\perp L_x w$, where $L_x = \frac{X}{\cos\theta}$ is the length of the interface between the flowing and static layers, and $v_\parallel = \alpha v_{in} = \alpha\sqrt{2gh}\sin\theta$, being v_{in} the velocity of the incoming grains (free fall) and $\alpha < 1$ a dimensionless constant that accounts for the energy loss after the impact on the tip of the pile of the grains coming from the container.

At the transition ($\theta \to \theta_s$) the thickness of the fluid layer reaches a minimum $\bar{\delta} = \delta_{stop}$, after which the flowing grains cannot "continually cover" the whole surface of the pile, therefore intermittency starts [20, 21, 26]. At this point, Eq. (2) transforms into the following:

$$X_c = \frac{3\alpha w\sin\theta_s}{\sqrt{2g}\mu_w\delta_{stop}^2}F_{in}h^{1/2} \tag{3}$$

Fig. 4 shows indeed that $P = X_c/(F_{in}\sqrt{h})$, which is the prefactor of Eq. (3), is roughly constant with no systematic dependence on the control parameters F_{in} and h. There is only a weak dependence observed for the lowest flux $F_{in} = 0.42$ cm^2/s for which this quantity slightly rises with h up to a value around 6 s/cm$^{3/2}$. Thus, Eq. (3) explains the general shape of the dependencies displayed in Fig. 3(a) and (b). These laws can be reproduced quantitatively using values shown in Table I, that correspond to a prefactor value of $P = X_c/(F_{in}\sqrt{h}) = 3.27 \pm 0.65$ s/cm$^{3/2}$. θ_s is taken from the experimental data while μ_w and δ_{stop} are taken from the literature typical

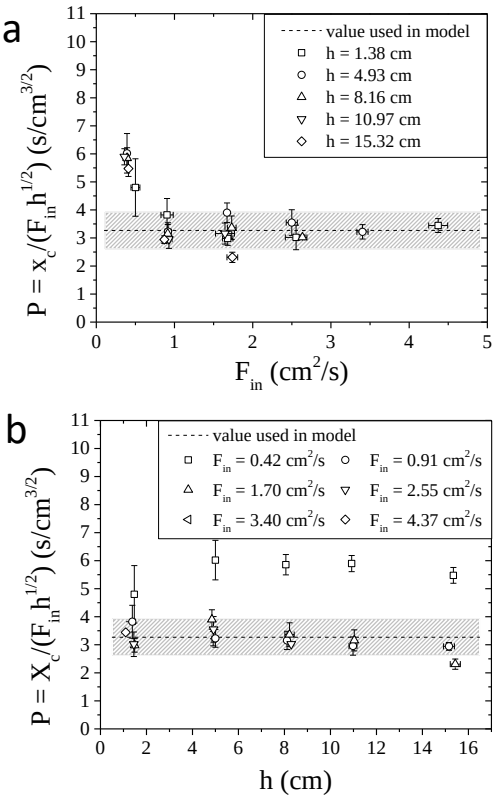

FIG. 4. Quantitative comparison between experiments and model. Dependence with the input flux (a) and with the deposition height (b) of the proportionality constant in Eq. (3), P. Black dashed lines represent the value of $P = X_c/(F_{in}\sqrt{h})$ used in our model to reproduce the experimental data and the height of the gray rectangles represents its standard error. $P_{model} = 3.27 \pm 0.65$ s/cm$^{3/2}$.

values of these quantities. That gives a value of $\alpha = 0.30$ which is our free parameter and suggests that the 70 % percent of the potential energy of the grains is dissipated due to the impact at the tip of the pile.

Magnitude	Value
θ_s	33.5°
μ_w	0.18 [21]
δ_{stop}	15 d = 0.15 cm [26]
α	0.30

TABLE I. Values of the quantities in eq. (3)

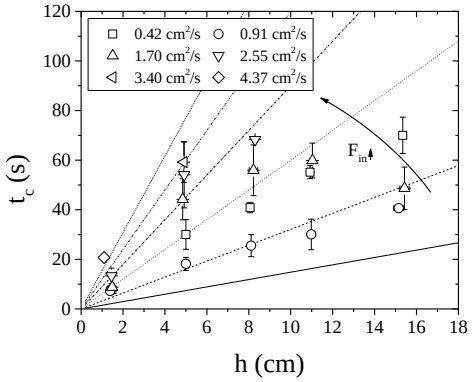

FIG. 5. Transition time dependency on the deposition height. Transition time as a function of deposition height for different input fluxes.

The agreement between the theoretical expression and the experimental measurements of X_c is satisfactory for all values of F_{in} and h tested, as seen on Figs. 3(a) and 3(b), comparing the theoretical expressions (lines) and experimental results (symbols). The only significant discrepancy is for the lowest input flux, where the model underestimates the value of X_c by a factor between 1.5 and 1.8. Apart from this outlying results at the lowest flux, and a point at $F_{in} = 1.7$ cm^2/s and $h = 15$ cm, all other experimental values of X_c lie within 18% of the theoretical value with fixed θ_s, μ_w, α and δ_{stop}.

Furthermore, taking into account that the conservation of mass imposes that the horizontal length of the pile scales with time as $t^{1/2}$ (see the fit displayed in Fig. 2), Eq. (3) immediately explains (at least semi-quantitatively) the experimental behavior illustrated in Fig. 5. It also predicts the behavior of t_c as a function of the input flux which, following the model, is given by (see the Appendix A),

$$t_c = \frac{9\alpha^2 w^2 \sin^2\theta_s \tan\theta_s}{4g\mu_w^2\delta_{stop}^4} F_{in} h \qquad (4)$$

Here the agreement between experimental data and theory is satisfactory as well, although less than for the value of X_c. Note that, apart from the lowest flux and two points with $F_{in} = 1.7$ cm^2/s, one with $h = 5$ cm and another with $h = 15$ cm, the experimental points lie within 23% of the theoretical value.

C. Predicting the transition: From fixed-h to variable-h piles

Differently from most of previous research, our experiments show the CIT in a completely controlled way: not only is the input flux controlled, but also the deposition height is fixed. In typical situations where some granular material is poured to form a growing heap, it is poured from a container without changing its position, so h decreases as the upper side of the heap grows. That behavior is showed for experiments we made with a fixed container and represented by the solid, decreasing lines in Fig. 6.

Fig. 6(a) shows how the deposition height decreases as the length of the pile increases while Fig. 6(b) shows its temporal evolution. Both behaviors can be modeled by applying the mass conservation principle, and approximating the pile as a triangular shape with fixed angle θ_s, height Y and base X. Since $Y + h = h_0$, $Y = X\tan\theta_s$, and from mass conservation $XY = 2Ft$, one obtains that h varies with the pile length as $h_0 - X\tan\theta_s$ and varies in time as $h_0 - \sqrt{2tF\tan\theta_s}$, where h_0 is the initial height of the container over the bottom of the Hele-Shaw cell and θ_s the critical angle of the pile surface. These expressions correspond to the two gray lines shown in Figs. 6 (a) and 6 (b). Their agreement with the experimental data, the black continuous line, is noticeable.

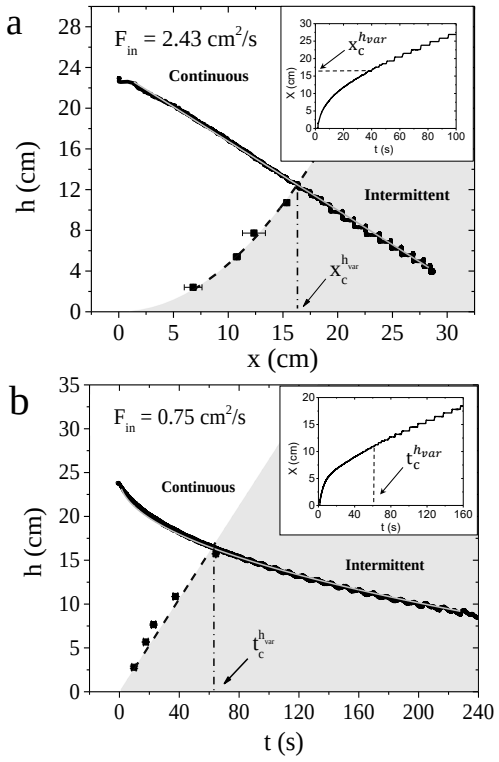

FIG. 6. Equivalence between fixed-h and variable-h experiments. The black solid lines show the deposition height for a variable-h experiment versus (a) the pile length and (b) the time, while the dashed increasing lines represent (a) a quadratic fit and (b) a linear fit to the dependence between the respective magnitudes at the transition for fixed-h experiments (squares are experimental points). Gray solid lines follow the law (a) $h = 23.5$ cm $-0.67x$ and (b) $h = 23.5$ cm $-(0.99$ cm$\cdot$s$^{-1/2})\sqrt{t}$. The insets display the time evolution of the pile horizontal length for variable-h experiments. (a) Input flow of 2.43 cm^2/s (b) Input flow of 0.75 cm^2/s.

The dashed lines in Fig. (6) are constructed by fits to the experimental data where X_c and t_c were obtained in different experiments controlling h (represented by squares). Each point of these lines corresponds to 6 (a) $X_c^{h_{fix}}$ and 6 (b) $t_c^{h_{fix}}$ for the different values of the fixed deposition height h_{fix}. The lines represent the interface between the continuous and the intermittent regimes for those input fluxes. Then, the length (time) at which the two curves intercept should match the transition length (time) for a free-h experiment, i.e., $X_c^{h_{fix}} = X_c^{h_{var}}$ ($t_c^{h_{fix}} = t_c^{h_{var}}$). The insets, which correspond to piles grown without controlling the deposition height, show that our prediction is correct in each case. Furthermore, using that idea it can be determined at which fixed-h the transition occurs at the same length or time for both kinds of experiments, fixed-h and variable-h.

IV. CONCLUSIONS

We performed a systematic study of the surface flow on a granular heap where grains are added from a controlled height, h. As the pile grows, the flow is first continuous, and then intermittent: for small piles, the free surface is smooth, but after reaching a horizontal pile size X_c avalanches flow down the hill, and step-like fronts then climb uphill until a new downhill avalanche occurs. We found that X_c grows linearly with the input flux, F_{in}, and as $h^{1/2}$ with the deposition height h. We explain these facts based on a model where mass and momentum are conserved taking into account the basal friction of the flowing grains with the quasi-static part of the heap as well as the friction with walls. Importantly, the model assumes that the layer of flowing grains is wedge-shaped in growing heaps, a fact that we demonstrate experimentally. Moreover, by systematically comparing experiments with controlled h and with non-controlled h (as typically reported in the literature) we are able to predict the values of X_c and t_c in the later case based on its values in the previous.

V. ACKNOWLEDGMENTS

We thank the support provided by Campus France Cuba, the French Embassy in Havana, the ITES, the University of Strasbourg, the INSU ALEAS program, the International Research Project France-Norway on Deformation Flow and fracture of disordered Materials IRP D-FFRACT and the Research Council of Nor-

way through its Centres of Excellence funding scheme, project number 262644. Discussions with Reinaldo García are gratefully acknowledged.

Appendix A: Deriving equations (3) and (4)

If we consider a flow of incompressible grains (ρ = constant) of thickness δ and width w on the free surface of a growing heap, using the Reynolds' transport theorem we can write the depth-averaged mass conservation equation for a control volume (CV), as the one showed in Figure 7. Here, $\vec{v}$ is measured relative to the control volume (CV) and the velocity along the x-direction considered constant $\frac{\partial v_x}{\partial x} = 0$ as it is suggested by experimental measurements [21, 26].

$$\begin{aligned} \frac{dm}{dt} &= \frac{\partial}{\partial t}\left(\int_{CV} \rho \, dV\right) + \int_{CS} \rho(\vec{v}\cdot\vec{n})\, dA \\ 0 &= \frac{\partial}{\partial t}\left(\rho w \delta dx\right) - \int \rho v_{\parallel} dA_1 + \int \rho v_{\perp} dA_2 + \int \rho v_{\parallel} dA_3 \\ 0 &= \rho\frac{\partial \delta}{\partial t} + \rho v_{\parallel}\frac{\partial \delta}{\partial x} + \rho v_{\perp} \end{aligned} \tag{A1}$$

The quasi-steady state solution gives

$$v_{\parallel}\frac{\partial \delta}{\partial x} = -v_{\perp} \tag{A2}$$

Now, doing the same analysis but for the linear momentum conservation,

$$\frac{d\vec{p}}{dt} = \frac{\partial}{\partial t}\left(\int_{CV} \vec{v}\rho \, dV\right) + \int_{CS} \vec{v}\rho(\vec{v}\cdot\vec{n}) dA \tag{A3}$$

and writing its force balance equation for the x-direction, we get,

$$\begin{aligned} \sum F_x &= \tau_{xx}\delta w - \left((\tau_{xx} + \frac{\partial \tau_{xx}}{\partial x}dx)(\delta + \frac{\partial \delta}{\partial x}dx)w\right) + \tau_{yx} w dx + 2\tau_{zx}\delta dx + \rho g \sin\theta \delta w dx \\ &= w dx\left(-\frac{\partial\left(\delta\tau_{xx}\right)}{\partial x} + \tau_{yx} + \tau_{zx}\frac{\delta}{w} + \rho g \delta \sin\theta\right) \end{aligned} \tag{A4}$$

In Eq. (A4) we take into account the normal and shear stresses in the x-direction on every control surface indicated in Fig. 7 as well as the shear stress on the walls confining the flow. Now, looking at the momentum exchange through the control surfaces,

$$\begin{aligned} \sum F_x &= \frac{\partial}{\partial t}\left(\int_{CV} \vec{v}\rho dV\right) + \int_{CS} \vec{v}\rho(\vec{v}\cdot\vec{n}) dA \\ &= \frac{\partial\left(v_{\parallel}\rho w \delta dx\right)}{\partial t} - \int v_{\parallel}\rho v_{\parallel} dA_1 + \int v_x \rho v_{\perp} dA_2 + \int v_{\parallel}\rho v_{\parallel} dA_3 \\ &= w dx\left(\rho\frac{\partial\left(v_{\parallel}\delta\right)}{\partial t}\right) - \rho v_{\parallel}^2 w\delta - (\rho v_x v_{\perp})|_{y=0} w dx + \rho v_{\parallel}^2 w\left(\delta + \frac{\partial \delta}{\partial x}dx\right) \\ &= w dx\left(\rho\frac{\partial\left(v_{\parallel}\delta\right)}{\partial t} - (\rho v_x v_{\perp})|_{y=0} + \rho v_{\parallel}^2\frac{\partial \delta}{\partial x}\right) \end{aligned} \tag{A5}$$

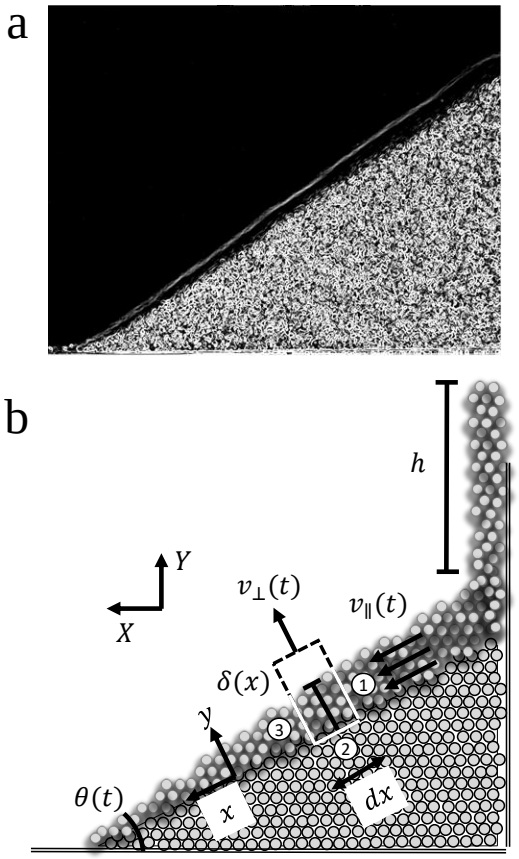

FIG. 7. (a) Flowing layer in a typical experiment during the continuous regime. The image is obtained from the overlay of 100 images (corresponding to 1/10 seconds) and then applying an edge detector. (b) Sketch used to derive the model equations. The region indicated with dashed lines represents the control volume (CV) while the solid white lines on top of them represent the control surfaces (CS) through which there is interchange of mass and momentum. The control volume moves with velocity $v_\perp$ to include only the fluid layer. The velocity $v_\parallel = \frac{1}{\delta w}\int_0^w \int_0^\delta v_x dz dy$.

Using Eq. A4 and A5,

$$\rho \frac{\partial \left(v_\parallel \delta\right)}{\partial t} + \rho v_\parallel^2 \frac{\partial \delta}{\partial x} = -\frac{\partial \left(\delta \tau_{xx}\right)}{\partial x} + \tau_{yx} + \tau_{zx}\frac{\delta}{w} + \rho g \delta \sin\theta + \left(\rho v_x v_\perp\right)|_{y=0} \tag{A6}$$

we get an expression for the momentum conservation in the (x) direction considering the interaction with the walls. Its quasi-steady state solution gives,

$$\begin{aligned} \rho v_\parallel^2 \frac{\partial \delta}{\partial x} &= -\frac{1}{2}\rho v_\parallel^2 \frac{\partial \delta}{\partial x} - \rho g \delta \cos\theta \tan\theta_s - \mu_w \rho g \delta \cos\theta \frac{\delta}{w} + \rho g \delta \sin\theta \\ v_\parallel \frac{\partial \delta}{\partial x} &= \frac{2 g \delta \cos\theta \left(\tan\theta - \mu_w \frac{\delta}{w} - \tan\theta_s\right)}{3 v_\parallel} \end{aligned} \tag{A7}$$

The normal stress τ_{xx} is considered as the dynamic pressure, equal to $\frac{1}{2}\rho v_\parallel^2$, and its vari-

ation in the flow direction (x) is neglected since changes in the layer thickness are small. The shear stresses $\tau_{yx} = \rho g \delta \cos\theta \tan\theta_s$ and $\tau_{zx} = \mu_w \rho g \delta \cos\theta$ are assumed as Coulomb's frictional stresses where $\tan\theta_s$ is the static friction of the pile μ_s and μ_w the dynamic friction coefficient of the grains with the walls. τ_{zx} is taken as suggested in [21]. $v_x|_{y=0}$ is expected to be equal or close to 0, so, $\rho v_x v_\perp$ is neglected. Combining equations (A2) and (A7),

$$L_x = \frac{3Q_{in}\alpha\sqrt{2gh}}{2g\bar{\delta}\cos\theta\left(-\tan\theta + \mu_w\frac{\bar{\delta}}{w} + \tan\theta_s\right)w} \tag{A8}$$

where $\bar{\delta} = (1/L_x)\int_0^{L_x}\delta dx$. We have used the fact that $Q_\perp = Q_{in} = v_\perp L_x w$, where $L_x = \frac{X}{\cos\theta}$ is the length of the interface between the the flowing and static layers, and $v_\parallel = \alpha v_{in}\sin\theta = \alpha\sqrt{2gh}\sin\theta$, being v_{in} the velocity of the incoming grains (free fall) and $\alpha < 1$ a dimensionless constant that accounts for the energy loss after the impact on the tip of the pile of the grains coming from the container.

At the transition ($\theta \to \theta_s$) the thickness of the fluid layer reaches a minimum $\bar{\delta} = \delta_{stop}$, after which the flowing grains cannot "continually cover" the whole surface of the pile, therefore intermittency starts [21, 26].

$$\lim_{\theta\to\theta_s} L_x = \frac{3\alpha\sqrt{h}Q_{in}\sin\theta_s}{\sqrt{2g}\delta_{stop}\cos\theta_s\mu_w\frac{\delta_{stop}}{w}w} \tag{A9}$$

$$X_c = \frac{3\alpha w\sin\theta_s}{\sqrt{2g}\mu_w\delta_{stop}^2}F_{in}h^{1/2} \tag{A10}$$

Assuming a triangular heap profile that grows with a constant angle θ_s, and using the principle of mass conservation we can write the following expression for the whole heap,

$$F_{in}t_c = \frac{1}{2}X_c^2\tan\theta_s \tag{A11}$$

Hence Eq. (4) can be obtained.

[1] J. B. Knight, H. M. Jaeger, and S. R. Nagel. Vibration-induced size separation in granular media: The convection connection. *Phys. Rev. Lett.*, 70:3728–3731, 1993.

[2] F. Melo, P. Umbanhowar, and H. L. Swinney. Transition to parametric wave patterns in a vertically oscillated granular layer. *Phys. Rev. Lett.*, 72:172–175, 1994.

[3] T. Le Pennec, K. J. Måløy, A. Hansen, M. Ammi, D. Bideau, and X. Wu. Ticking hour glasses: Experimental analysis of intermittent flow. *Phys. Rev. E*, 53:2257–2264, 1996.

[4] S. L. Conway, D. J. Goldfarb, T. Shinbrot, and B. J. Glasser. Free surface waves in wall-bounded granular flows. *Phys. Rev. Lett.*, 90:074301, 2003.

[5] N. Taberlet, P. Richard, E. Henry, and R. Delannay. The growth of a super stable heap: An experimental and numerical study. *Europhysics Letters (EPL)*, 68(4):515–521, 2004.

[6] H. Elbelrhiti, P. Claudin, and B. Andreotti. Field evidence for surface-wave-induced instability of sand dunes. *Nature*, 437:720–723, 2005.

[7] E. Martínez, C. Pérez-Penichet, O. Sotolongo-Costa, O. Ramos, K. J. Måløy, S. Douady, and E. Altshuler. Uphill solitary waves in granular flows. *Phys. Rev. E*, 75:031303, 2007.

[8] Ø. Johnsen, R. Toussaint, K. J. Måløy, E. G. Flekkøy, and J. Schmittbuhl. Coupled air/granular flow in a linear hele-shaw cell. *Phys. Rev. E*, 77:011301, 2008.

[9] F. Pacheco-Vázquez, G. A. Caballero-Robledo, J. M. Solano-Altamirano, E. Altshuler, A. J. Batista-Leyva, and J. C. Ruiz-Suárez. Infinite penetration of a projectile into a granular medium. *Phys. Rev. Lett.*, 106:218001, 2011.

[10] M. J. Niebling, R. Toussaint, E. G. Flekkøy, and K. J. Måløy. Dynamic aerofracture of dense granular packings. *Phys. Rev. E*, 86:061315, 2012.

[11] E. Altshuler, H. Torres, A. González-Pita, G. Sánchez-Colina, C. Pérez-Penichet, S. Waitukaitis, and R. C. Hidalgo. Settling into dry granular media in different gravities.

Geophysical Research Letters, 41(9):3032–3037, 2014.

[12] F. K. Eriksen, R. Toussaint, A. L. Turquet, K. J. Måløy, and E. G. Flekkøy. Pressure evolution and deformation of confined granular media during pneumatic fracturing. *Phys. Rev. E*, 97:012908, 2018.

[13] A. L. Turquet, R. Toussaint, F. K. Eriksen, G. Daniel, O. Lengliné, E. G. Flekkøy, and K. J. Måløy. Source localization of microseismic emissions during pneumatic fracturing. *Geophysical Research Letters*, 46(7):3726–3733, 2019.

[14] V. L. Díaz-Melián, A. Serrano-Muñoz, M. Espinosa, L. Alonso-Llanes, G. Viera-López, and E. Altshuler. Rolling away from the wall into granular matter. *Phys. Rev. Lett.*, 125:078002, 2020.

[15] M. Espinosa, V. L. Díaz-Melián, A. Serrano-Muñoz, and E. Altshuler. Intruders cooperatively interact with a wall into granular matter. *Granular Matter*, 24(1):1–8, 2022.

[16] H. M. Jaeger, S. R. Nagel, and R. P. Behringer. Granular solids, liquids, and gases. *Reviews of Modern Physics*, 68(4):1259, 1996.

[17] B. Andreotti, Y. Forterre, and O. Pouliquen. *Granular media: between fluid and solid*. Cambridge University Press, 2013.

[18] S. Douady, B. Andreotti, and A. Daerr. On granular surface flow equations. *The European Physical Journal B-Condensed Matter and Complex Systems*, 11(1):131–142, 1999.

[19] D. V. Khakhar, A. V. Orpe, P. Andresén, and J. M. Ottino. Surface flow of granular materials: model and experiments in heap formation. *Journal of Fluid Mechanics*, 441:255–264, 2001.

[20] GDR MiDi. On dense granular flows. *The European Physical Journal E*, 14:341–365, 2004.

[21] P. Jop, Y. Forterre, and O. Pouliquen. Crucial role of sidewalls in granular surface flows: consequences for the rheology. *Journal of Fluid Mechanics*, 541:167–192, 2005.

[22] P. Jop, Y. Forterre, and O. Pouliquen. A constitutive law for dense granular flows. *Nature*, 441(7094):727–730, 2006.

[23] Y. Forterre and O. Pouliquen. Flows of dense granular media. *Annual Review of Fluid Mechanics*, 40(1):1–24, 2008.

[24] P. Jop. Rheological properties of dense granular flows. *Comptes rendus physique*, 16(1):62–72, 2015.

[25] J. Rajchenbach. Flow in powders: From discrete avalanches to continuous regime. *Phys. Rev. Lett.*, 65:2221–2224, 1990.

[26] P.-A. Lemieux and D. J. Durian. From avalanches to fluid flow: A continuous picture of grain dynamics down a heap. *Phys. Rev. Lett.*, 85:4273–4276, 2000.

[27] E. Altshuler, O. Ramos, E. Martínez, A. J. Batista-Leyva, A. Rivera, and K. E. Bassler. Sandpile formation by revolving rivers. *Phys. Rev. Lett.*, 91:014501, 2003.

[28] E. Altshuler, R. Toussaint, E. Martínez, O. Sotolongo-Costa, J. Schmittbuhl, and K. J. Måløy. Revolving rivers in sandpiles: From continuous to intermittent flows. *Phys. Rev. E*, 77:031305, 2008.

[29] R. Fischer, P. Gondret, and M. Rabaud. Transition by intermittency in granular matter: From discontinuous avalanches to continuous flow. *Phys. Rev. Lett.*, 103:128002, 2009.

[30] L. Domínguez-Rubio, E. Martínez, and E. Altshuler. Opto-mechanical system for the controlled growth of granular piles. *Revista Cubana de Física*, 32(2):111–114, 2015.

[31] L. Alonso-Llanes, L. Domínguez-Rubio, E. Martínez, and E. Altshuler. Intermittent and continuous flows in granular piles: Effects of controlling the feeding height. *Revista Cubana de Física*, 34(2):133–135, 2017.

[32] The distance from the bottom is taken as half the width of the input jet of sand feeding the pile.

To go beyond (literally) From growing to stationary piles

I. CONTINUOUS TO CONTINUOUS

Consider a sand pile that grows into a Hele-Shaw cell as the one described in the previous paper. As our model is only written to describe the flow during the continuous regime we will consider first a situation in which the heap reaches the outlet of the cell while is still in the this flow regime. As we explained before, the shape of the fluid layer while the heap is growing is wedge-shaped. This is due to the exchange of grains between the two phases of the heap: the fluid and the solid, and it is effectively from the first to the second, resulting in a decrease of the thickness of the flowing layer from the higher to the lower end of the heap. However once the heap reaches the outlet and starts to spill, the shape of the fluid layer changes: it becomes a layer of constant thickness throughout the entire pile. Figure 1 shows the shape of fluid layer of a stationary pile, obtained of the same manner than the one showed in the main article for a growing heap.

The passing from a situation like the previously discussed in the thesis to an open system (or stationary) has never been studied, and it is a potentially difficult task. However, the mass conservation equation proposed in our model above correctly describes the transition, based on the following expression:

$$v_{\parallel}\frac{\partial h}{\partial x} = v_{\perp} \tag{1}$$

In equation (1), which corresponds to equation (A2) of the manuscript if $v_{\perp} = 0$, i.e. the heap is not growing, and the average velocity of the fluid layer parallel to the free surface $v_{\parallel}$ does not change, so the variation of the layer thickness $\frac{\partial h}{\partial x}$ is 0 as in the experimental observations.

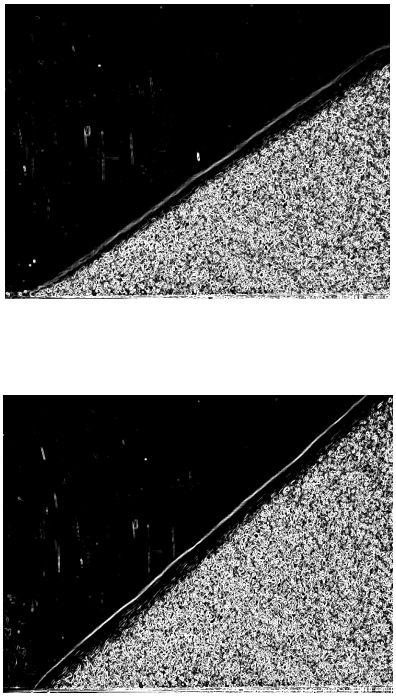

FIG. 1. Comparison between the flowing layer in (top) a growing heap and (bottom) an stationary heap.

II. INTERMITTENT TO CONTINUOUS/INTERMITTENT

If we consider the case of passing from a pile that grows in an intermittent regime (not described by our model), the situation that arises when the stationary pile spills can involve both a continuous or an intermittent regime, this will depend on the flow rate and on the size of the pile when it reaches the edge of the cell.

The transition from intermittent to continuous may be due to a reduction in the effective friction between the fluid layer and the solid layer. This justifies that, in order to stop the flow in a length equal to or less than that cor-

responding to the free surface of the pile, a smaller mass flow would be needed. In fact, we were able to verify with preliminary experiments that the flow that produces the transition in a growing heap differs, and is greater, than the flow that produces the transition in a stationary pile (if the latter has a horizontal size equal to X_c).

CHAPTER 5

Ground-based close-range photogrammetry for the monitoring of erosion: a preliminary study on a Cuban sandy coastal dune

Pending submission

L. Alonso-Llanes et al..

Résumé (French abstract)

La photogrammétrie est considérée comme une excellente alternative aux techniques coûteuses telles que la détection et la télémétrie par ondes lumineuses (LiDAR), qui peut également atteindre une grande précision dans la production de modèles numériques d'élévation (DEM). Ici, nous étudions l'évolution d'une dune de sable située sur une plage à l'est de La Havane. Après une période de 8 mois, nous avons mesuré une perte d'environ 1350 kg/m^2 (13500 tonnes/ha) équivalente à un taux d'érosion intense de 0,9 m. Les restrictions sanitaires liées au COVID-19 ont empêché l'accès au site étudié pendant près de deux ans, ce qui a interrompu temporairement l'étude qui était planifiée de façon régulière lors de cette thèse. Nous présentons ici les premiers résultats issus de l'analyse des deux premières campagnes de terrain.

Ground-based close-range photogrammetry for the monitoring of erosion: a preliminary study on a cuban sandy coastal dune

L. Alonso-Llanes,[1,2,*] J. L. Llicas,[1] E. Altshuler,[1] and R. Toussaint[2,3,†]

[1] *Group of Complex Systems and Statistical Physics, Physics Faculty, University of Havana, 10400 Havana, Cuba*
[2] *Université de Strasbourg, CNRS, Institut Terre et Environnement de Strasbourg, UMR7063, 67000 Strasbourg, France*
[3] *SFF PoreLab, The Njord Centre, Department of Physics, University of Oslo, P.O. Box 1074 Blindern, 0316 Oslo, Norway*

Photogrammetry is considered an excellent alternative to expensive techniques such as Light Detection and Ranging (LiDAR) that can also achieve high accuracy in the production of Digital Elevation Models (DEM). Here, we study the evolution of a sand dune located on a beach east of Havana. After a period of 8 months we measured a loss of approximately 1350 kg/m^2 (13500 ton/ha) equivalent to an intense erosion rate of 0.9 m.

I. INTRODUCTION

Digital Elevation Models (DEMs) are very useful sources of information for numerous studies in geosciences [1–6]. They are a representation of the topographic surface of the Earth, buildings or any other surface objects, i.e. an array of points in an area with their x, y, and z coordinates determined and whose creation is the first step in many studies of geomorphology, hydrology, and geophysics.

Nowadays, there exist many technologies capable of produce high-resolution DEMs with vertical accuracy as high as 10 centimeters, as it is the case of the Light Detection and Ranging (LiDAR) technique [7, 8].

However, the use of this technique is very expensive since it includes, apart from a laser scanner, a Global Positioning System (GPS), and an Inertial Navigation System (INS) [7, 8], which makes it unaffordable for certain studies, especially in developing countries. In these situations, photogrammetry is considered an excellent alternative that can also achieve high accuracy [9, 10]. According to the American Society for Photogrammetry and Remote Sensing, photogrammetry is defined as the art, science, and technology of obtaining reliable information about physical objects and the environment through processes of recording, measuring, and interpreting digital imagery. Through metric photogrammetry, precise measurements from photos and other information sources can be made to determine, in general, the relative locations of points, which enables finding distances, angles, areas, volumes, elevations, sizes and shapes of objects [9].

FIG. 1. The strong wind and sea waves associated to hurricane Irma removed several meters from the sand dune at "Santa María" beach in Havana, by September 2017. (Photo by E. Altshuler)

Recent advances in computer vision have made more flexible the reconstruction of 3D surfaces allowing the development of new photogrammetric algorithms with this purpose: bundle adjustment, camera auto (or self)-calibration, as well as digital image matching [9, 11].

Bundle adjustment is an iterative process to estimate the location in the space of 3D points

* lalonso@fisica.uh.cu
† renaud.toussaint@unistra.fr

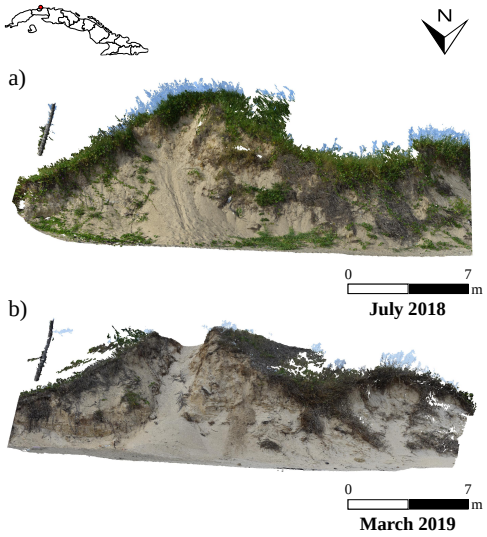

FIG. 2. Location and view of the point clouds of a portion of the dune under study at "Santa María" beach in Havana, Cuba.

from camera images. It includes not only the location of the points but also the location of the cameras when taking the images and where they were looking to. The technique consists of estimating projection matrices and 3D points which project to measured image points (from the photos) and also minimize the image distance between the reprojected point and detected (measured) image points for every view in which the 3D point appears.

Digital image matching techniques fall into three general categories: area-based methods, feature-based methods, and hybrid methods. Area-based methods perform image matching by numerical comparison on small subarrays of each image (normalized cross-correlation is perhaps the simplest area-based method). Feature-based methods are more complicated and involve feature extraction, which is composed of edges at different scales, with subsequent comparison based on feature characteristics such as size and shape. Feature-based image comparison requires techniques from the field of artificial intelligence in computer science. Hybrid methods are a combination of the first two approaches.

Photogrammetry can be used for determining erosion, which is one of the most common phenomena affecting sandy beaches and its ecosystems along the whole planet [12, 13]. Inevitably, climate change impacts on these systems will only exacerbate this situation. The shoreline retreat is recognized as a burgeoning threat because of global climate change and other anthropogenic activities that alter the natural processes of sustaining beaches and coasts. Cuba, being an island, must face this situation in order to take care of its beaches and ecosystems, since they constitute a fundamental asset for its tourism industry, beyond their intrinsic environmental values. This work presents a preliminary study of the transformation, due to erosion, of a sand dune located on a Cuban beach, using photogrammetry.

II. STUDY SITE AND DATA ACQUISITION

The dune studied is a sandy dune about 4 - 5 meters high and several tens of meters wide, located on one of the tourist beaches (Santa María beach) at the east of Havana, Cuba (Fig. 2). At present, its dynamics is controlled by local hydro-meteorological conditions and the human action of both visitors and the authorities in charge of the area's maintenance cleanliness. During the last few years substantial changes in sand dunes can be appreciated by simple eye inspection as a result of hurricane activity, usually during the period between June and November (see Fig. 1). The relatively high rates of change that occur during this period pose a great challenge for displacement measurements, since they often lead to signal decorrelation in the multi-temporal analysis of DEM models. On the other hand, they also make long-term maintenance of in-situ measurement devices difficult, although in this case this is not the only impediment: being a public place, human presence can be also invasive.

Our team has conducted ground-based image acquisition since the summer of 2018 at regular intervals. A Nikon D3300 camera with an 18 - 55 mm zoom lens has been used for this purpose. All acquired images were obtained with the same focal length (18mm), to avoid

possible influences on the reconstruction, with a compromise to have sufficiently high shutter speeds while using a small aperture to ensure deep depth of field. Lighting conditions in most cases allowed a good compromise between these parameters while maintaining the sensor sensitivity at minimum (ISO - 100). Images were captured at approximately the same time of day to minimize the influence of shadows, and at distances from the target surface between 2 and 20 meters with a resolution of 6000x4000 in JPEG format.

Some ground control points (GCPs) were visually identified in natural objects located in stable parts outside the main study region and known distances were used for the model scaling. However, some of them moderately changed position or disappeared after large magnitude events, so we were forced to manually intervene in the alignment of the models corresponding to different dates.

III. PROCESSING METHODS

Surface reconstruction is performed with the non-free software Agisoft Photoscan Professional™ which is a stand-alone software product that performs photogrammetric processing of digital images and generates 3D spatial data for use in GIS applications [14]. Photoscan [15] contains tools for tie point extraction, pose estimation, camera calibration, bundle adjustment, dense matching, georeferencing and many others.

For the comparison of point clouds corresponding to different acquisition times, different approaches are often used. In many cases, interpolations of the point clouds are performed for subsequent comparison. However, this procedure may introduce artifacts that affect the accuracy. Another technique used is the so-called Cloud-to-Mesh (C2M), which interpolates a surface from one of the two point clouds and calculates the distance along the surface normal [16, 17]. This approach poses problems in areas where the two point clouds do not overlap so that to obtain accurate measurements, it is necessary to remove all non-overlapping areas during manual editing, which is often time-consuming. In our study we used the Multiscale Model to Model Cloud Comparison (M3C2) which does not require explicit interpolation of the surfaces, but estimates surface normals and distances directly from the point clouds [17]. This method tends to give more accurate results since it avoids possible artifacts from interpolation and consists of two steps, in a first step the surface normals at each point are computed considering all points in a vicinity of size $D/2$ (D is a scale factor), usually from the oldest point cloud. Then, distances are calculated at each point as the average distance between all points in a vicinity of size $d/2$ (where d is the projection scale). The scale D should

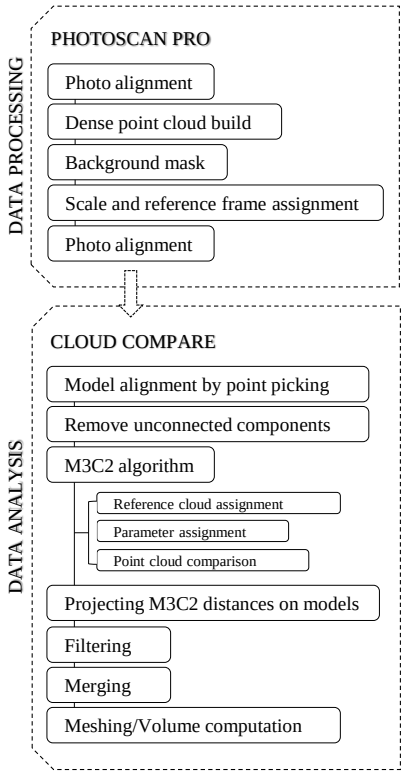

FIG. 3. Generalized workflow for data processing (dune reconstruction) and analysis (change detection).

be chosen sufficiently large to ensure that the distance measurement is independent of the surface roughness, and a range of d of 0.3 - 2 m is recommended. To promote greater robustness in the calculation of distances, large scale parameters were selected, since the shape and roughness of the surface can vary considerably between acquisition dates. An interesting feature of the M3C2 algorithm is the possibility to estimate a 95%-confidence interval for significant changes between two point clouds. The calculation of the confidence interval is based, among other things, on the local surface roughness.

An open source 3D point cloud editing and processing software, Cloud Compare [18], was used to perform the comparison among point clouds (compute M3C2 distances). Volume estimation were obtained by projecting M3C2 distances on models. To determine the removed volume, regions with negative distances were filtered out from the point clouds being compared. The resulting point clouds were subdivided into connected components where those with less than 30 points were disregarded. The next step is to construct meshes with those components coinciding between the two point clouds. For this purpose the normals of one of the matching components must be inverted so that all normals point outwards from the volume to be considered. At this point, a Poisson surface reconstruction is applied for each component [19]. This way is preferred over the other ways of estimating the volume since it does not need rather flat or properly oriented clouds (i.e. with the Z dimension as the vertical one). The same procedure described above is then applied to the regions where there were increases in material. The total removed/deposited volume is the sum of the volumes of each calculated component.

Figure 3 shows a simplified workflow for both reconstruction and comparison between models built from different acquisition dates.

IV. RESULTS AND DISCUSSION

Our results focus on the changes that occurred between two dates corresponding to a period of just under a year (July 2018 - March 2019). In this, period Cuba was affected, among other atmospheric phenomena, by Hurricane Michael, which caused considerable damage to infrastructure during its passage through the west of the country. With its action (direct or not), a good part of the material of the dune under study was removed and with it, some of the natural references of the area that would be used when comparing the elevation models generated on both dates. However, although with a slightly more manual intervention, it was possible to align point clouds of the two dates in a portion of the dune (about 200 m^2) with some of the references that remained in place.

Figure 2(a) shows a point cloud of the studied portion of the dune obtained during the acquisition in the summer of 2018. Figure 2(b) shows a similar portion of the dune acquired during the early spring of 2019. By simple inspection, some evident changes are identified in the amount of sand, but also in the vegetation –a feature characteristic of the season that introduced uncertainty in any quantification of sand volume. It is important to keep in mind that in order to obtain good temporal comparisons between models obtained in places where considerable changes are expected during the study period, it is advisable to include in them features (natural or not) with high probability of remaining stationary, if possible evenly distributed throughout the region of interest and its surroundings. These will play an important role in the alignment of the point clouds and thus in the corresponding measurement accuracy. The changes are quantified and represented in Fig. 4, through the M3C2 distances ($D = 0.5$m, 95% confidence interval) projected on the point cloud acquired in July 2018.

A relevant finding is that there was relatively almost no material gain during the time analyzed (about 20 cm in certain spots showed in red). This indicates that the material that was removed from the higher parts of the dune was also mostly removed from the site, probably as a result of the high tides associated with the natural phenomena that occurred during that period. The differences in height found between the clouds of constructed points reach values of up to 2 meters (vegetation included). However, height variations around 0.5 m are

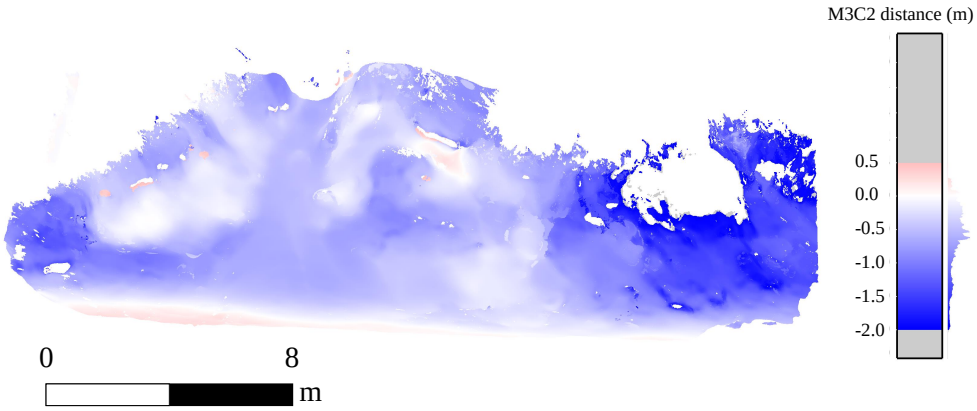

FIG. 4. M3C2 distances projected onto the point cloud corresponding to July 2018. Blue color indicates where there was material loss while red indicates where there was material gain. The uncertainty values of these distances are upper bounded by a value of 0.02 m.

predominant, similar values were reported in analysis of coastal changes in the U.S. after hurricane Sandy in 2014 [20].

The calculation of the removed volume resulted in a value of about 180 m^3, which corresponds to approximately 1350 kg/m^2 (13500 ton/ha). The amount of lost sand is equivalent to approximately a rate of 0.9 m/yr, so it can be classified as erosion, close to intense, according to the beach erosion classification scheme proposed in [13]. This value is close to the reported averaged values of annual erosion (1.2 m/yr) that Cuban beaches suffer [21] taking into account that the study period includes only 8 months.

V. CONCLUSIONS

A ground-based photogrammetric analysis was conducted to quantitatively study the temporal evolution of a dune on a Cuban sandy beach. For this purpose, two point clouds separated by a period of 8 months were obtained and compared using the Multiscale Model to Model Cloud Comparison (M3C2) method. From the analysis we quantified a loss of material volume of about 180 m^3 in an area of 200 m^2, equivalent to an erosion rate of 0.9 m/yr. A possible extra analysis, to go further, would be to look at the erosion rate as function of the (largest) slope, for all points in the model, evaluating the slope at a certain scale. More precise measurements of this and other dunes at "Santa María" beach should include the setting of artificial reference features capable of remaining immobile during the study period.

ACKNOWLEDGMENTS

We thank the support provided by the French Embassy in Havana through its Cooperation and Cultural Action Service (SCAC), Campus France, the ITES and the University of Strasbourg. We also thank to he INSU ALEAS program, the International Associate Laboratory France-Norway on Deformation Flow and fracture of disordered Materials LIA D-FFRACT and the Research Council of Norway through its Centres of Excellence funding scheme, project number 262644.

[1] M. R. James and S. Robson. Straightforward reconstruction of 3d surfaces and topography with a camera: Accuracy and geoscience ap-

plication. *Journal of Geophysical Research: Earth Surface*, 117(F3), 2012.

[2] M.J. Westoby, J. Brasington, N.F. Glasser, M.J. Hambrey, and J.M. Reynolds. 'structure-from-motion' photogrammetry: A low-cost, effective tool for geoscience applications. *Geomorphology*, 179:300–314, 2012.

[3] Mark A. Fonstad, James T. Dietrich, Brittany C. Courville, Jennifer L. Jensen, and Patrice E. Carbonneau. Topographic structure from motion: a new development in photogrammetric measurement. *Earth Surface Processes and Landforms*, 38(4):421–430, 2013.

[4] U. Niethammer, M.R. James, S. Rothmund, J. Travelletti, and M. Joswig. Uav-based remote sensing of the super-sauze landslide: Evaluation and results. *Engineering Geology*, 128:2–11, 2012. Integration of Technologies for Landslide Monitoring and Quantitative Hazard Assessment.

[5] Arko Lucieer, Steven M. de Jong, and Darren Turner. Mapping landslide displacements using structure from motion (sfm) and image correlation of multi-temporal uav photography. *Progress in Physical Geography: Earth and Environment*, 38(1):97–116, 2014.

[6] M. R. James and N. Varley. Identification of structural controls in an active lava dome with high resolution dems: Volcán de colima, mexico. *Geophysical Research Letters*, 39(22), 2012.

[7] George L. Heritage and Andrew R. G. Large. *Laser Scanning for the Environmental Sciences*. Blackwell Publishing Ltd, 2009.

[8] Pinliang Dong and Qi Chen. *LiDAR Remote Sensing and Applications*. Taylor & Francis, 2017.

[9] Paul R. Wolf, Bon A. Dewitt, and Benjamin E. Wilkinson. *Elements of Photogrammetry with Applications in GIS*. McGraw-Hill Education, 2014.

[10] John Fryer, Harvey Mitchell, and Jim H Chandler. *Applications of 3D measurement from images*. Whittles, 2007.

[11] R Hartley and A Zisserman. *Multiple view geometry in computer vision*. Cambridge University Press, 2013.

[12] Omar Defeo, Anton McLachlan, David S. Schoeman, Thomas A. Schlacher, Jenifer Dugan, Alan Jones, Mariano Lastra, and Felicita Scapini. Threats to sandy beach ecosystems: A review. *Estuarine, Coastal and Shelf Science*, 81(1):1–12, 2009.

[13] Arjen Luijendijk, Gerben Hagenaars, Roshanka Ranasinghe, Fedor Baart, Gennadii Donchyts, and Stefan Aarninkhof. The State of the World's Beaches. *Scientific Reports*, 8(1):6641, 2018.

[14] Agisoft. `http://agisoft.com`. Accessed: 2020-06-16.

[15] Currently named Agisoft Metashape Professional.

[16] P. Cignoni, C. Rocchini, and R. Scopigno. Metro: Measuring error on simplified surfaces. *Computer Graphics Forum*, 17(2):167–174, 1998.

[17] Dimitri Lague, Nicolas Brodu, and Jérôme Leroux. Accurate 3d comparison of complex topography with terrestrial laser scanner: Application to the rangitikei canyon (nz). *ISPRS Journal of Photogrammetry and Remote Sensing*, 82:10–26, 2013.

[18] Daniel Girardeau-Montaut. http://www.danielgm.net/cc/. Accessed: 2022-06-20.

[19] Michael Kazhdan, Matthew Bolitho, and Hugues Hoppe. Poisson surface reconstruction. In *Proceedings of the fourth Eurographics symposium on Geometry processing*, volume 7, 2006.

[20] K.L. Sopkin, H.F. Stockdon, K.S. Doran, N.G. Plant, K.L.M. Morgan, K.K. Guy, and K.E.L. Smith. Hurricane sandy—observations and analysis of coastal change, 2014.

[21] R. Rodríguez Paneque and Charles W. Finkl. Erosion of Carbonate Beaches on the Northeastern Coast of Cuba. *Journal of Coastal Research*, 36(2):339 – 352, 2020.

Conclusions

Intruder penetration has been studied under different circumstances, focusing on rotation and preferential orientation. Additionally, the continuous to intermittent transition in dense granular flows developed over a growing granular pile has been studied. In particular, the presented studies have reached the following conclusions:

- We have fully characterized the horizontal repulsion of solid intruders as they penetrate a quasi-2D granular bed near a wall. Our experiments reveal that the interaction with the wall additionally produces rotation of the intruder around its axis of symmetry. We conclude that non-zero frictional forces between the intruder surface and the surrounding grains are essential to obtain the rotation effect, which was corroborated by DEM simulations. Finally, we suggest that the repulsion and rotation of an intruder released near a vertical wall can be largely reproduced by replacing the wall with a second intruder released next to the original one.

- We have studied the behavior of cylindrical objects as they sink into a dry granular bed fluidized by horizontal oscillations, as a model system to understand the effects of earthquake-related fluidization of soils on human constructions and other objects like rocks. We have found that cylinders with flat bottoms sink vertically, while those with a "foundation" attached to their bottom, tilt laterally besides their vertical sinking. DEM simulations suggest that differences can be associated with the jamming of the particles in the

region of the foundation, which can increase the effective friction at the bottom generating force chains capable of preventing the recovery of the vertical orientation after the oscillation-induced rotation. However, the tilting scenario tends to dominate, regardless the nature of the intruder's foundation, when strong enough lateral shaking is applied.

- We have systematically studied the penetration of a square prism intruder released at different angles of attack inside a Hele-Shaw cell (away from its side walls). During penetration, the intruder rotates in such a way that its final angular position is close to zero, i.e., its bottom surface parallel to the bottom of the container. Similar behaviors were observed for all the different initial angles of the intruder, except for 45 degrees, where on average the angular position remained unchanged. We proposed a phenomenological model based on resistive force theory (RFT) to describe its penetration and rotation dynamics under non-quasistatic conditions, showing that RFT theory is capable of semi-quantitatively describe both tilting and sinking motions.

- We have performed a systematic study of the surface flow on a granular heap where grains are added from a controlled height. As the pile grows, the established flow is first continuous, and then intermittent. We have found that the size of the base of the pile at which this change in regime occurs (X_c) grows linearly with the input flux, and is proportional to the squared root of the deposition height. We explain these facts based on a model where mass and momentum are conserved taking into account the basal friction of the flowing grains with the quasi-static part of the heap as well as the friction with walls. Importantly, we observed that the layer of flowing grains is wedge-shaped in growing heaps. By systematically comparing experiments with controlled and non-controlled deposition height (as typically reported in the literature) we were able to predict the values of X_c in the latter case based on its values in the former.

- A ground-based photogrammetric analysis was conducted to quantitatively study the evolution of a dune on a Cuban sandy beach. For this purpose, two point clouds separated by a period of 8 months were obtained and compared

using the Multiscale Model to Model Cloud Comparison (M3C2) method. We measured a loss of material volume of about 180 m^3 in an area of 200 m^2, which is equivalent to an erosion rate of approximately 0.9 m/yr.

Perspectives

Our contributions to the understanding of the rotation of intruders that penetrate granular media provide a new dimension in the comparison of these (granular materials) with conventional fluids. The rotation found in penetrations close to a vertical wall bear similarities to analogue experiments in fluids, where it is also appreciated, in addition to lateral repulsion/attraction to the boundary. On the other hand, the preference in orientation shown by flat-lying intrusions, both in light and agitated beds, could suggests new elements to be taken into account in the study of sediment transport, since the existence of shape-fabrics in sedimentary deposits was recognized at an early date. The study of the dynamics of objects on agitated soils can serve as a toy model for investigations of the performance of human structures in which the foundations could be relevant.

Furthermore, the dependencies found for the occurrence of transition in growing granular piles could find practical application in the industry for activities involving the transportation and storage of granular materials. The phenomena that usually appear once the transition is reached can be detrimental in certain aspects and affect, for example, the proper mixing of the components that make up the granular material.

Acknowlegdments

Just as a granular medium owes much of what it is to the particles that compose it, the completion of this thesis would not have been possible without the support of many who were there for me in one way or another throughout the duration of this PhD.

- I would like to express my deepest gratitude to my supervisors. Alt, Renaud, thank you for being such excellent persons and for giving me the opportunity to work and share with you all these years. It has been inspiring, interesting and fun. Thank you for your patient guidance, enthusiastic encouragement and helpful criticism. I will always be deeply grateful to you.

- I would like to extend my sincere thanks to all the co-authors, without whom the articles or drafts would not have been what they are today. It has been a pleasure to work with you all.

- Words cannot express my gratitude to Yerila. Thank you for sharing these years with me, for believing in me and for so much support.

- I want to thank all my family for their encouragement and support over all these years, especially to my wonderful mother. To them I owe much of what I am today.

- I am grateful to all my office mates and fellow PhD students in Strasbourg, Monem Ayaz, Shahar Ben-Zeev, Mathilde Desrues, Tom Vincent-Dospital

and Bérénice Vallier for sharing with me many pleasant moments and for all the interesting discussions on a plethora of topics. You guys have made my stays easier and more fun, thank you.

- I am also grateful to all my colleagues and office mates at the Physics Faculty in Havana for all this enriching time with them and for all the good moments we had.

- I thank to the members of the Photovoltaic Lab in Havana for allowing me to share good times with them and for letting me use their facilities as another member. I especially want to thank Lídice Vaillant for always looking out for me and for helping me in everything she could. Thank you also for the good advice.

- I would like to thank Roberto Mulet for always keeping an eye on my progress, for all the help and advice, and for being so contagiously optimistic.

- I thank to the Cubans at Nancy, Claudia de Melo, Alejandro Borroto, Mariana Miranda, Alexis García and Adrián Benedit for all the good times we have had together and for the help and advice.

- I'd like to acknowledge Aime Pelaiz for being a great dean and for always getting me out of trouble with the bureaucracy.

- I'd also like to acknowledge the French embassy in Cuba, Campus France and IPGS/ITES for supporting my mobility to France during these years.

- I thank the Institute of Materials Science and Technology (IMRE) in Havana, especially its direction, for allowing me to stay late into the night and on weekends for conducting experiments.

- I'd like to recognize the administrative staff of ITES (formerly IPGS) for their kindness, patience and for always making sure that everything related to my mobility was in order. Special thanks to Dilek Karayagit and Binta Mesmacque for being so dedicated, and so cheerful.

- I am grateful to the staff of the European Doctoral College (CDE), especially Virginie Herbasch for being such a nice person and for taking care of my co-supervision agreement. I thank the International Doctoral Program (PDI) for accepting my application and for all the great conferences organized on science and Europe from which I learned a lot. I would like to extend my thanks to everyone in the PDI, especially the Katherine Johnson cohort for sharing many fun and learning moments. To the CDE residency staff, I thank you for hosting me every year.

- I'd like to acknowledge Jean Philippe Malet for accepting to be part of my supervisory committee and for his help in obtaining satellite images of the dunes for possible future studies.

- Lastly, I would like to thank the referees and examiners for agreeing to be part of my jury and for the time they will spend on assessing my work.

Remerciements

De même qu'un milieu granulaire doit beaucoup de ce qu'il est aux particules qui le composent, l'achèvement de cette thèse n'aurait pas été possible sans le soutien de nombreuses personnes qui ont été là pour moi d'une manière ou d'une autre pendant toute la durée de ce doctorat.

- Je tiens à exprimer ma plus profonde gratitude à mes encadrants. Alt, Renaud, merci d'être d'excellentes personnes et de m'avoir donné l'opportunité de travailler et de partager avec vous toutes ces années. Cela a été inspirant, intéressant et amusant. Merci pour vos conseils patients, vos encouragements enthousiastes et vos critiques utiles. Je vous en serai toujours profondément reconnaissant.

- Je tiens à adresser mes sincères remerciements à tous les coauteurs, sans lesquels les articles ou les ébauches n'auraient pas été ce qu'ils sont aujourd'hui. Ce fut un plaisir de travailler avec vous tous.

- Les mots ne peuvent exprimer ma gratitude envers Yerila. Merci d'avoir partagé ces années avec moi, d'avoir cru en moi et de m'avoir tant soutenu.

- Je tiens à remercier toute ma famille pour ses encouragements et son soutien pendant toutes ces années, en particulier ma merveilleuse mère. C'est à eux que je dois beaucoup de ce que je suis aujourd'hui.

- Je suis reconnaissante à tous mes collègues de bureau et mes camarades doctorants à Strasbourg, Monem Ayaz, Shahar Ben-Zeev, Mathilde Desrues,

Tom Vincent-Dospital et Bérénice Vallier pour avoir partagé avec moi de nombreux moments agréables et pour toutes les discussions intéressantes sur une pléthore de sujets. Vous avez rendu mes séjours plus faciles et plus agréables, merci.

- Je suis également reconnaissant à tous mes collègues et camarades de bureau de la Faculté de Physique de La Havane pour ce temps enrichissant passé avec eux et pour tous les bons moments que nous avons passés.

- Je remercie les membres du laboratoire photovoltaïque de La Havane pour m'avoir permis de partager de bons moments avec eux et pour m'avoir laissé utiliser leurs installations en tant que membre supplémentaire. Je tiens tout particulièrement à remercier Lídice Vaillant pour avoir toujours veillé sur moi et m'avoir aidé dans tout ce qu'elle pouvait. Merci également pour les bons conseils.

- Je voudrais remercier Roberto Mulet pour avoir toujours gardé un œil sur mes progrès, pour toute l'aide et les conseils, et pour être si contagieusement optimiste.

- Je remercie les Cubains de Nancy, Claudia de Melo, Alejandro Borroto, Mariana Miranda, Alexis García et Adrián Benedit pour tous les bons moments que nous avons passés ensemble et pour l'aide et les conseils.

- Je tiens à remercier Aime Pelaiz pour avoir été un doyen formidable et pour m'avoir toujours tiré d'affaire avec la bureaucratie.

- Je tiens également à remercier l'Ambassade de France à Cuba, Campus France et l'IPGS/ITES pour avoir soutenu ma mobilité en France pendant ces années.

- Je remercie l'Institut des Sciences et Technologies des Matériaux (IMRE) à La Havane, en particulier sa direction, pour m'avoir permis de rester tard dans la nuit et les week-ends pour réaliser des expériences.

- Je tiens à remercier le personnel administratif de l'ITES (anciennement IPGS) pour sa gentillesse, sa patience et pour avoir toujours veillé à ce que

tout ce qui concerne ma mobilité soit en ordre. Je remercie tout particulièrement Dilek Karayagit et Binta Mesmacque pour leur dévouement et leur bonne humeur.

- Je remercie le personnel du Collège Doctoral Européen (CDE), en particulier Virginie Herbasch, pour sa gentillesse et pour s'être occupée de mon contrat de co-supervision. Je remercie le Programme Doctoral International (PDI) d'avoir accepté ma candidature et pour toutes les merveilleuses conférences organisées sur la science et l'Europe, qui m'ont beaucoup appris. Je tiens à remercier tous les membres du PDI, en particulier la cohorte Katherine Johnson, pour avoir partagé de nombreux moments de plaisir et d'apprentissage. Au personnel de la résidence du CDE, je vous remercie de m'accueillir chaque année.

- Je tiens à remercier Jean Philippe Malet pour avoir accepté de faire partie de mon comité de suivi et pour son aide dans l'obtention d'images satellites des dunes pour d'éventuelles études futures.

- Enfin, je tiens à remercier les rapporteurs et examinateurs pour avoir accepté de faire partie de mon jury et pour le temps qu'ils consacreront à l'évaluation de mon travail.

Fluidized granular matter: sedimentation and dense flows

Abstract

Granular media are ubiquitous in nature and of utmost importance for Earth sciences. A distinguishing feature of these is that although their constituent particles are solid, as a whole they may behave as solids, liquids or gases. During the penetration of an intruder into a granular bed, solid and fluidlike behaviors coexist and, under certain conditions, this penetration may involve rotation of the object. However, despite significant research efforts devoted to understanding of the penetration, rotation has been a topic rarely documented in the literature. Another scenario involving solid and fluidlike behaviors is that of granular heap. Many complex phenomena have been found in the dense flows established on its surface, such as the transition between continuous and intermittent flows (CIT). In spite of the many advances in the physics of granular flows, the study of these during the continuous regime in situations of greater practical utility such as growing heaps is not common. This thesis studies the sedimentation of solid intruders in granular cells under different conditions: close to a vertical wall, in a horizontally agitated cell or with different initial orientations, with particular emphasis on the rotation described by them. On the other hand, the CIT in a growing granular heap is also studied.

Keywords: granular media, sedimentation, settling, penetration, tilting, dense flows, flow transition

---

Matière granulaire fluidisée : sédimentation et écoulements denses

Résumé

Les milieux granulaires sont omniprésents dans la nature et revêtent une importance capitale pour les sciences de la Terre. Ils se distinguent par le fait que, bien que leurs particules constitutives soient solides, dans leur ensemble, ils peuvent se comporter comme des solides, des liquides ou des gaz. Lors de la pénétration d'un intrus dans un lit granulaire, les comportements solide et fluide coexistent et, dans certaines conditions, cette pénétration peut impliquer une rotation de l'objet. Cependant, malgré d'importants efforts de recherche consacrés à la compréhension de la pénétration, la rotation a été un sujet rarement documenté dans la littérature. Un autre scénario impliquant des comportements de type solide et fluide est celui du tas granulaire. De nombreux phénomènes complexes ont été découverts dans les flux denses établis à sa surface, tels que la transition entre les flux continus et intermittents (CIT). Malgré les nombreuses avancées dans la physique des écoulements granulaires, l'étude de ceux-ci en régime continu dans des situations de plus grande utilité pratique comme les tas en croissance n'est pas courante. Cette thèse étudie la sédimentation d'intrus solides dans des cellules granulaires dans différentes conditions : près d'une paroi verticale, dans une cellule agitée horizontalement ou avec différentes orientations initiales, avec un accent particulier sur la rotation décrite par celles-ci. D'autre part, le CIT dans un amas granulaire en croissance est également étudié.

Mots clés : milieux granulaires, sédimentation, décantation, pénétration, basculement, écoulements denses, transition d'écoulement

Laciel ALONSO-LLANES

Matière granulaire fluidisée

Résumé

Les milieux granulaires sont omniprésents dans la nature et revêtent une importance capitale pour les sciences de la Terre. Ils se distinguent par le fait que,bien que leurs particules constitutives soient solides, dans leur ensemble,ils peuvent se comporter comme des solides, des liquides ou des gaz. Lors de la pénétration d'un intrus dans un lit granulaire, les comportements solides et fluides coexistent et, dans certaines conditions, cette pénétration peut impliquer une rotation de l'objet. Cependant, malgré d'importants efforts de recherche consacrés à la compréhension de la pénétration, la rotation a été un sujet rarement documenté dans la littérature. Un autre scénario impliquant des comportements de type solide et fluide est celui du tas granulaire. De nombreux phénomènes complexes ont été découverts dans les flux denses établis à sa surface, tels que la transition entre les flux continus et intermittents (CIT). Malgré les nombreuses avancées dans la physique des écoulements granulaires, l'étude de ceux-ci en régime continu dans des situations de plus grande utilité pratique comme les tas en croissance n'est pas courante. Cette thèse étudie la sédimentation d'intrus solides dans des cellules granulaires dans différentes conditions: près d'une paroi verticale, dans une cellule agitée horizontalement ou avec différentes orientations initiales, avec un accent particulier sur la rotation décrite par celles-ci. D'autre part, le CIT dans un amas granulaire en croissance est également étudié.

Mots clés : milieux granulaires, sédimentation, décantation, pénétration, basculement, écoulements denses, transition d'écoulement

Résumé en anglais

Granular media are ubiquitous in nature and of utmost importance for Earth sciences. A distinguishing feature of these is that although their constituent particles are solid, as a whole they may behave as solids, liquids or gases. During the penetration of an intruder into a granular bed, solid and fluid-like behaviors coexist and, under certain conditions, this penetration may involve rotation of the object. However, despite significant research efforts devoted to understanding of the penetration, rotation has been a topic rarely documented in the literature. Another scenario involving solid and fluid-like behaviors is that of granular heap. Many complex phenomena have been found in the dense flows established on its surface, such as the transition between continuous and intermittent flows (CIT). In spite of the many advances in the physics of granular flows, the study of these during the continuous regime in situations of greater practical utility such as growing heaps is not common. This thesis studies the sedimentation of solid intruders in granular cells under different conditions: close to a vertical wall, in a horizontally agitated cell or with different initial orientations, with particular emphasis on the rotation described by them. On the other hand, the CIT in a growing granular heap is also studied.

Keywords: granular media, sedimentation, settling, penetration, tilting, dense flows, flow transition